CILIUM-AUTONOMOUS REGULATION OF TUBULIN TRANSPORT BY INTRAFLAGELLAR TRANSPORT IN *CHLAMYDOMONAS REINHARDTII*

by

JULIE MELISSA CRAFT

(Under the Direction of Karl Lechtreck)

ABSTRACT

The microtubule-based axoneme is the defining characteristic of all eukaryotic flagella and cilia. Assembly of this structure during ciliogenesis requires a vast translocation of the microtubule subunit, the α/β tubulin heterodimer, from the cytoplasm to the site of growth, the distal tip of cilia. Herein this work, we investigate tubulin transport in cilia, inlcuding the means of transport, its regulation, and timing. In *Chlamydomonas reinhardtii*, we express fluorescently tagged $\alpha-$ and $\beta-$ tubulins and observe via *in vivo* total internal reflection fluorescence (TIRF) microscopy. Both subunits are bona fide cargoes of intraflagellar transport (IFT), the devoted ciliary active transport system; tubulin also diffuses into the cilium. The protruding C-terminal E-hooks of $\alpha-$ and $\beta-$ tubulin are not essential for transport by IFT, but removal of β-tubulin E-hook significantly reduced transport frequency suggesting that is does provide enhanced stability of the heterodimer-IFT particle interaction. The transport frequency of GFP-tubulin is strongly upregulated during ciliary growth and IFT trains carry more tubulin as cargo than during non-growth. Thus cells regulate

the amount of tubulin cargo on IFT trains; the differential loading of IFT could explain this phenomenon. Further, cells possessing both growing and non-growing cilia selectively elevate IFT particles carrying tagged tubulin in only the actively growing cilia. We posit that cells regulate the amount of cargo loading; upon receipt of an incomplete growth status signal, the cells respond with an increase of cargo loading in a cilium-autonomous manner. Likewise, cells approximately double the intraciliary pool of soluble tubulin. We propose that IFT functions to increase the local soluble concentration of tubulin at the growing tip to facilitate timely axonemal elongation. Thus, IFT functions as a tubulin pump to enrich tubulin in cilia; high tubulin concentrations will promote microtubule extension, and inasmuch, ciliary growth.

INDEX WORDS: Cilia, Flagella, Intraflagellar Transport, Tubulin

CILIUM-AUTONOMOUS REGULATION OF TUBULIN TRANSPORT BY INTRAFLAGELLAR TRANSPORT IN *CHLAMYDOMONAS REINHARDTII*

by

JULIE MELISSA CRAFT

B.S., The University of Georgia, 2008

A Dissertation Submitted to the Graduate Faculty of The University of Georgia in Partial Fulfillment of the Requirements for the Degree

DOCTOR

OF PHILOSOPHY

ATHENS, GEORGIA

2015

CILIUM-AUTONOMOUS REGULATION OF TUBULIN TRANSPORT BY INTRAFLAGELLAR TRANSPORT IN *CHLAMYDOMONAS REINHARDTII*

by

JULIE MELISSA CRAFT

Major Professor: Karl Lechtreck

Committee: Jacek Gaertig
James Lauderdale
Vincent Starai

Electronic Version Approved:

Suzanne Barbour
Dean of the Graduate School
The University of Georgia
December 2015

ACKNOWLEDGEMENTS

I am especially grateful to my major professor Dr. Lechtreck for his guidance through my project and for providing a fostering environment for my scientific development. I am so thankful to have matured into a (somewhat) better scientist under his direction; he fully embodied the term *mentor.* I would like to acknowledge past mentors, Drs. Matt Collins and Juan Bustamante for being wonderful scientific examples to a naïve student. I would also like to thank my committee members, Drs. Jacek Gaertig, James Lauderdale, and Vincent Starai. I am thankful to Dr. Gaertig for his creative and insightful suggestions to help further my work. A special thanks to Drs. James Lauderdale and Marcus Fechheimer who gave much support and guidance over the years. To past and current Lechtreck lab members, thanks for making this fun, tolerating my somewhat eccentric behavior, and enlightening conversations. I'd like to thank members of Gaertig lab- who knew lab meetings could be so entertaining!

Beyond the realm of science, I would like to acknowledge several people. To my parents, Joe and Deann Craft, and family, thank you for supporting me over all the many, many years I've been in school and imparting a strong work ethic. A special thanks to my *scientific partner in crime* (and piñatas), Dr. Hillary Shane. I'd like to thank m'lady Kenji Johnson, a pal and a confidant. To a young grasshopper, Aaron Harris, thanks for helping to keep things lighthearted- keep your head down and your chin up! And finally, I owe a debt of gratitude to my fiancé, Dave Van De Weghe for going through this journey with me and being a

constant source of support and inspiration.

TABLE OF CONTENTS

Page

APPENDICES

Page

LIST OF TABLES

Page

LIST OF FIGURES

Page

CHAPTER 1

INTRODUCTION AND LITERATURE REVIEW

1.1 Cilia: Conserved organelles with diverse functions

Cilia and flagella (interchangeable terms) are specialized, cylindrical protrusions emanating from the cell body. A cilium is not a membrane bound organelle, but it is partially isolated from the rest of the cell by the transition zone. Cilia are devoid of ribosomes and all ciliary proteins must be transported in and out of the organelle; this feat is achieved in parts by intraflagellar transport (IFT), a bidirectional transport system which moves along axonemal microtubules via molecular motors. Cilia, the axoneme, and IFT are evolutionarily highly conserved from protists to metazoans. Here I will give a brief overview of the structure.

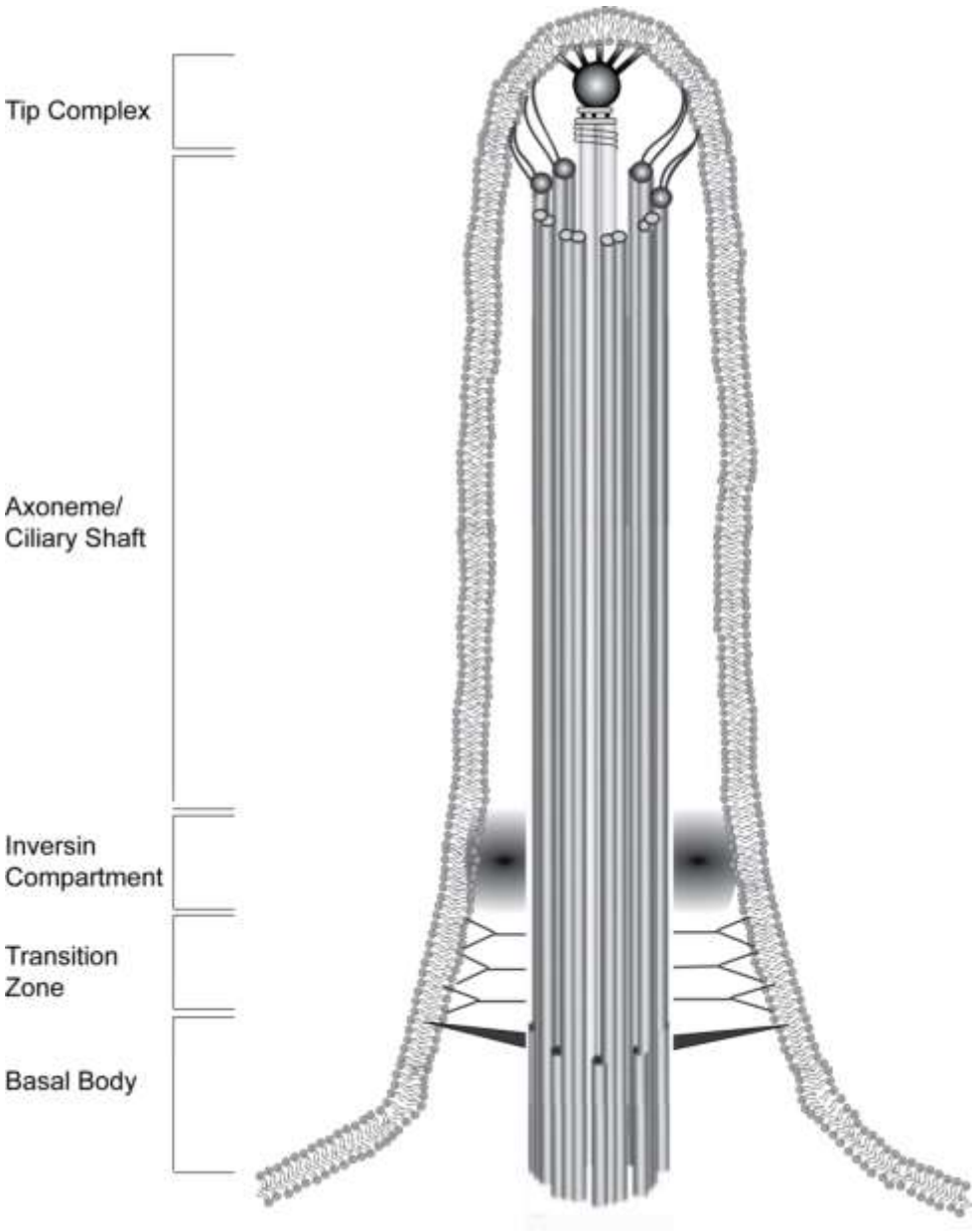

Figure I. Cartoon schematic of motile ciliary compartments. The ciliary membrane is continuous with the plasma membrane. The basal body serves as the microtubule organizing center for the axoneme. The transition zone lies distal to the basal bodies, with inversin compartment just distal thereof. The axoneme is a 9+2 microtubular arrangement. The enigmatic tip complex links the axonemal microtubules to the membrane.

The basal bodies

Basal bodies are required for cilia formation and are located at the ciliary base. They are formed of nine short triplet microtubules (A, B, and C microtubules) in a barrel fashion (Geimer and Melkonian, 2004). The nine ciliary outer doublet microtubules are nucleated and continuous with the A and B tubules of the basal body (Ringo, 1967). When not associated with the cilium, these structures are referred to as centrioles; centrioles form the microtubule organizing center (MTOC) during mitotic spindle formation. When not in division, the centrioles are repurposed as the MTOC for cilium formation; when division resumes, the cilium resorbs and the basal bodies are centrioles once again. Therefore, ciliogenesis is tightly linked to cell cycle progression (Pugacheva et al, 2007; Pan and Snell, 2007). In the first stages, a ciliary vesicle forms at the distal end of the basal body and this structure translocates to the cell cortex (Sorokin, 1968). In epithelial cells, the planar cell polarity pathway aids in positioning the basal bodies (Marshall, 2008). Then, the ciliary vesicle, which has already begun to accumulate ciliary membrane proteins, fuses with the plasma membrane and cilium growth commences (Lu et al., 2015).

Once the cilium is formed, the basal bodies continue to serve as an organizing center for protein entry into the cilium proper. IFT proteins, motors, and cargoes can be seen accumulating in this region. It is thought that it is in this region where IFT trains assemble (i.e., IFT particles arrange into complexes, associate with motors, and load cargoes).

The transition zone

The transition zone begins at the end of the basal body and in *C. reinhardtii*, encompasses ~50nm distal to the ciliary base (Geimer and Melkonian, 2004). The most proximal region contains the transition fibers that form a propellor like array that emanate from the distal region of the B tubules of the basal bodies to the plasma membrane. These transition fibers anchor ciliary microtubules to the cililary membrane via specialized proteins (Graser et al., 2007; Deane et al., 2001). Above the transition fibers lie the Y-shaped connectors that also function to stabilize the axoneme/membrane connection (O'Toole et al., 2007). The transition zone is assembled from protein modules in a heirarchial order: The JBTS module is required for the assembly of other transition zone components, the NPHP and MKS modules (Garcia-Gonzalo et al., 2011; Sang et al., 2011; Williams et al., 2011; Chih et al., 2011). Distal to the transition zone proper is the inversin compartment (Shiba et al., 2010). These modules are thought to interact in a complex fashion to control entry and exit of proteins from the cilium; a diffusion barrier in this region assists in ciliary compartmentalization from cell body cytoplasm (reviewed in Hu and Nelson, 2011). Many causative proteins for ciliopathies localize to these regions (see Appendix 2). Since this is the site of entry into the cilium proper, the transition zone is aptly located to function as a protein sorting area to maintain proper protein content in cilia.

The axoneme

The microtubular axoneme serves as the scaffold for all varieties of cilia. Motile cilia have the canonical 9+2 microtubular arrangement, yet it is not entirely inviolable. This configuration includes nine peripheral doublet outer microtubules consisting of an A and B tubule. The A tubules serves as the scaffold for inner and outer dynein arms that drive microtubule sliding, while IFT motors translocate upon the B tubule (Pigino et al., 2009). The two central pair microtubules and their associated projections lie inside the axonemal cylinder and are required for complex waveform. Also required for motility, the radial spokes physically contact the central pair and outer doublet microtubules (Oda et al., 2014a; reviewed in Smith and Yang, 2004).

Nodal cilia retain a simple helical movement with the 9 + 0 axonemal configuration. These axonemes lack the machinery for complex wave form (i.e., central apparatus and radial spokes), but retain the dynein arms (Supp et al., 1997). During development, these cilia are at the embryonic node where the vortical movement generates a leftward fluid flow that drives an asymmetric distribution of morphogens; this leads to left-right asymmetry in the node and, ultimately, in the body plan (Nonaka et al., 1998; Praetorius and Spring, 2005).

The 9+0 axonemal arrangement is predominately found in non-motile cilia. These axonemes are void of all motility-associated structures. Lacking motility, these cilia have sensory functions. These cilia are called primary cilia; they were first denoted as such in studies of ciliated epithelia in which the primary cilia arises first before the formation of multiple motile cilia (Sorokin, 1968).

Further, the axonemal microtubules serve as the track upon which IFT trains translocate. Axonemal microtubules comprise the scaffold onto which other axonemal complexes dock (e.g., inner dynein arms and outer dynein arms). These complexes dock at regular repeats and components are just beginning to be identified that govern this finely tuned process for structural repeats (Oda et al., 2014b). The axoneme is highly complex structure with ~600-1000 distinct polypeptides; this creates a challenge for sorting and transporting proteins in required amounts.

The ciliary tip

A complex structure resides at the ciliary tip, of which little is known. The ultrastructure was described in *Chlamydomonas* and *Tetrahymena* as two distal plates with an electron-dense ball at the end of the central pair microtubules in connection with the ciliary membrane (Dentler and Rosenbaum, 1977; Sale and Satir, 1977; Dentler, 1980). Transmission electron micrographs revealed carrot-shaped filaments partially inserted into the distal lumen of the A tubules of the doublets, and connecting them to the ciliary membrane (Dentler, 1980). It is proposed that this structure facilitates the integrity of the axonemes association with the ciliary membrane (Dentler, 1980). Further, cargoes of IFT are unloaded in this area and incorporated into the growing axoneme from the tip. This structure could be involved with the addition of tubulin at the growing distal plus tips of axonemal microtubules (Dentler, 1984).

1.2 Intraflagellar transport

Twenty years ago, a bidirectional movement of granules in the cilia of *Chlamydomonas* was observed with differential interference contrast microscopy (Kozminksi et al., 1993). This movement occurred between the axoneme and ciliary membrane and was thus termed intraflagellar transport (IFT) (Kozminksi et al., 1993). Formally, IFT is a bi-directional movement of multi-megadalton protein composites (IFT trains) along the length of the cilium. This system brings axonemal precursors and other required proteins into the organelle.

IFT is indispensable for maintaining cilia, with the notable exception of mammalian sperm (San Agustin et al., 2015). This transport system delivers macromolecules needed for maintenance and assembly since the cilium is devoid of ribosomes. IFT motors, IFT particles, and cargoes concentrate at the base of the cilium near the transitional fibers, and all form ordered IFT trains before the initiation of transport (Iomini et al. 2001; Deane et al., 2001). IFT trains translocate from the base of the cilium to the distal tip by anterograde IFT (Iomini et al., 2001). Heterotrimeric kinesin-II is the motor responsible for anterograde transport, moving with a velocity of ~2 μm/sec for *C. reinhardtii* (Walther et al., 1994; Cole et al.,1998). At the tip, the cargoes are unloaded from the anterograde IFT (Iomini et al., 2001). Cargoes bound to exit the cilium are loaded onto retrograde IFT trains, which translocate to the base of the cilium (Iomini et al., 2001). Cytoplasmic dynein 1b is the motor responsible for retrograde transport, moving with velocity of ~4 μm/sec for *C. reinhardtii* (Signor et al., 1999; Pazour et al., 1999; Cole et al., 2003). It is known that IFT maintains

a steady rate independent of ciliary length; this suggests that IFT may function as a continuous conveyor belt that is capable of interacting and translocating a wide range of proteins (Craft et al., 2015; Dentler, 2005; Engel et al., 2009).

IFT particles are composed of ~22 proteins organized into two complexes, IFT-A and IFT-B (Cole et al., 1998; Follit et al., 2009; Cole et al., 2003). IFT particle proteins are strongly conserved among ciliated organisms and listed in Appendix 1. These proteins are rich in several domains with protein-protein implications, such as WD, coiled-coiled, and tetratricopeptide; it is postulated that these domains facilitate interactions with a range of cargoes (Cole et al., 2003). The BBSome also cycles in conjuction with IFT; it is not required for IFT, but is thought to serve as a specialized cargo adapter for membrane associated proteins and involved in their export from cilia (Jin et al., 2010; Lechtreck et al., 2009; Berbari et al., 2008).

It is presently unclear how IFT interacts with its cargoes. How does the cell move all proteins needed to build a cilium into this organelle? Do individual binding sites exist for all cargoes? Does IFT respond to ciliary deficiencies with increased transport? Being able to observe IFT and its cargoes simultaneously enables us to begin to answer these questions.

1.3 Cilia in human health and disease

All three aforementioned forms of cilia are found in the human body: motile (9+2 arrangement), primary cilia (9+0), and nodal cilia (9+0). Motile cilia function throughout the body to generate flow, e.g., aiding in mucociliary clearance in the lung airways, promoting cerebral spinal fluid flow in the brain

ventricles, and sperm propulsion. Most differentiated cells in the body possess a single non-motile primary cilium used for signaling and sensing a variety of cues ranging from light and odorants to mechanical stimuli (Pugacheva et al., 2007).

Defects in IFT and other processes that influence ciliary composition will affect all cilia in the body, thus resulting in disorders with a multi-organ phenotype. When cilia are not formed or have improper protein content, a variety of disorders present that are collectively called ciliopathies. These disorders can result in blindness, mental retardation, hydrocephalus, infertility, heart defects, situs inversus, polydactyl, and obesity (Fig. II). A comprehensive list of ciliopathies, the causative genes, and the sub-ciliary localization of the gene products can be found in Appendix 2.

The lack of ciliary motility causes a condition referred to as primary ciliary dyskinesia (PCD). PCD is a heterogenic disease with a prevalence of 1 in 20,000 births and is caused when motile cilia are not able to generate proper motion with the canonical frequency and beat pattern (Pazour et al., 2002; Ibanez-Tallon et al., 2003). Chronic respiratory problems arise from difficulties in mucociliary clearance, as cilia normally act to move mucus along the respiratory tract (Lee et al., 2011; Snell et al., 2004). Hydrocephalus often occurs, as ependymal cilia normally function to move cerebrospinal fluid throughout the ventricular system of the brain (Lee, 2011; Snell et al., 2004). Another common pathological manifestation is infertility, predominately in men as sperm lack proper locomotion and less commonly in women via disruptions of oviduct cilia (Pazour et al., 2002; Lee, 2011;Ibanez-Tallon et al., 2003; Snell et al. 2004).

Also occurring in a subset of PCD patient is *situs inversus*, which is reversed viscera placement due to defective nodal cilia resulting in a randomization of the left-right body axis (Okada et al., 1999;Pazour et al., 2002). The majority of PCD cases arise from defects in inner or outer dynein arms (Escudier et al., 2009).

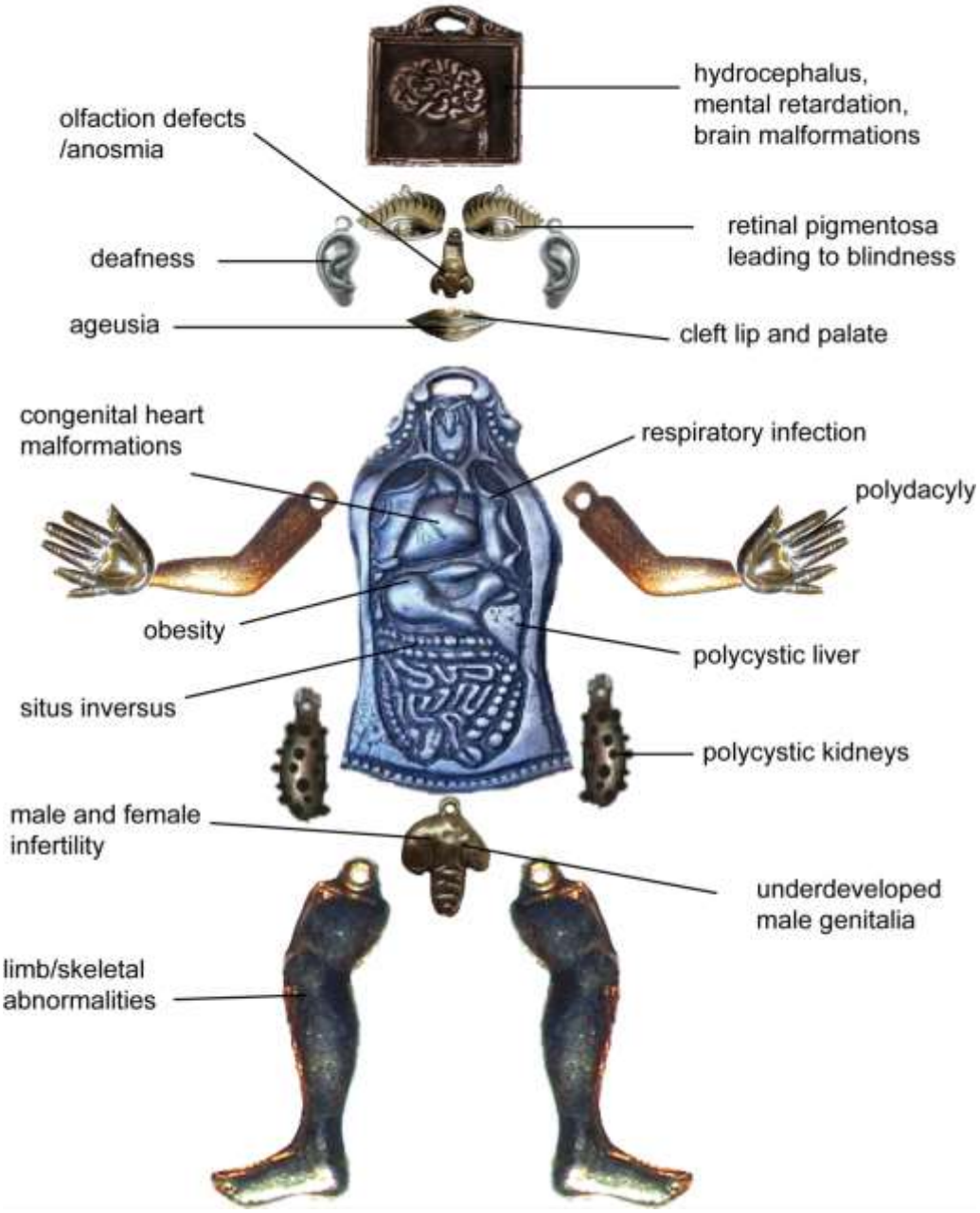

Figure II. Pleiotropic manifestations of ciliopathies. Given the near ubiquitous nature of cilia in the human body, dysfunction often leads to a multi-organ phenotype.

1.4 Ciliary Assembly

Cilia were first described in 1675 by Anthony Van Leeuwenhoek as he examined rain water and noted tiny animalcules with 'incredibly thin feet, or little legs, which were moved very nimbly.' (Dobell,1932). This organelle was later termed cilia (latin for eyelash). Advances were made in determining the ultrastructure of cilia as transmission electron microscopy became available in the 1940's and 50's (Porter, 1945; Sedar and Porter, 1955; reviewed in Satir, 1999).

The initial works in cilia biology found that protozoans deflagellate in the transient presence of acidic media. After recovery from pH shock, cells regenerate this organelle (Rosenbaum and Child, 1967). This *de novo* ciliary regeneration allowed for observation and analysis of ciliogenesis. After a short lag phase, cilia grow at a constantly decelerating rate until reaching full length (Rosenbaum and Child, 1967). This regeneration was not fully dependent on new protein synthesis as experiments with cycloheximide indicated the presence of a precursor pool in the cell body (Rosenbaum and Child, 1967). It was posited at this time that the ciliary growth zone was at the distal tip (Rosenbaum and Child, 1967). To further dissect the kinetics of ciliary regeneration, it was discovered that mechanical shearing of *Chlamydomonas* could amputate just one cilium; this technique generates cells with one growing cilium and one non-growing cilium (long-short cell) (Rosenbaum et al., 1969). The amputated cilium will elongate while simultaneously the intact cilium will slowly resorb (Rosenbaum et al., 1969). This usually continues until both cilia are of about equal length,

then they both elongate together to full length. In these long-short cells, the addition of colchicine, an inhibitor of microtubule synthesis, specifically inhibits elongation in the short regenerating cilium (Rosenbaum et al., 1969). This also work confirmed that precursors are preferentially incorporated into the growing tip region (Rosenbaum et al., 1969). Taken together, these works laid a solid foundation for investigating ciliary assembly.

1.5 Ciliary Tubulin

With the delineated kinetics of cilia regeneration, the accompanying precursor protein synthesis was explored. Deflagellation induces synthesis of ciliary proteins and specifically tubulin synthesis (Weeks and Collis 1976). At maximum, about 45 minutes post deflagellation, tubulin accounts for ~14% of total protein synthesis (Weeks and Collis 1976). After 180 minutes post deflagellation, only very low levels of tubulin synthesis was found (Weeks and Collis 1976). This work was expounded upon later with pulse-labeling experiments; radiography of whole cell protein identified with some certainty α- and β-tubulin (Lefebvre et al., 1978). This labeling remained high until cilia reached full length (Lefebvre et al., 1978). Collectively, these finding mimicked the deceletory kinetics of ciliary regeneration detailed in early works: a strong and robust burst of *de novo* tubulin synthesis occurs concomitantly with ciliary regeneration, then is greatly reduced as ciliary growth is complete.

Microtubules are intrinsically polar and have a plus-end and minus-end; this polarity is due to all α/β heterodimers have the same orientation with β-tubulin pointing to the plus-end (Allen and Borisy, 1974; Borisy, 1978; Summers

and Kirschner, 1979). β-tubulin hydrolyzes GTP after incorporation into the microtubules, creating a transient GTP cap on the plus end of growing microtubules. Microtubules grow faster at the plus end which is located at the distal tip of cilia (Allen and Borisy, 1974; Dentler et al., 1974; Euteneuer and McIntosh, 1981). With the previous findings implicating the ciliary distal tip as the growth zone, these data confirmed that the axoneme is oriented accordingly.

To examine tubulin during ciliogenesis, an HA-tagged tubulin was expressed in *Chlamydomonas* and the mating reaction was used to introduce the tagged-tubulin to wildtype cells while regenerating cilia (Johnson and Rosenbaum, 1992). Once in the shared cytoplasm of the quadriflagellate, the HA-tubulin had access to the growing cilia and immunofluorescence revealed incorporation was limited to the distal plus tip (Johnson and Rosenbaum, 1992). This approach confirmed that the site of tubulin addition during regeneration is at the tip, with immunogold labeling recapitulating these findings (Johnson and Rosenbaum, 1992). This distal incorporation of epitope tagged tubulin was dependent upon IFT; it was found that the plus end of ciliary microtubules undergoes turnover and that this turnover was strongly reduced in the absence of IFT (Marshall and Rosenbaum, 2001).

To investigate IFT and tubulin during ciliary assembly, a tagged tubulin isotype was expressed in *C. elegans* (Hao et al., 2011). Upon direct observation of this tagged tubulin, tagged IFT particles could be seen, but the tubulin could not be visualized (Hao et al., 2011). Photobleaching was then used in conjunction with post-acquisition analysis to reveal faint tubulin tracks, indicative

of tubulin transport by IFT (Hao et al., 2011). Specific dynamics were unable to be gathered via this experimental method.

Recently, *in vitro* work has identified a tubulin-binding module on the IFT particle (Bhogaraju et al., 2013). They found that the N-terminus of IFT81 recognizes the α/β tubulin heterodimer interface with high specificity and the basic N-terminus of IFT74 recognizes the acidic E-hook of β-tubulin to increase the affinity of the interaction by ~16x (Bhogaraju et al., 2013). This *in vitro* work implicates IFT74 and IFT81 may directly bind and transport tubulin in a living cell (Bhogaraju et al., 2013).

Poised on the work described here, the stage is set to investigate tubulin dynamics *in vivo* and how this is influenced during ciliary regeneration.

1.6 *Chlamydomonas* as a model

Chlamydomonas is a unicellular green algae found throughout the world. The defining features of *Chlamydomonas* include an overall polar structure with two 12 μm long motile cilia on the apical end of an ovoid cell body. The cell body is encased by a cell wall, and notably contains an eye spot for sensing light and a single cup-shaped chloroplast surrounding the nucleus. The two cilia emanate from anterior basal bodies and possess the 9 + 2 microtubular structure of the axoneme. Encased in the nucleus, *C. reinhardtii* has a sequenced haploid genome of ~120 Mbp (*Chlamydomonas Sourcebook*, 2009).

C. reinhardtii is easy and economical to culture. In a flask with minimal media, one can achieve approximate synchronous cultures by alternating light dark cycles. A liquid culture will expand via asexual division. In a 24-hour

period, each cell typically undergoes two to three mitotic divisions, giving rise to four to eight daughter cells respectively (*Chlamydomonas Sourcebook*, 2009). Quick culturing allows for a fast pace for experiments.

One major advantage to working with *Chlamydomonas* resides in the ability to deflagellate cells. Cells will deflagellate in the transient presence of acidic media and upon recovery, will regenerate their cilia in ~ one hour. This feature allows for observation of *de novo* cilia assembly. Further, the biochemical isolation of cilia can be easily achieved. One can mass deflagellate a culture and proceed to isolate cilia. Once a pure cilia sample is obtained, this can be fractionated into axonemes, membrane, and matrix. This allows for protein biochemisty via Western blot analysis or other methods including immunoprecipitations and mass spectrometry.

The mating cycle of *Chlamydomonas* can be exploited for complementation assays. Mating competency is induced upon nitrogen starvation (Sager and Granick, 1953). When gametes are mixed, they recognize one another via mating-type specific adhesion molecules on their cilia, and fuse cell bodies to form a zygote (Adair, 1985). A quadriflagellated zygote is formed; the zygote remains motile for approximately four to six hours, at which point the cilia resorb (*Chlamydomonas Sourcebook*, 2009). During this quadriflagellate stage, the zygote has a one cell body and two sets of biochemically distinct cilia from each parental gamete. If one parental strain (donor strain) expresses a fluorescently tagged ciliary protein, once a zygote with a shared cytoplasm is

formed, we can observe the tagged protein entering the initially fluorophore-free acceptor cilia.

Chlamydomonas is particularly well suited for Total Internal Reflection Fluorescence Microscopy (TIRFM). Only fluorophores in close proximity to the coverslip will be excited via this technique; fluorophores in the flagella will be exicted, while the cytoplasmic pool in the cell body is largely outside of the TIRF excitation field (Engel et al, 2009). Via this approach, we can see single fluorescently-tagged ciliary proteins moving *in vivo*.

Together with the expression of fluorescently tagged proteins, the points listed above make *C. reinhardtii* an ideal model to investigate ciliary tubulin.

1.7 Summary and Structure of Dissertation

Gaining knowledge on how cilia grow and are maintained is pivotal to advancing our understanding of this organelle in a normal cell biological context and, notably, in human disease. In investigating how a cilium is built and the involved protein logistics, we reveal unforeseen regulatory events and inherent complexity of cargo-IFT interactions. There is a growing, albeit inadequate, number of bona fide cargoes of IFT. By examining the most abundant protein in cilia, tubulin, we are poised to ascertain basic truths about how this transport system interacts with proteins.

In Chapter 2 of this dissertation we will describe how tubulin transport is regulated according to growth status and how this regulation is cilium-autonomous. We hypothesis that IFT functions as a tubulin pump to ensure the critical concentration of soluble tubulin is met for microtubule polymerization and

therefore axonemal elongation. In Chapter 3 of this dissertation, we investigate how the tubulin heterodimer interacts with IFT for robust transport. We generated a variety of mutants of the C-terminal E-hooks of α– and β– tubulin. This approach involves fluorescently-tagging E-hook mutants and examining transport via TIRFM. We demonstrate that E-hooks of α- and β- tubulin are not necessary for IFT transport. We posit diffusion is the major contributor of supplying unpolymerized soluble tubulin for axonemal incorporation. To conclude, Chapter 4 will discuss the implications of cargo regulation as shown in Chapter 2 with respect to models of ciliary growth. Our work herein provided the most direct and convincing argument that swayed the field to the current differential cargo loading model. Future directions for this work will then be discussed.

CHAPTER 2

TUBULIN TRANSPORT BY IFT IS UPREGULATED DURING CILIARY GROWTH BY A CILIUM-AUTONOMOUS MECHANISM[1]

[1] Craft, J.M., Harris, J.A., Hyman, S., Kner, P., Lechtreck, K.F. 2015 *The Journal of Cell Biology.* 208 (2)223-237. Reprinted here with permission of the publisher via Rockfeller University Press Copyright Policy: Original Author Reuse : Permission on file

2.1 Abstract

The assembly of the axoneme, the structural scaffold of cilia and flagella, requires translocation of a vast quantity of tubulin into the growing cilium, but the mechanisms that regulate the targeting, quantity, and timing of tubulin transport are largely unknown. In *Chlamydomonas*, GFP-tagged α-tubulin enters cilia as an intraflagellar transport (IFT) cargo and by diffusion. IFT-based transport of GFP-tubulin is elevated in growing cilia and IFT trains carry more tubulin. Cells possessing both nongrowing and growing cilia selectively target GFP-tubulin into the latter. The preferential delivery of tubulin boosts the concentration of soluble tubulin in the matrix of growing versus steady-state cilia. Cilia length mutants show abnormal kinetics of tubulin transport. We propose that cells regulate the extent of occupancy of IFT trains by tubulin cargoes. During ciliary growth, IFT concentrates soluble tubulin in cilia and thereby promotes elongation of the axonemal microtubules.

2.2 Introduction

Microtubules, polymers of α- and β-tubulin dimers, are the major structural element of motile and nonmotile cilia and flagella (Borisy and Taylor, 1967). Microtubules form the scaffold onto which other axonemal structures such as dynein arms and radial spokes are attached; they also serve as tracks for intraflagellar transport (IFT), a bidirectional motility which is required for ciliary assembly (Kozminski et al., 1993, 1995). During ciliary growth, large amounts of tubulin dimers need to be transported into the organelle. Like cytoplasmic microtubules, the axonemal microtubules grow through the addition

of tubulin subunits to the distal plus-ends (Witman, 1975; Euteneuer and McIntosh, 1981; Johnson and Rosenbaum, 1992). Thus, the delivery of tubulin into cilia and its translocation to the ciliary tip are prerequisites for ciliary assembly. Several lines of evidence suggest that inside cilia, tubulin is transported by IFT. In the conditional *Chlamydomonas fla10-1* mutant, the incorporation of epitope-tagged tubulin at the distal end of cilia is decreased after a shutdown of IFT (Marshall and Rosenbaum, 2001). In vitro, tubulin dimers directly interact with a tubulin-binding module formed by the IFT particle proteins IFT74 and IFT81 (Bhogaraju et al., 2013). Expression of fluorescent tubulin in *Caenorhabditis elegans* revealed weak tracks, possibly representing tubulin transport in sensory cilia, and FRAP analysis supported the notion that tubulin transport is IFT-dependent (Hao et al., 2011). It remains largely unknown how tubulin transport is coordinated with ciliary growth. Insufficient delivery of tubulin could result in slower growth and shorter cilia, whereas an excess of tubulin might promote the assembly of excessively long cilia. Defects in ciliary length impair the motile and sensory functions of cilia and have been linked to ciliary diseases (Mahjoub et al., 2005; Tammachote et al., 2009; Ko et al., 2010; Özgül et al., 2011; Mahjoub and Stearns, 2012; Tam et al., 2013). In the unicellular alga *Chlamydomonas reinhardtii*, IFT and protein transport inside cilia can be imaged with single particle sensitivity using total internal reflection fluorescence (TIRF) microscopy (Lechtreck, 2013; Wren et al., 2013). Recently, stable expression of a fluorescent protein-tagged α-tubulin was accomplished in *C. reinhardtii* (Rasala et al., 2013). Ciliogenesis can be experimentally induced by

removing the existing cilia (Rosenbaum et al., 1969), allowing for an in-depth study of the relationship between tubulin transport and ciliary growth using direct imaging. A genetic analysis of the regulation of tubulin transport is aided by numerous *C. reinhardtii* mutants with defects in ciliary assembly and length control. Here, using two-color imaging, we show that GFP–α-tubulin is primarily transported by IFT but some GFP-tubulin also enters cilia by diffusion. The frequency of tubulin transport events by anterograde IFT was greatly increased during ciliary growth. We find that *C. reinhardtii* cells possess the ability to preferentially direct IFT-bound tubulin into growing cilia, indicating that tubulin transport is regulated in a cilium-autonomous manner. Dysregulation of tubulin transport was observed in the cilia length mutants *short flagella2* and *long flagella2-1*, indicating a possible link between the ciliary length regulation and tubulin transport by IFT. During ciliary growth, the concentration of soluble tubulin in the ciliary matrix was elevated substantially above that of steady-state cilia. We propose a model in which cells use IFT to regulate the concentration of soluble tubulin inside cilia; a high concentration of tubulin in the matrix will promote microtubule polymerization and ciliary growth.

2.3 GFP-tagged and endogenous α-tubulin have similar properties

To express GFP–α-tubulin in *C. reinhardtii* for imaging in vivo, we used the recently described fusion construct consisting of the zeocin resistance gene *BLE* and the *TUA2* gene separated by the viral 2A sequence encoding a self-cleaving peptide and replaced the original mCerulean with the brighter superfolder GFP (hereafter referred to as GFP; Rasala et al., 2013). *In vivo*

microscopy revealed the presence of GFP–α-tubulin in cilia and cell body microtubules (Fig. 1 A; Rasala et al., 2013). Western blotting of whole cells with anti-GFP identified a major ~78 kD and a minor ~104 kD band that were both also recognized by anti–α-tubulin (Fig. 1 B). The former represents GFP–α-tubulin; the latter, largely excluded from cilia (Fig. 1 B), is the uncleaved ble-GFP–α-tubulin fusion protein. The expression levels of GFP–α-tubulin varied between individual transformants. In the strain GFP-Tub1, which was used in most experiments, GFP–α-tubulin amounted to ~15% of the endogenous α-tubulin (Fig. 1 B). To determine the distribution of GFP-tagged and endogenous α-tubulin, cells were fractionated and analyzed by Western blotting (Fig. 1, B–D). Staining with anti–α-tubulin revealed that ~80% of endogenous tubulin resides in the cell body and ~20% enters the cilia; a similar partition was observed for GFP–α-tubulin with ~90% in the cell body and ~10% in cilia (Fig. 1, C and F). Inside steady-state cilia, both tagged and endogenous tubulin showed a similar distribution with ~90% incorporated into the axoneme and <10% remaining soluble in the membrane+matrix fraction (MM fraction; Fig. 1, D and G). Immunoprecipitation using anti-GFP beads revealed that GFP–α-tubulin forms a complex with endogenous β-tubulin in the ciliary matrix (Fig. S1, A and B). Axonemal tubulin is known to undergo numerous posttranslational modifications (PTMs; Gaertig and Wloga, 2008). Western blots of fractionated cilia probed with PTM-specific antibodies showed that GFP–α-tubulin undergoes K40 acetylation and polyglutamylation, especially in the axoneme (Fig. 1 E and Fig. S1 C). In

summary, GFP–α-tubulin behaves largely similar to the endogenous protein, validating its use as a reporter of tubulin transport.

2.4 Tubulin enters cilia by IFT and diffusion

Tubulin is a cargo of IFT. To image GFP–α-tubulin during transport, cilia were first photobleached to eliminate the signal resulting from the presence of GFP–α-tubulin in the axonemes and then analyzed by TIRF microscopy. Kymograms (time-space plots) showed individual GFP–α-tubulin particles diffusing inside cilia or undergoing active transport with constant velocities indicative for IFT (Fig. 2 A). Anterograde transport progressed at 1.68 μm/s (±0.21 μm/s; *n* = 1,404 particles) and occurred with a frequency of 0.3 particles/min in steady-state cilia (± 0.7 particles/min, *n* = 78 cilia); retrograde transport events were rarely observed and had a velocity of 3.05 μm/s (±1.1 μm/s, *n* = 35; Fig. 2 A, a and b). IFT moved the majority of GFP–α-tubulin particles directly from the ciliary base to the tip (98% of 1,281 particles; Fig. 2 B, a); transitions of GFP–α-tubulin from IFT to diffusion indicative of unloading along the ciliary shaft were observed as well (Fig. S2, C and D). To test directly if tubulin moves in association with IFT trains, GFP–α-tubulin was expressed in an *ift20-1*IFT20-mCherry strain (Fig. S3 B). Two-color imaging showed comigration of the tagged tubulin and IFT20-mCherry indicating that tubulin is a bona fide cargo of IFT (Fig. 2 B).

Recent data revealed that the acidic C-terminal domain (E-hook) of β-tubulin but not that of α-tubulin is required for the *in vitro* interaction between tubulin dimers and IFT74–IFT81 complexes (Bhogaraju et al., 2013). We

designed modified GFP–α-tubulins in which the E-hook was replaced with the corresponding region of β-tubulin, altered to substitute seven glutamate residues with alanine or glutamine, or removed entirely (Table S1). The altered α-tubulin molecules were expressed (as ~5–15% of the endogenous α-tubulin; Fig. S3 A), transported by IFT, and incorporated into the axoneme (Table S1). Thus, our in vivo observations agree with the earlier in vitro study showing that the C-terminal E-hook of α-tubulin is dispensable for tubulin binding to IFT trains. The modified tubulins were expressed in the presence of endogenous wild-type tubulin indicating that *C. reinhardtii* tolerates some E-hook–deficient GFP–α-tubulins; a deletion of the E-hook from all of either α- or β-tubulin is lethal in *Tetrahymena* (Duan and Gorovsky, 2002).

Tubulin enters cilia by diffusion. To improve imaging of diffusing tubulin, photobleached cilia were observed at elevated laser intensities which quickly bleached most GFP preventing crowding of the cilia with fluorescent α-tubulin. For some experiments, superfolder GFP was replaced with the brighter mNeonGreen (Shaner et al., 2013). 64 individual GFP–α-tubulin particles were tracked while diffusing inside the ciliary shaft and the mean of the square displacement was determined in 30 subsequent frames (Fig. 2 C). This resulted in a 1D diffusion coefficient of 1.76 ± 0.18 $\mu m^2/s$ for GFP–α-tubulin, a value similar to that determined for similarly sized soluble proteins diffusing in cilia (Lin et al., 2013). In agreement with this high mobility of GFP–α-tubulin, we observed “jumps” over almost the entire length of a cilium (Fig. 2 A, d; and Fig. S2, A, E, and I). In the vicinity of the ciliary tip, GFP-tagged tubulin mostly displayed a

reduced mobility as reflected by a diffusion coefficient of ~0.18 ± 0.02 $\mu m^2/s$ (*n* = 58 trajectories; Fig. 2 A, d; Fig. S2, A, C, D, and F, white arrowheads). The reduced mobility of GFP-tubulin in the distal ~0.5-μm ciliary segment could result, for example, from interactions with other proteins. Infrequently, GFP–α-tubulin diffusing near the tip of steady-state cilia was observed becoming stationary, which is indicative of incorporation into the axoneme (Fig. S2, F–H).

Although IFT-based transport of tubulin was rare in steadystate cilia, diffusing GFP-tubulin continuously entered fully photobleached cilia from the base (Fig. 2 A, c; Fig. S2 I). To test whether active IFT is required for the diffusional entry of tubulin into cilia, we expressed GFP–α-tubulin in the *C. reinhardtii fla10-1* mutant; IFT can be switched-off in this strain by incubating the cells at 32°C for several hours (Kozminski et al., 1995). IFT of GFP–α-tubulin was observed in *fla10-1* and wildtype steady-state cilia at the permissive temperature albeit at low frequencies (Fig. 2, D, a, and E). Cycloheximide (CHX) limits ciliary regeneration to half-length and we previously observed elevated transport of the axonemal protein DRC4 in such cilia (Wren et al., 2013). Similarly, an increased frequency of tubulin transport was observed in half-length cilia assembled by control or *fla10-1* in the presence of CHX at the permissive temperature (Fig. 2 E). After shifting such cells to 32°C for 180 min, IFT-like movements of GFP–α-tubulin were frequent in cilia of control cells but were not observed in the *fla10-1* cells; entry of GFP–α-tubulin by diffusion, however, continued (Fig. 2, D, b, and E). A strain expressing IFT20-mCherry in the *fla10-1 ift20-1*background was used to verify that IFT was indeed abolished at the

conditions used (Fig. 2 D, c and d). The data indicate that GFP–α-tubulin enters cilia by diffusion.

2.5 The frequency of tubulin transport by IFT is regulated by the assembly status of cilia

To determine whether IFT transports more tubulin when cilia grow, we compared the transport frequencies of GFP–α-tubulin between steady-state and growing cilia. After amputation of cilia by a pH shock, cells regenerate full-length cilia within ~90 min. Partially regenerated cilia were bleached and tubulin influx and incorporation into the cilia were analyzed (Fig. 3 A). Fluorescent tubulin was rapidly added to the tip and the fluorescent distal parts of cilia lengthened, revealing that cilia continue to grow under TIRF illumination while immobilized in the observation chamber (Fig. 3 B). In growing cilia (~3–10 μm in length), GFP–α-tubulin moved by anterograde IFT with a greatly elevated mean frequency of 18.3 ± 6.9 particles/min (*n* = 110 cilia) versus ~0.3 particles/min observed in steady-state cilia of the same strain (Fig. 3 C). The transport frequency of GFP–α-tubulin remained elevated until cilia reached ~10 μm in length and was then reduced to 1 ± 2.2 particles/min in cilia of 10–12 μm in length (*n* = 49 cilia) before returning to the pre-deciliation level (~0.3 ± 0.75 particles/min, *n* = 80 cilia at >2 h after pH shock; Fig. 3, C and D). The pattern indicates a strong length dependency of IFT-based tubulin transport and matches the deceleratory kinetics of cilia regeneration in *C. reinhardtii* with rapid elongation until cilia reach ~10 μm, followed by slower growth until cilia reach their final length of ~12 μm

(Rosenbaum et al., 1969; Engel et al., 2009). In summary, tubulin transport by anterograde IFT is up-regulated during ciliary growth.

2.6 IFT particles carry more tubulin during ciliary growth

The observed increase in the transport of tubulin in growing cilia could be caused by an increase in the amount of tubulin carried by a given number of IFT trains or by an increase in the number of IFT trains without changing the tubulin load per train. In *C. reinhardtii*, similar amounts of IFT material are thought to be present in cilia regardless of their length (Marshall et al., 2005; Engel et al., 2009). Two-color imaging was used to determine the share of IFT particles participating in GFP-tubulin transport in regenerating and steady-state cilia (Fig. 3, E–G). Photobleaching of the entire cilia using increased 488-nm laser intensity also greatly diminished the signal from IFT20-mCherry making quantitative analyses unreliable. We therefore used a brief, focused laser beam in epifluorescence (~3 µm diameter; ~100–300 ms in duration) to bleach a ciliary segment and imaged the cilia in TIRF as particles reentered the bleached area (Fig. 3, E and F). IFT occupancy, i.e., the share of IFT20-mCherry–tagged anterograde IFT trains carrying GFP–α-tubulin, decreased from ~80% during the initial rapid growth to ~10% as cilia approached full length and even lower rates in fully regenerated and steady-state cilia (means were 45 ± 21% vs. 4.5 ±3.5%, respectively; P = 2.2 × 10^8; Fig. 3 G). As previously shown, the IFT frequency was largely independent of ciliary length (Fig. S4 A; Dentler, 2005; Engel et al., 2009). In conclusion, IFT trains in regenerating cilia carry a larger load of tubulin than those in nongrowing cilia.

2.7 Cilium-autonomous regulation of tubulin transport by IFT

How do cells regulate the loading of cargo onto IFT particles? To begin addressing this question, we tested whether tubulin transport is regulated at the cilium or cell level. After shearing of just one of the two cilia, cells will partially resorb the remaining cilium while regrowing the missing one giving so-called longshort cells (Fig. 4 A and see Fig. 6 E; Rosenbaum et al., 1969). An elevated tubulin transport in both cilia of a long-short cell would indicate a cell-wide regulation, whereas an increase limited to the growing cilium would indicate a regulation that operates at the single cilium level. The mean GFP–α-tubulin IFT frequencies were 20.5 particles/min for the short and 3.3 particles/min for the long cilia of long-short cells (*n* = 17; ±11.6 and 3.2 particles/min, respectively; Fig. 4, B and C). In all longshort cells analyzed, the transport frequency in the short cilium exceeded that of the long one; this difference decreased as both cilia approached a similar length (Fig. 4 D).

As an alternative approach that does not require mechanical shearing, we generated long-short cells by mating GFP–α-tubulin–expressing gametes with full-length cilia to wild-type gametes that were deciliated by a pH shock and regenerating cilia (Fig. 5, A and B, a and b). The resulting zygotes, initially possessing two long GFP-positive and two short GFP-negative cilia, will equalize the length of all four cilia by partially resorbing the long ones and adding new tubulin to the short ones (Fig. 5 B, c–g; Ludington et al., 2012). Tubulin transport in all four cilia of such zygotes was analyzed after photobleaching (Fig. 5 C). The frequency of tubulin transport by anterograde IFT in the short growing cilia

surpassed that of the nongrowing long cilia (Fig. 5 D). As the four cilia approached equal length, the transport frequency in the initially long cilia increased, whereas that in the initially short ones decreased (Fig. S4 D). Based on the study of long-short cells, we conclude that the frequency of IFT-based tubulin transport events is controlled cilium-autonomously.

2.8 The concentration of soluble tubulin is increased in growing cilia

In steady-state cilia, ~10% of the total tubulin was in the detergent soluble MM fraction (Fig. 1 D). The elongation of microtubules depends, among other factors, on the availability of α/β-tubulin dimers (Desai and Mitchison, 1997; Howard, 2001). Western blotting and FRAP analysis were used to test whether steady-state and growing cilia differ in the concentration of soluble tubulin. Steady-state, growing, and fully regenerated cilia were separated into axonemal and MM fractions; loading was adjusted to represent equal volumes of MM (Fig. 6 A). Western blots revealed that the amount of soluble tubulin was doubled from ~10 to 20% of the total ciliary tubulin in growing versus nongrowing flagella (Fig. 6 A; for quantification see Fig. S4, B and C).

For FRAP analysis, ciliary segments were spot bleached. An exchange of axonemal tubulin with GFP–α-tubulin laterally along the ciliary shaft was not observed in this study. Thus, axonemal GFP–α-tubulin will remain bleached. Soluble, unbleached GFP–α-tubulin from other ciliary segments or de novo imported from the cell body will move into the bleached region, and fluorescence recovery reflects the concentration of mobile GFP-tubulin in the cilium (Fig. 6 B). FRAP analysis showed recovery rates of 2 ± 1% of the pre-bleach fluorescence

for nongrowing cilia (*n* = 16), whereas ~15.6 ± 10% of the signal intensity recovered in growing cilia (*n* = 18; Fig. 6, C and D). In growing cilia, GFP-tubulin moving on IFT trains through the bleached region contributes to the recovery, but over time the diffused background staining significantly increased, indicating an increase in the concentration of GFP-tubulin diffusing inside cilia (Figs. 3 F, 6 F, and S5 B). Repeated bleaching of the same ciliary segment was followed by a recovery of similar strength (~5% for steady-state and ~15% for growing cilia; Fig. S5), indicative of an ongoing de novo import of GFP–α-tubulin into cilia.

An increase in the concentration of soluble tubulin in cilia could result from an increase in soluble tubulin in the cell body of regenerating cells. FRAP of long-short cells, however, showed that recovery was significantly stronger in the short cilium than in the long one (39 ± 10% vs. 4.3 ± 3%; Fig. 6, E–H; Fig. S5, C and D). Thus, distinct concentrations of soluble tubulin can be established in the two cilia of the same cell. We conclude that the concentration of soluble tubulin is elevated in growing cilia. A high concentration of tubulin in the ciliary matrix is likely to promote elongation of the axonemal microtubules.

2.9 Defective regulation of tubulin transport in ciliary length mutants

Because microtubules are the major structural elements of cilia, defective regulation of tubulin transport could affect ciliary length. We expressed GFP–α-tubulin in *lf2-1* (*long flagella2*) and *shf2* (*short flagella2*) mutants and selected transformants expressing similar amounts of GFP-tubulin as the control strain GFP-Tub1 (Fig. S3 C). *lf2-1* has cilia of variable length with some 2–3× longer than wild type, whereas cilia reach only 6–8 μm in *shf2*. *LF2* encodes a CDK-like

kinase, whereas the molecular defect in *shf2* is unknown (Kuchka and Jarvik, 1987; Tam et al., 2007). In steady-state *lf2-1* cilia, the mean frequency of GFP–α-tubulin transport was higher than in steady-state wild-type cilia; a length dependent decrease in frequency was not observed (Fig. 7 A). Cilia regeneration in *lf2-1* was slow and irregular in onset with many cells failing to reassemble cilia (Barsel et al., 1988). In the *lf2-1* cells that regenerated cilia, the frequency of tubulin transport was somewhat higher but showed a similar lack of length dependency. The frequency of IFT was slightly reduced in *lf2-1* (unpublished data). *lf2-1* cells apparently fail to properly regulate the IFT-based transport of tubulin in response to changes in ciliary length.

In steady-state cilia of *shf2*, the frequency of tubulin transport decreased with increasing ciliary length and tubulin transport was rarely observed in *shf2* cilia longer than ~6 μm, a length at which wild-type cilia showed robust trafficking of tubulin (Figs. 7 A and 3 D). IFT (based on DIC microscopy) appeared normal in the longer *shf2* cilia (unpublished data). Many *shf2* cells failed to regenerate cilia but the regrowth kinetics was largely normal in those that did (Kuchka and Jarvik, 1987). Regenerating *shf2* cilia showed a similar steep down-regulation of tubulin transport frequency with increasing ciliary length as described for *shf2* in steady-state. The data suggest that *shf2*, although able to increase tubulin transport frequency in short regenerating cilia, prematurely down-regulates tubulin transport by IFT. The data show that an abnormal regulation of tubulin transport occurs in mutants with defects in ciliary length regulation.

2.10 Discussion

IFT functions as a tubulin transporter. Ciliary assembly requires a massive translocation of tubulin from the cell body into the growing organelle. In *C. reinhardtii*, almost 800,000 tubulin dimers, corresponding to ~20% of the cell's total tubulin, are required to assemble its two 12-µm-long 9+2 cilia (Bhogaraju et al., 2014b; see Materials and methods). IFT is essential for the assembly of cilia and flagella in most eukaryotes and thought to be the major pathway of protein transport in cilia (Rosenbaum and Witman, 2002). Recent data, however, have shown that numerous proteins move into cilia in an IFT-independent manner. Ectopic cytosolic proteins up to a size of ~50 kD enter cilia by passive diffusion; even proteins up to ~650 kD appear to diffuse slowly into cilia (Kee et al., 2012; Breslow et al., 2013; Lin et al., 2013). In *C. reinhardtii*, the transmembrane protein SAG1 and the membrane-associated phospholipase D will enter cilia in the absence of IFT (Belzile et al., 2013; Lechtreck et al., 2013A). Furthermore, certain transmembrane proteins (SSTR3, Smo) diffuse inside the ciliary membrane while associating only transiently—if ever—with IFT (Ye et al., 2013). These findings raised the question which proteins are the actual cargoes of IFT. Several TRP channels were reported to move by IFT and the BBSome cycles through cilia by associating to IFT trains (Blacque et al., 2004; Qin et al., 2004; Huang et al., 2007; Lechtreck et al., 2009). Also, IFT powers gliding and ciliary surface motility in *C. reinhardtii* presumably due to its interaction with the ciliary transmembrane protein FMG-1B (Collingridge et al., 2013; Shih et al., 2013). We recently showed that the axonemal proteins PF16, DRC2, and DRC4 are

cargoes of IFT and that entry of DRC4-GFP into cilia is largely diminished in the absence of IFT (Wren et al., 2013). Defects in the IFT complex B protein IFT46 and or its interacting partner ODA16p largely prevent the transport of outer arm dynein to its ciliary docking sites (Hou et al., 2007; Ahmed et al., 2008). Thus, IFT plays a role in the transport of axonemal proteins, several of which are transported in large complexes feasibly rendering transport by diffusion inefficient. Several studies provided evidence that tubulin is a cargo of IFT but direct imaging of tubulin transport by IFT and the quantification of such events has been challenging (Marshall and Rosenbaum, 2001; Hao et al., 2011; Bhogaraju et al., 2013; Brust-Mascher et al., 2013). Here, we show that GFP-tagged tubulin moves in association with IFT particles inside cilia indicating that IFT functions as tubulin transporter.

Cilium-autonomous regulation of tubulin transport by IFT. In growing cilia, the frequency of GFP-tubulin transport by IFT was greatly elevated. Taking into account that only a fraction of the total tubulin in cilia was tagged, extrapolation of the data indicates that IFT trains in growing cilia carry a larger tubulin load than those in steady-state cilia. Previously, we showed that the IFT-based transport of the axonemal protein DRC4 is strongly increased during ciliary growth (Wren et al., 2013). It is likely that the transport of many other ciliary proteins is also enhanced when cilia elongate. Although some differences in the velocity, size, and frequency of IFT in growing vs. steady-state cilia of *C. reinhardtii* have been reported, the number of IFT particles inside cilia is largely length-independent (Dentler, 2005; Marshall et al., 2005; Engel et al., 2009). In

conclusion, IFT trains are highly loaded with cargo during ciliary growth; then, the number and velocity of IFT trains might limit the rate of ciliary elongation. Indeed, the 60% reduction in IFT frequency observed in the IFT kinesin mutant *fla3-1* results in sluggish regrowth of nearly full-length cilia (Mueller et al., 2005). In steady-state cilia, IFT particles carry less cargo probably running well below capacity. This would allow the cells to quickly adjust ciliary protein content and length in response to developmental or environmental cues by altering cargo loading of IFT (Wren et al., 2013).

Currently, it is unknown how the amount of cargo transported by IFT into cilia is regulated. In a simple model, an increase in the concentration of soluble tubulin in the cell body would make more tubulin available as cargo for IFT and promote tubulin transport into cilia (Chan and Marshall, 2012; Goehring and Hyman, 2012). Indeed, primary cilia elongate when the level of soluble cytoplasmic tubulin is increased by drug-induced microtubule depolymerization (Sharma et al., 2011). During ciliary growth, kinesin-13 may depolymerize cell body microtubules in *C. reinhardtii* to provide tubulin for axonemal assembly (Wang et al., 2013). Remarkably, in cells possessing growing and nongrowing cilia, the frequency of IFT-based GFP-tubulin transport was strongly elevated in the growing over the nongrowing cilia. We conclude that a general increase in tubulin supply in the cell body is insufficient to explain the increase in IFT-based tubulin transport just into growing cilia of long-short cells. Our data suggest that tubulin import into cilia is regulated locally within the basal body–cilium entity. An increase in admission of tubulin to the cilium could involve a change in the

transition zone (TZ), located between the basal body and the cilium proper. TZ proteins are hotspots for ciliopathy related mutations which alter the protein composition of cilia, and the TZ is thought to function as a ciliary gate regulating protein entry into the organelle (Craige et al., 2010; Omran, 2010; Williams et al., 2011; Kee and Verhey, 2013). The TZ could respond to changes in the ciliary length by permitting IFT particles carrying a large load into growing cilia while preventing such particles from entering steady-state cilia. Such a model of size-based exclusion of IFT trains at the TZ would require the constant presence of both loaded and unloaded IFT particles. The share of IFT trains occupied with GFP-tubulin in nongrowing and growing cilia ranges from <10 to ~80%, rendering this model unlikely.

Alternatively, cargo loading onto IFT particles could be regulated. Dikaryon experiments showed that IFT proteins from distinct basal body–cilia units mix rapidly (Wren et al., 2013). Therefore, an increase in cargo loading onto IFT must happen locally at the base of a growing cilium, for example, by increasing the affinity of IFT carriers for cargo proteins. In C. *reinhardtii*, IFT particle and motor proteins are concentrated at the transitional fibers, which are located proximal to the TZ (Deane et al., 2001). The transitional fibers could increase the local concentration of IFT and cargoes and thereby promote the formation of IFT–cargo complexes. The anterograde IFT motor subunit KAP is more abundant at the base of growing cilia (Ludington et al., 2013), which might suggest that transitional fibers at the base of growing cilia have a higher capacity to bind IFT material. We propose a model in which cells measure the length of

their cilia; cilia of insufficient length generate a signal that alters the property of the ciliary base, resulting in an increased loading of IFT particles and/or facilitated admission of highly loaded IFT trains into the cilium, which will augment the amount of tubulin transported into the cilium in need (Fig. 7 B).

Ciliary length defects are associated with dysregulation of tubulin transport. Sensing of ciliary length is likely to involve various protein kinases whose mutations lead to length defects (Berman et al., 2003; Tam et al., 2007; Lefebvre, 2009; Cao et al., 2013; Tam et al., 2013). LF2p, for example, is a CDK kinase which, together with LF1p and LF3p, forms the length regulating complex (LRC; Tam et al., 2007). LF2p homologues are also involved in ciliary length control in mammals and *C. elegans* (Ko et al., 2010; Phirke et al., 2011). In *lf2-1*, the frequency of tubulin transport was largely independent of ciliary length and remained elevated in *lf2-1* cilia that were longer than wild-type cilia. A failure to adjust tubulin transport with respect to ciliary length could explain the phenotype of *lf2-1* characterized by slow regeneration kinetics, and variable ciliary length with some abnormally long cilia (Barsel et al., 1988). The LRC is located in the cell body of *C. reinhardtii*, but its molecular role is unknown (Tam et al., 2007). Based on its localization, the LRC could function in adjusting IFT-based tubulin transport in response to signals from the ciliary length sensor.

Shorter-than-normal cilia could result from a failure to incorporate precursors into the cilium, an increased disassembly rate, or an insufficient delivery of precursors. The latter was observed in the short flagella mutant *shf2*. Tubulin transport was down-regulated well before cilia reached wild-type length.

The phosphorylation pattern of the aurora-like kinase CALK can be used as an indicator of the assembly state of cilia. At the onset of ciliary growth, phosphorylation and dephosphorylation occur at distinct sites, followed by a gradual return to a pattern characteristic for full-length steady-state cilia (Luo et al., 2011; Cao et al., 2013). *shf2* displays a CALK phosphorylation state typical for short, growing cilia (Luo et al., 2011; Cao et al., 2013). This suggests that *shf2* cells still sense the insufficient length of their cilia but fail to respond appropriately by maintaining a high tubulin influx via IFT.

In our study, we did not address the question of why the longer cilia of long-short cells retract. In those long cilia, tubulin transport via IFT—although well below that of short cilia—was actually somewhat above the steady-state levels (Fig. 4 C). Also, the breakdown of the axoneme is likely to increase the levels of soluble tubulin inside the shortening long cilia. Thus, ciliary shortening appears not to be driven by a shortage of tubulin, suggesting that the intraciliary tubulin concentration is not the sole factor regulating ciliary growth. We posit that the resorption involves an up-regulation of the cilia disassembly pathway in the long cilia. Putative players in the disassembly pathway are microtubule-destabilizing proteins such as kinesin-13 and CNK2. Mutants in the latter assemble the missing cilium of long-zero cells at normal rates but fail to resorb the remaining long cilium, supporting the notion that ciliary assembly and disassembly in long-short cells are distinctly regulated (Hilton et al., 2013).

IFT promotes ciliary growth by concentrating tubulin. GFP-tubulin enters cilia by both diffusion and IFT, raising the question of the respective roles

in supplying tubulin for ciliary assembly. Tubulin dimers (110 kD) are above the predicted size exclusion limit of ~50 kD for free diffusion of soluble protein into the cilium (Kee et al., 2012; Breslow et al., 2013). Distinct concentrations of soluble tubulin were observed in cilia of a given cell, indicating the absence of diffusive equilibration. We estimate (see Materials and methods) that the concentration of soluble tubulin in the ciliary matrix of growing cilia is higher than that in the cytoplasm; the absence of a cell body–to–cilia gradient in tubulin concentration rules out a net influx of tubulin into cilia by diffusion. In *fla10-1*, GFP-tubulin continued to enter cilia by diffusion in the absence of IFT but the cilia do not elongate. Similarly, ciliary elongation ceased in *shf2* after IFT of GFP-tubulin was down-regulated despite the continued entry of GFP-tubulin by diffusion. We conclude that the entry of tubulin into cilia by diffusion is insufficient to provide enough tubulin to promote ciliary growth.

Tubulin concentration has a strong impact on microtubule growth in vitro and in vivo, with high concentrations of tubulin suppressing catastrophe frequency and increasing the polymerization rate (Pedigo and Williams, 2002). In the cytoplasm, proteins such as XMAP215 act as microtubule polymerases at MT plus ends putatively by increasing the local tubulin dimer concentration (Al-Bassam and Chang, 2011). Messages of specific tubulin isoforms are recruited to microtubule plus-ends in the axonal growth cone to locally increase tubulin expression (Preitner et al., 2014). In growing cilia, large amounts of tubulin released from IFT into the cilium will increase the concentration of soluble tubulin in the matrix. We noticed a reduced mobility of tubulin in the vicinity of the ciliary

tip, which could result from tubulin interactions with other proteins; IFT proteins, for example, are typically accumulated at the ciliary tip and possess tubulin binding motifs (Bhogaraju et al., 2014b). Further, GFP-tubulin was predominately released from IFT near the ciliary tip; reduced mobility and preferred unloading could further increase the tubulin concentration locally at the tip.

We predict that the concentration of soluble tubulin in the matrix of growing cilia is in the range of 300 μM (see Materials and methods). Although some of the tubulin is sequestered onto IFT, the concentration is well above the concentrations (~20 μM) required for microtubule assembly in vitro or in the cytoplasm. *C. reinhardtii* cilia elongate at ~350 nm/min compared with 20–60 μm/min observed for microtubules in the cytoplasm (Srayko et al., 2005). However, during axonemal assembly, nine doublet microtubules and two singlet microtubules are assembled simultaneously within the comparably small volume of the cilium. About 2,500 dimers are required to elongate a singlet microtubule by 20 μm, whereas the assembly of 350 nm of 9+2 microtubules consumes ~10,000 dimers. We estimate ~18,000 dimers to be present in the matrix of a 4-μm-long cilium (see Materials and methods). Thus, soluble tubulin in the ciliary matrix will be rapidly consumed during ciliary growth and the matrix pool must be equally rapidly replenished to ensure continued elongation of the axoneme. A unifying feature of most cilia is doublet microtubules, the assembly of which has not yet been reconstituted in vitro and could require very high concentrations of tubulin dimers. In summary, due to its architecture and its position within the small volume of the cilium, axonemal assembly could require exceptionally high

concentrations of soluble tubulin. Several IFT complex B proteins contain tubulin-binding motifs—confirmed and predicted—and estimates suggest that IFT has the capacity to transport tubulin in amounts required during ciliary assembly (Bhogaraju et al., 2014). Although additional factors are likely involved in determining the rate of ciliary elongation (most notably the rate of axoneme depolymerization), tubulin transport by IFT and the resulting high concentration of tubulin in the ciliary matrix are likely prerequisites for the rapid elongation of axonemal microtubules. We propose that IFT functions as a tubulin pump to increase the concentration of tubulin inside growing cilia. Higher tubulin concentrations will promote the growth of the axonemal microtubules and thereby elongation of the cilium.

2.11 Figures

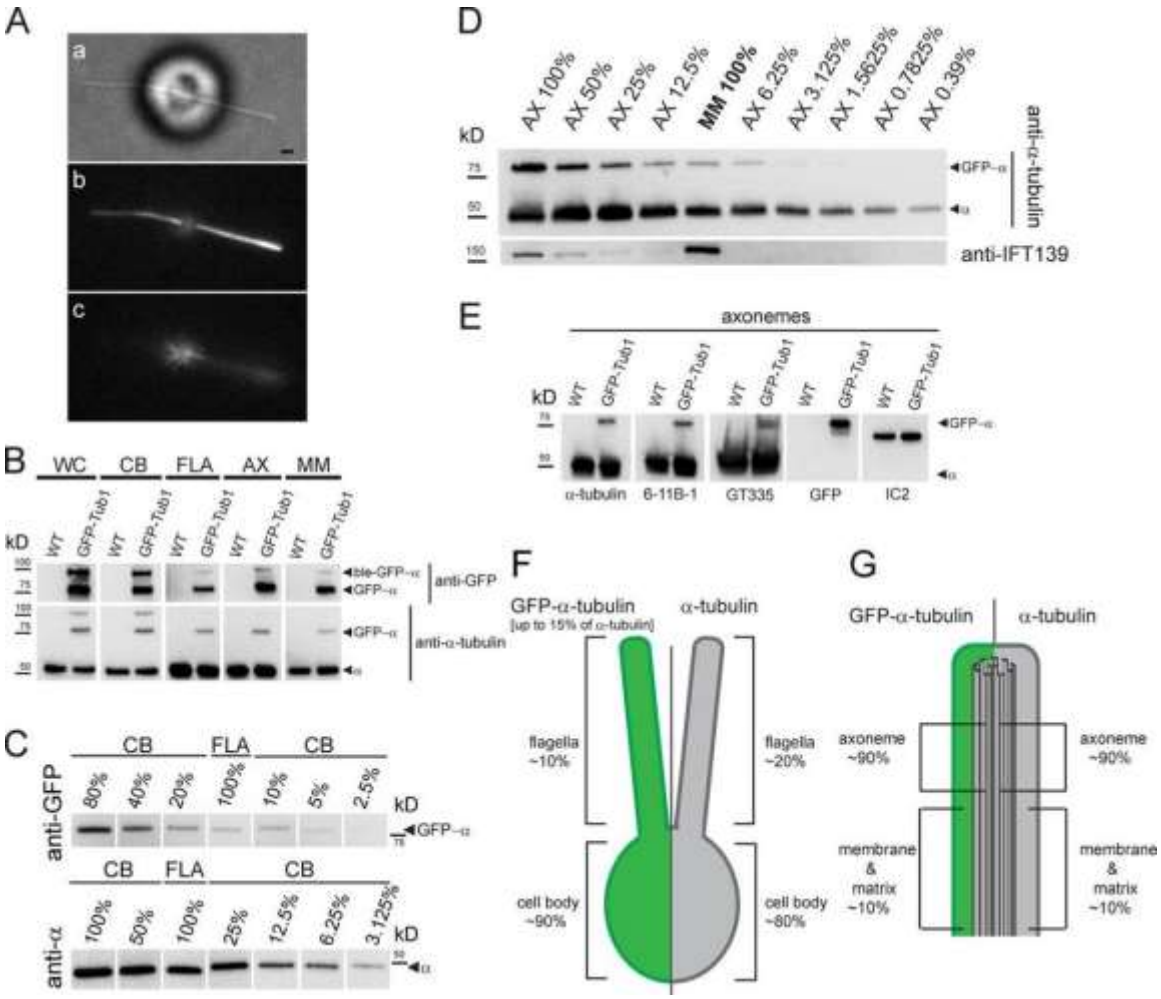
A
a
b
c
D
AX 100%
AX 50%
AX 25%
AX 12.5%
MM 100%
AX 6.25%
AX 3.125%
AX 1.5625%
AX 0.7825%
AX 0.39%
kD
75
50
150
GFP-α
α
anti-α-tubulin
anti-IFT139
E
axonemes
kD
WT
GFP-Tub1
GFP-α
α
α-tubulin
6-11B-1
GT335
GFP
IC2
B
WC
CB
FLA
AX
MM
kD
ble-GFP-α
GFP-α
anti-GFP
anti-α-tubulin
C
CB
FLA
CB
anti-GFP
80%
40%
20%
100%
10%
5%
2.5%
kD
GFP-α
CB
FLA
CB
anti-α
100%
50%
100%
25%
12.5%
6.25%
3.125%
kD
α
F
GFP-α-tubulin
[up to 15% of α-tubulin]
α-tubulin
flagella
~10%
flagella
~20%
cell body
~90%
cell body
~80%
G
GFP-α-tubulin
α-tubulin
axoneme
~90%
axoneme
~90%
membrane
&
matrix
~10%
membrane
&
matrix
~10%

Figure 1. GFP-tagged and endogenous α-tubulin have similar properties. (A) Bright-field (a) and TIRF (b and c) images of a live cell expressing GFP–α-tubulin. The two focal planes show cilia (b) and cell body microtubules (c). Bar, 1 μm. (B) Western blot analysis of wild type (WT) and the GFP–α-tubulin expressing strain GFP-Tub1. Whole cells (WC), cell bodies (CB), isolated cilia (FLA), axonemes (AX), and MM fractions were loaded and probed with antibodies to GFP and α-tubulin. The bands corresponding to α-tubulin, GFP–α-tubulin, and the uncleaved ble-GFP–α-tubulin are marked. (C) Western blots probed with anti–α-tubulin and anti-GFP showing different dilutions of the cell body (CB) sample in comparison to the undiluted cilia sample (FLA). The amounts of endogenous and tagged tubulin in cilia correspond to ~20 and ~10% of the respective cell body tubulin. (D) Western blot showing a dilution series of axonemes (AX) and undiluted MM of strain GFP-Tub1 to determine the distribution of tagged and endogenous tubulin inside cilia. The blot was probed with antibodies to α-tubulin and the matrix protein IFT139. (E) Western blots of wild-type and GFP-Tub1 axonemes probed with antibodies to α-tubulin, acetylated α-tubulin (6-11B-1), polyglutamylated tubulin (GT335), GFP, and, as a loading control, IC2, an outer arm dynein intermediate chain. (F and G) Schematic presentations of the distribution of GFP-tagged tubulin and endogenous tubulin in whole cells (F) and cilia (G).

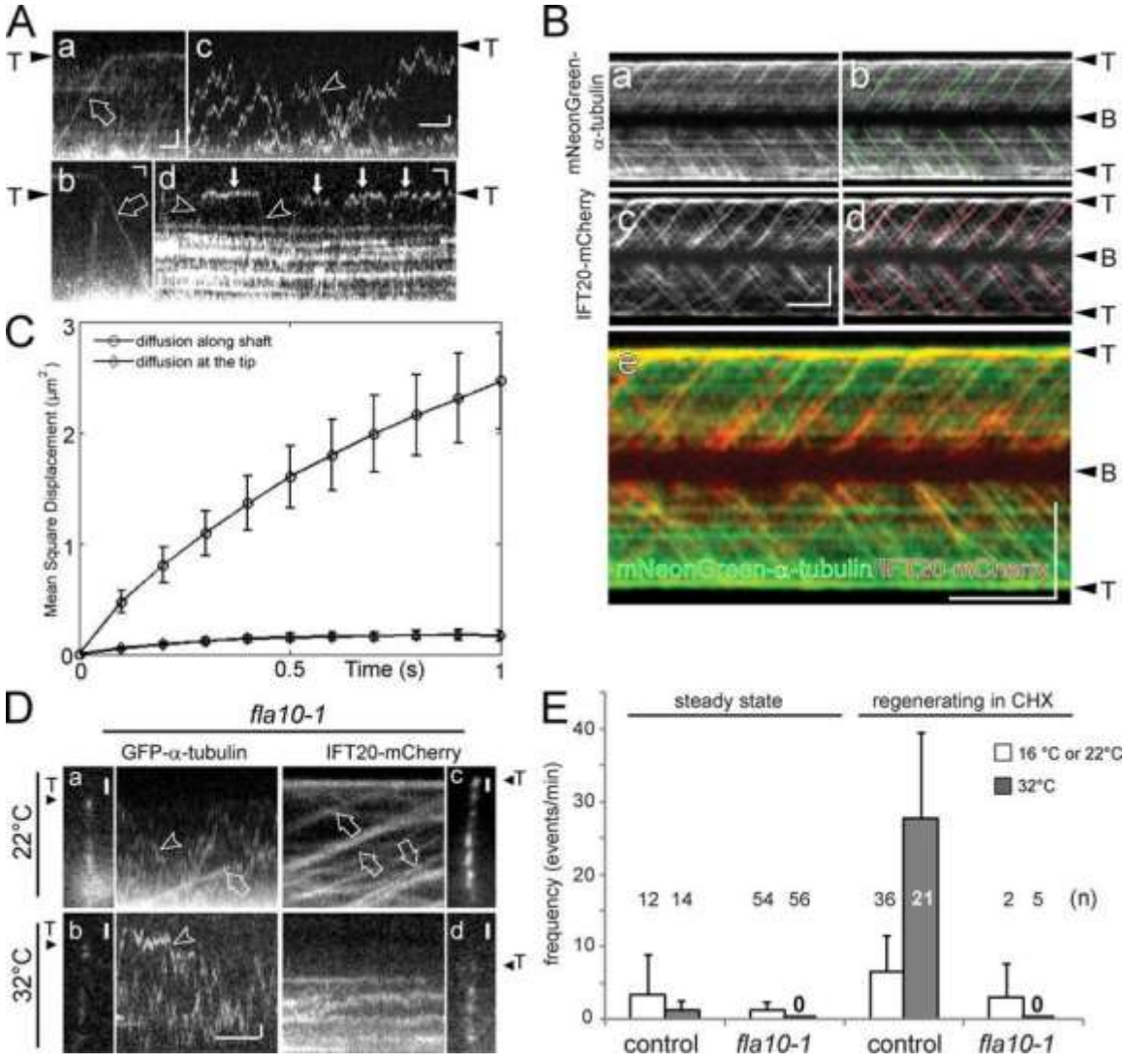
A
T
a
c
T
b
d
T
B
mNeonGreen-α-tubulin
IFT20-mCherry
B
C
diffusion along shaft
diffusion at the tip
Mean Square Displacement (μm²)
Time (s)
0
0.5
1
2
3
D
fla10-1
GFP-α-tubulin
IFT20-mCherry
22°C
32°C
E
steady state
regenerating in CHX
16 °C or 22°C
32°C
frequency (events/min)
12 14
54 56
36 21
2 5
(n)
control
fla10-1
control
fla10-1

Figure 2. Tubulin enters cilia by IFT and diffusion. (A) Gallery of kymograms depicting GFP–α-tubulin (or, in c, mNeonGreen-tubulin) moving inside cilia by anterograde IFT (open arrow in a), retrograde IFT (open arrow in b), and diffusion (arrowheads in c and d). Anterograde transport results in trajectories running from the bottom left (ciliary base) to the top right (ciliary tip; T); retrograde transport events result in top-left to bottom-right trajectories. (c) Tubulin diffusing inside the ciliary shaft; (d) reduced mobility of GFP–α-tubulin in the vicinity of the tip (filled arrows). Bars, 1 μm and 1 s. (B) Kymograms from simultaneous imaging of mNeonGreen–α-tubulin (a and b) and IFT20-mCherry (c and d) in growing cilia; IFT-like trajectories are marked in b and d. A merged kymogram is shown in e. A Western blot of this strain is shown in Fig. S3 B. Bars, 5 μm and 5 s. (C) Mean square displacement versus time for 64 sfGFP–α-tubulin particles diffusing inside the shaft and 58 particles diffusing near the tip of steady-state cilia. The standard error of the mean at each value is indicated. A linear fit to the data at the short time points, which is likely to represent pure diffusion, results in diffusion coefficients of ~1.8 $\mu m^2/s$ and ~0.2 $\mu m^2/s$ for 1D diffusion of GFP-tubulin along the ciliary shaft and at the tip, respectively. (D) Still images and kymograms of *fla10-1* cells expressing either GFP–α-tubulin (a and b) or IFT20-mCherry (c and d) at the permissive temperature (22°C; a and c) and after >180 min at 32°C (b and d). IFT-like trajectories for tubulin and IFT20 were only observed at 22°C (open arrows in a and c). Diffusion of GFP–α–tubulin

(arrowhead in b) into photobleached cilia continued at 32°C in the absence of detectable IFT (d). Bars, 1 μm and 1 s. (E) Frequency of anterograde GFP–α-tubulin transport by IFT in *fla10-1*and control cells (*FLA10 ift20-1* IFT20 mCherry). Steady-state cilia and cilia regenerated in the presence of CHX were compared; at 32°C, IFT-like tubulin transport was robust in control cells but not observed in *fla10-1* cells. *fla10-1* regenerates cilia only slowly at room temperature (~22°C); most measurements are based on cells regenerating cilia at 16°C. Error bars indicate SEM.

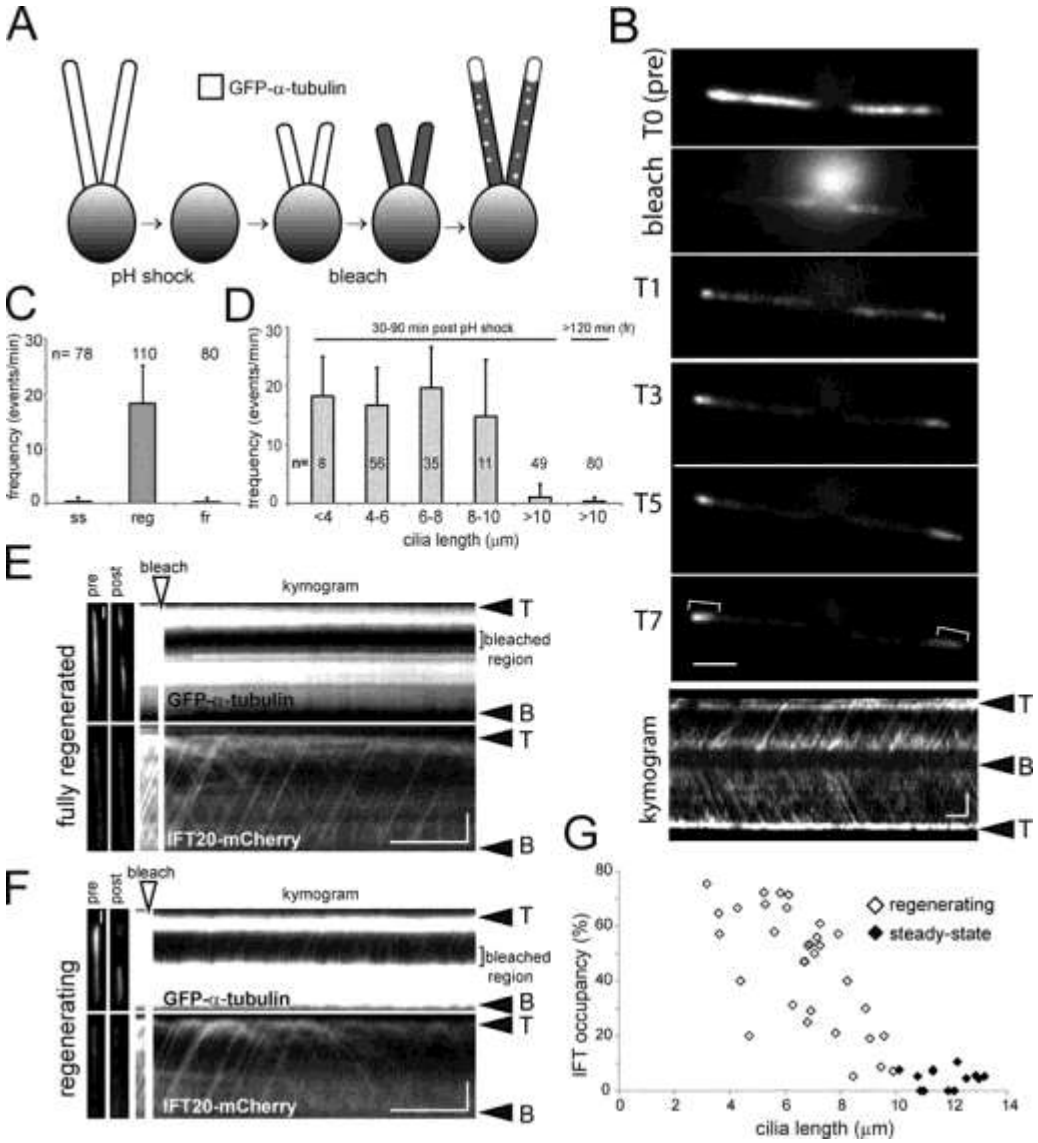
A
GFP-α-tubulin
pH shock
bleach
B
T0 (pre)
bleach
T1
T3
T5
T7
kymogram
T
B
T
C
frequency (events/min)
n= 78
110
80
ss
reg
fr
D
30-90 min post pH shock
>120 min (hr)
frequency (events/min)
n=
8
56
35
11
49
80
<4
4-6
6-8
8-10
>10
>10
cilia length (μm)
E
pre
post
bleach
kymogram
T
bleached region
fully regenerated
GFP-α-tubulin
B
T
IFT20-mCherry
B
F
pre
post
bleach
kymogram
T
bleached region
regenerating
GFP-α-tubulin
B
T
IFT20-mCherry
B
G
IFT occupancy (%)
regenerating
steady-state
cilia length (μm)

Figure 3. IFT particles carry more tubulin during ciliary growth. (A) Schematic presentation of the experimental design. Cells were deciliated by a pH shock and allowed to partially regrow cilia. Then, the cilia were bleached and the entry and assembly of unbleached GFP–α-tubulin was analyzed by TIRF. (B) Individual frames from videos captures before (T0), during (bleach), and at various time points (T1–T7 in min) after bleaching of the cilia. Brackets: unbleached GFP-tubulin added at the ciliary tip as cilia elongate. Bar, 2 μm. Bottom: kymogram of the same cell showing numerous IFT-like GFP-tubulin tracks. Bar, 2 μm and 2 s. (C) Mean frequency of GFP-tubulin transport by anterograde IFT in steady-state (ss), regenerating (reg), and fully regenerated (fr) cilia. Error bars indicate the standard deviation. (D) Analysis of GFP-tubulin transport frequency by anterograde IFT in regenerating cilia of various lengths. Error bars indicate SEM. (E and F) Segments of the cilia of cells coexpressing GFP–α-tubulin and IFT20-mCherry were bleached using a focused laser beam and protein traffic in the bleached region was analyzed by twocolor TIRF microscopy. The kymogram of a cell with fully regrown flagella (E) shows numerous IFT20-mCherry trajectories, whereas transport of GFP–α-tubulin was not observed. In contrast, most IFT20-mCherry trajectories align with GFP–α-tubulin trajectories in the regenerating cilium (F). Bars, 2 μm and 5 s. (G) Scatter plot of the occupancy rate (the percentage of IFT20-mCherry particles moving together with GFP–□-tubulin) in cilia of different length. Cells with regenerating (white marks) or nongrowing (steady-state and fully regenerated, black marks) cilia were analyzed (*n* = 32 and 13 cilia, respectively).

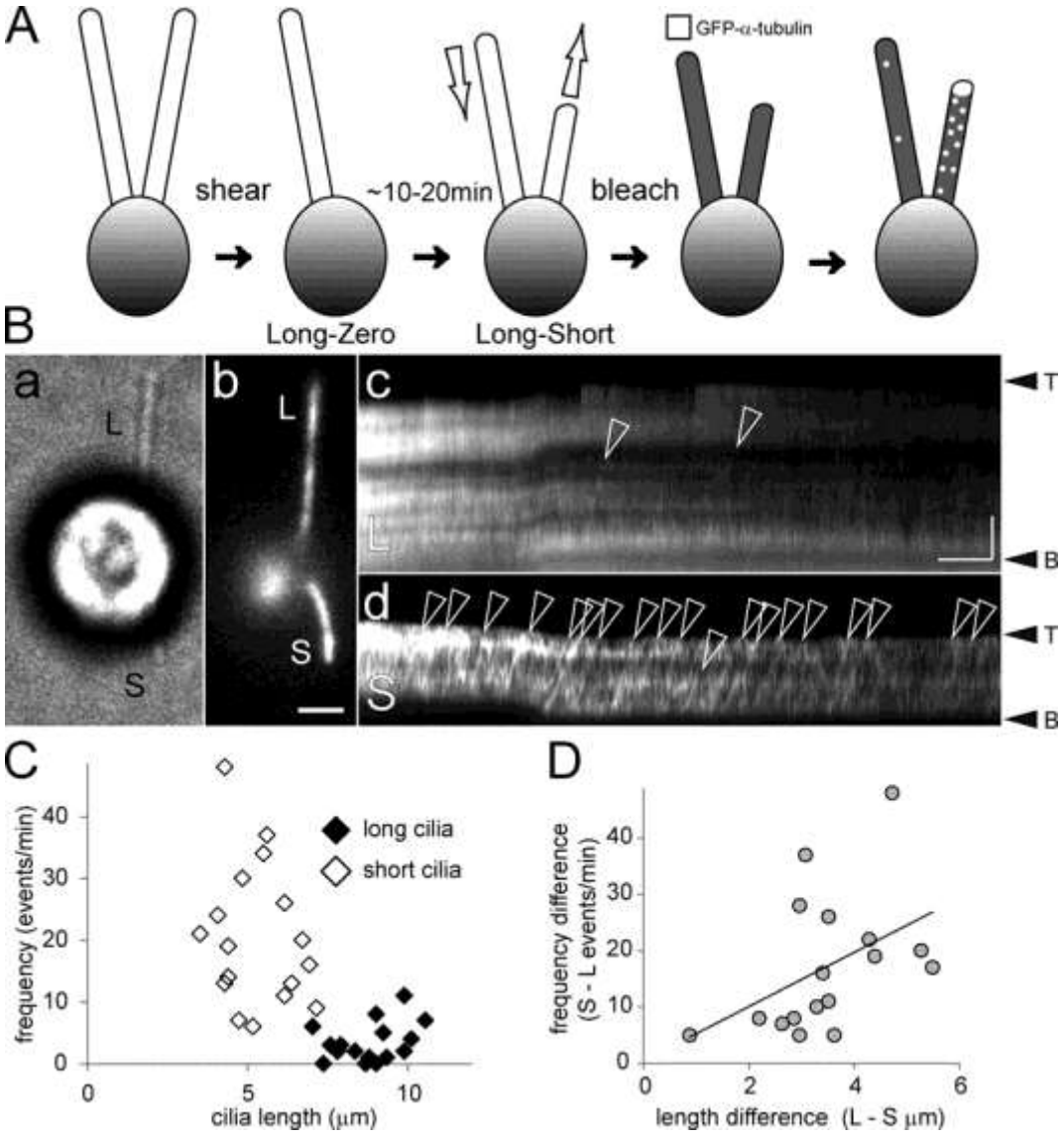
A
GFP-α-tubulin
shear
~10-20min
bleach
Long-Zero
Long-Short
B
a
L
S
b
L
S
c
T
B
d
S
T
B
C
frequency (events/min)
long cilia
short cilia
cilia length (μm)
D
frequency difference (S - L events/min)
length difference (L - S μm)

Figure 4. Cilium-autonomous regulation of tubulin transport by IFT. (A) Schematic presentation of the long-short experiment to generate cells with growing and nongrowing cilia. (B) Bright-field (a), TIRF image (b), and corresponding kymograms (c and d) of a long-short cell. Numerous GFP–α-tubulin transport events (open arrowheads) were observed in the short (S) cilium (d), whereas only a few such events were detected in the long (L) flagellum (c). Bars, 2 μm and 5 s (b and c). (C) Scatter plot of the frequencies of GFP–α-tubulin transport in short (open diamonds) and long (filled diamonds) cilia of long-short cells. (D) The difference in tubulin transport frequencies between the long and the short cilia of given cells diminished as the difference in length between the two cilia decreased (*n* = 17).

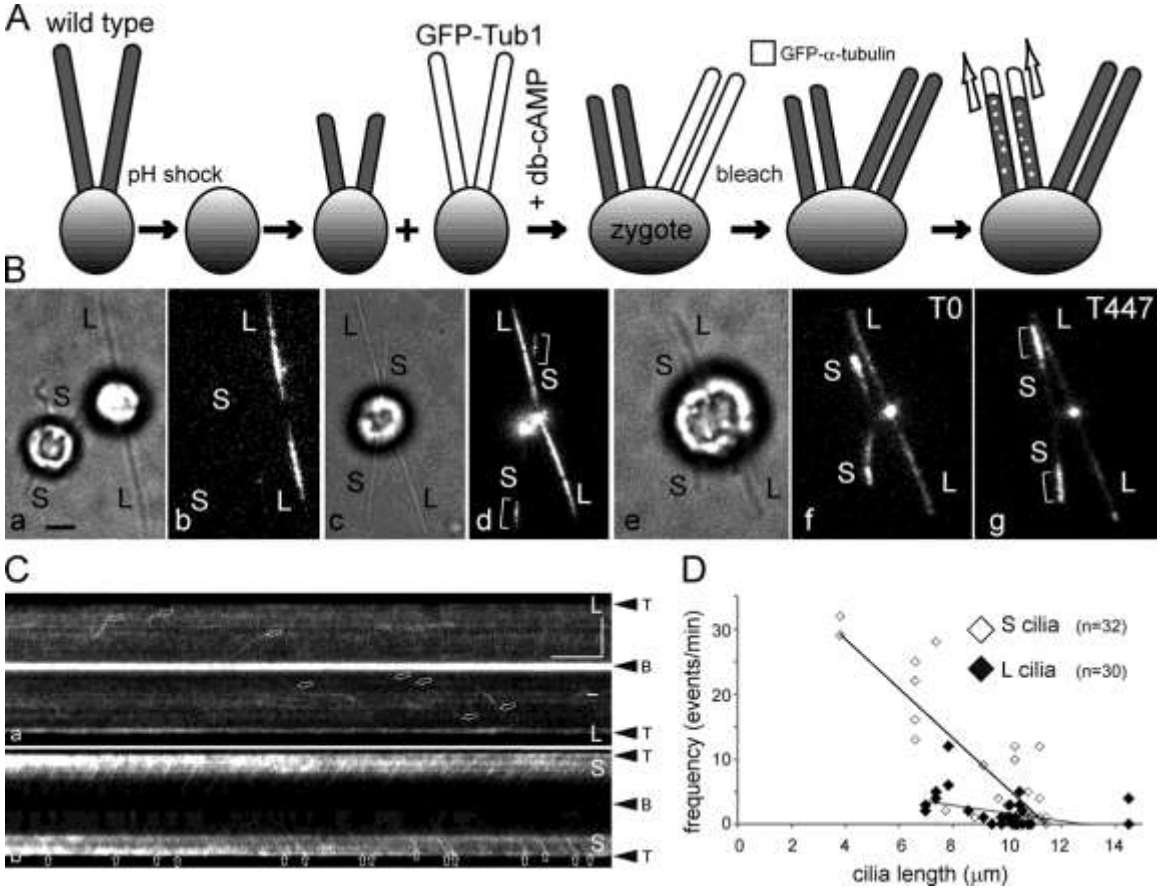
A
wild type
pH shock
GFP-Tub1
+ db-cAMP
GFP-α-tubulin
bleach
zygote
B
T0
T447
C
D
S cilia (n=32)
L cilia (n=30)
frequency (events/min)
cilia length (μm)

Figure 5. Cells direct tubulin flux specifically into growing cilia. (A) Schematic presentation of the experimental design. Wild-type gametes were deciliated by a pH shock, allowed to initiate cilia regeneration, and fused to GFP–α-tubulin expressing gametes with full-length cilia. Cell fusion was promoted by adding 15 mM dibutyryl cAMP (Pasquale and Goodenough, 1987). The resulting long-short zygotes will initially possess two short, regenerating cilia and two steady-state, GFP-positive cilia. To analyzed GFP-tubulin transport, all four cilia were photobleached. (B) Bright-field (a, c, and e) and TIRF images (b, d, f, and g) of gametes (a and b) and zygotes (c–g). S, regenerating cilia. L, long flagella derived from the GFP–α-tubulin donor strain. Brackets indicate ciliary segments assembled after cell fusion. Note elongation of short cilia depicted in e–g; the time points (in seconds) are indicated. Bar, 2 μm. (C) Kymograms of the long (L) and short (S) cilia of the zygote shown in B (e–g). Arrows: GFP-tubulin trajectories. Bars, 5 μm and 5 s. (D) Scatter plot showing the frequency of anterograde GFP-tubulin trajectories in wild-type–derived regenerating cilia (S cilia, open diamonds) and GFP-Tub1–derived cilia (L cilia, closed diamonds) of eight long-short zygotes. Mean values were 7.8 ± 10 versus 1.8 ± 2.6 events/min, respectively; P = 0.0016. Some data points with zero transport events and similar ciliary length overlap. See Fig. S4 for a histogram of the data.

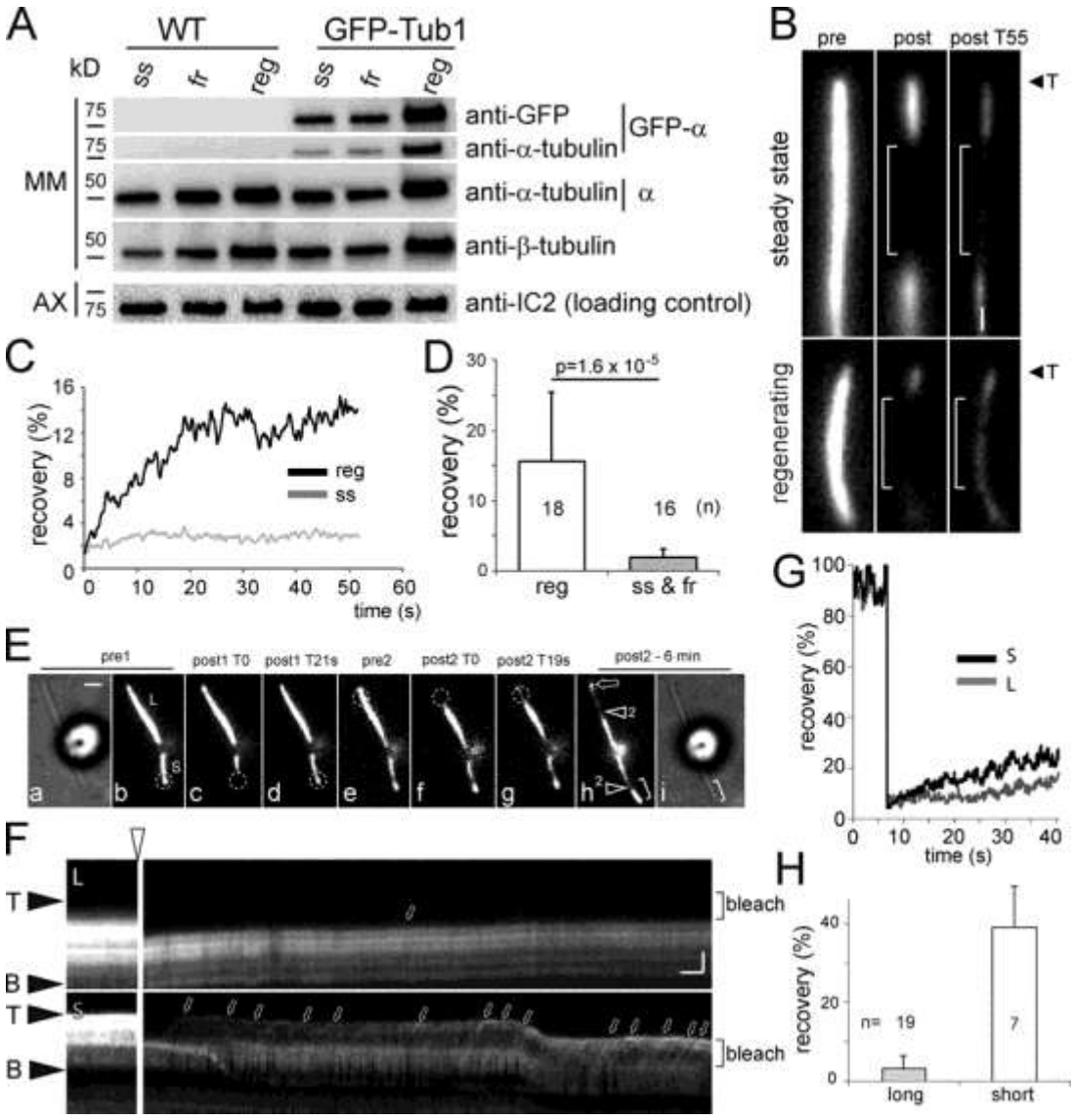
A
WT
GFP-Tub1
kD
ss
fr
reg
ss
fr
reg
MM
AX
75
75
50
50
75
anti-GFP
anti-α-tubulin
GFP-α
anti-α-tubulin
α
anti-β-tubulin
anti-IC2 (loading control)
B
pre
post
post T55
steady state
regenerating
T
T
C
recovery (%)
reg
ss
time (s)
D
p=1.6 x 10-5
recovery (%)
18
16
(n)
reg
ss & fr
E
pre1
post1 T0
post1 T21s
pre2
post2 T0
post2 T19s
post2 - 6 min
a
b
c
d
e
f
g
h
i
L
S
F
T
B
T
B
L
S
bleach
bleach
G
recovery (%)
S
L
time (s)
H
recovery (%)
n= 19
7
long
short

Figure 6. The concentration of soluble tubulin is increased in growing cilia. (A) Western blot comparing the amounts of tubulin in the MM fractions of steady-state (ss), fully regenerated (fr), and regenerating (reg) cilia. MM fractions were loaded to represent matching volumes of MM. Toward this end, loading was adjusted for equal amounts of axonemal proteins in the corresponding axonemal fractions based on anti-IC2 staining. See Fig. S4 D for quantification of band intensities. (B–D) FRAP analysis of steady-state and growing cilia. (B) After local bleaching of cilia using a focused laser beam (brackets), partial recovery of GFP–□-tubulin fluorescence was observed. Shown are images before (pre), and immediately (after T0) and 55 s (after T55) after photobleaching. Bar, 1 µm. (C) Single measurements of the fluorescence recovery (in % of the pre-bleaching intensity) in the bleached areas of a steady-state and a regenerating cilium. (D) Mean FRAP of regrowing (reg; *n* = 18) versus steady-state and fully regenerated (ss & fr; *n* = 16) cilia. Error bars indicate SEM. (E and F) FRAP analysis of a long-short cell. (E) Still images showing a long-short cell before (pre1) and immediately (post1 T0) and 21 s (post1 T21) after spot bleaching of the short cilium (S); pre2, post2 T0, and post2 T19 indicate similar steps for the long cilium. Dashed circle: position of the bleaching laser. Arrow in h: incorporation of GFP-tubulin into the long cilium. Arrowheads with 2 indicate additional areas bleached between post2 T19s and post2–6 min. Note considerable elongation of the initially short cilium (after 6 min; indicated by brackets). Bar, 2 µm. (F) Kymograms showing FRAP in the long (L) and the short (S) cilium of a given cell. Open arrowhead: bleaching steps. Small arrows: GFP–α-tubulin trajectories.

Note recovery of a diffuse background of GFP–α-tubulin in the bottom panel. Bar, 2 μm and 2 s. (G) Single measurements of the fluorescence recovery (in percentage of the pre-bleaching intensity) in the bleached areas of the short and long cilia shown in F. (H) Mean FRAP of short and long cilia of long-short cells. Newly assembled axonemal segments (see brackets in E, h) were excluded from FRAP analysis. Error bars indicate SEM.

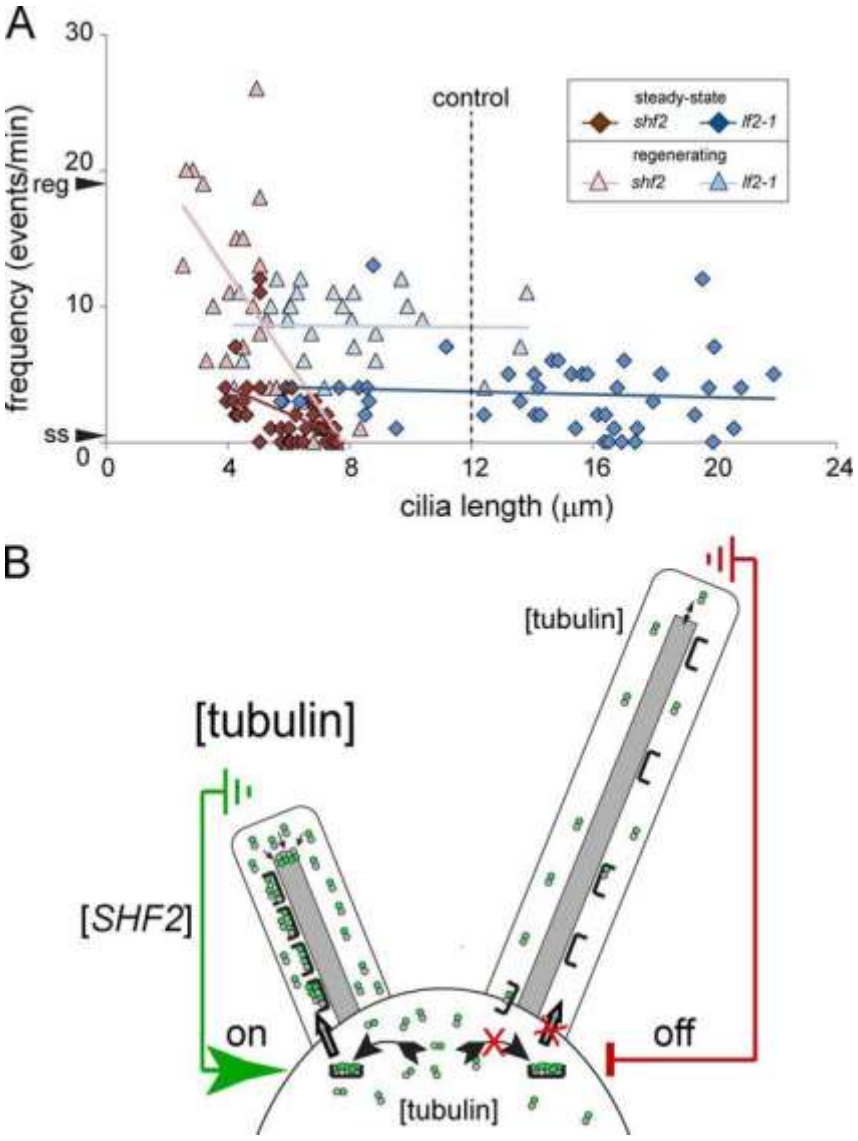
A
30
20
reg
10
ss
0
frequency (events/min)
control
steady-state
shf2
lf2-1
regenerating
shf2
lf2-1
0
4
8
12
16
20
24
cilia length (μm)
B
[tubulin]
[tubulin]
[SHF2]
on
off
[tubulin]

Figure 7. Regulation of tubulin transport in cilia. (A) Scatter plot of the frequencies of tubulin transport by anterograde IFT in *shf2* (red symbols) and *lf2-1* mutant cilia (blue symbols). Diamonds: steady-state cilia; triangles: regenerating cilia. Trend lines are given for each dataset. *n* = 27, 43, 29, and 44 for *lf2-1* regenerating and steady-state and *shf2* regenerating and steady-state, respectively, from a single experiment. The mean ciliary length of control cilia, and the frequencies of tubulin transport in steadystate and regenerating control cilia (arrowheads) are indicated. (B) Model of the regulation of tubulin transport. Incompletely assembled cilia (left) induce a signal resulting in increased loading of IFT particles with tubulin (curved arrow) or facilitated access of highly loaded IFT particles into cilia. Augmented tubulin transport will increase the concentration of soluble tubulin in the cilia matrix and promote the polymerization of axonemal microtubules. Mutants in *SHF2* prematurely down-regulate tubulin transport (A), suggesting that SHF2 functions in maintaining a high tubulin flux into cilia until steady-state length is reached. Full-length cilia (right) inhibit tubulin loading onto IFT or admission of highly loaded IFT trains into cilia.

2.12 Supplementary Figures

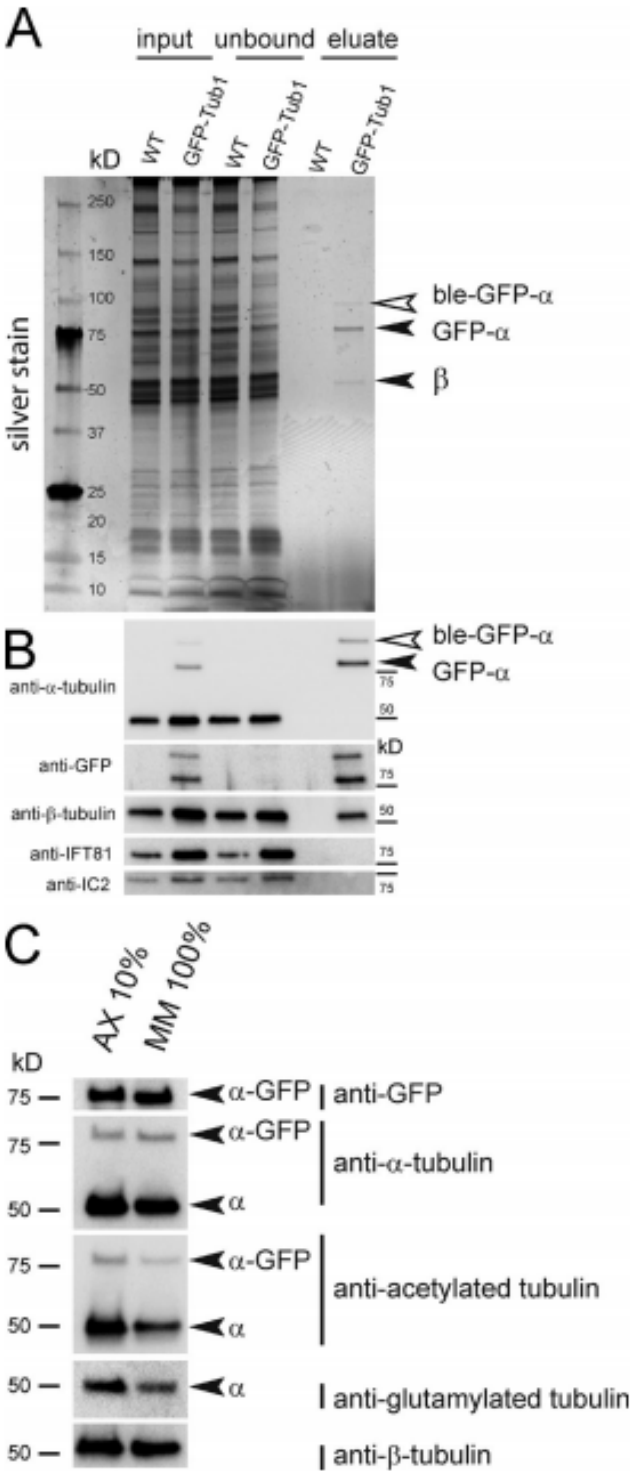

Figure S1. GFP–α-tubulin interacts with endogenous β-tubulin. Ciliary matrix obtained from strain GFP-Tub1 and a wild-type control was incubated with anti-GFP (i.e., GFP nanobody or GFP binding protein) beads to purify GFP–α-tubulin and associated proteins. (A) Silver-stained gel showing the ciliary matrix (input), the unbound fraction (flow through), and the eluted fraction (eluate). GFP–α-tubulin, β-tubulin, and the uncleaved ble-GFP–α-tubulin fusion protein are marked by arrowheads; the mean band intensity of the latter was 22% compared with that of cleaved GFP-tubulin (±8%, *n* = 7 flagellar preparations). (B) Western blot analysis of the fractions with the antibodies as indicated. Under the chosen stringent conditions (wash with 250 mM NaCl in HMEK), endogenous α-tubulin did not coimmunoprecipitate with GFP-tubulin. (C) Comparison of soluble and insoluble ciliary tubulin. Western blot of axonemal and MM fractions isolated from strain GFP-Tub1 analyzed with the antibodies indicated. Loading was adjusted to present similar amounts of tubulin in both fractions.

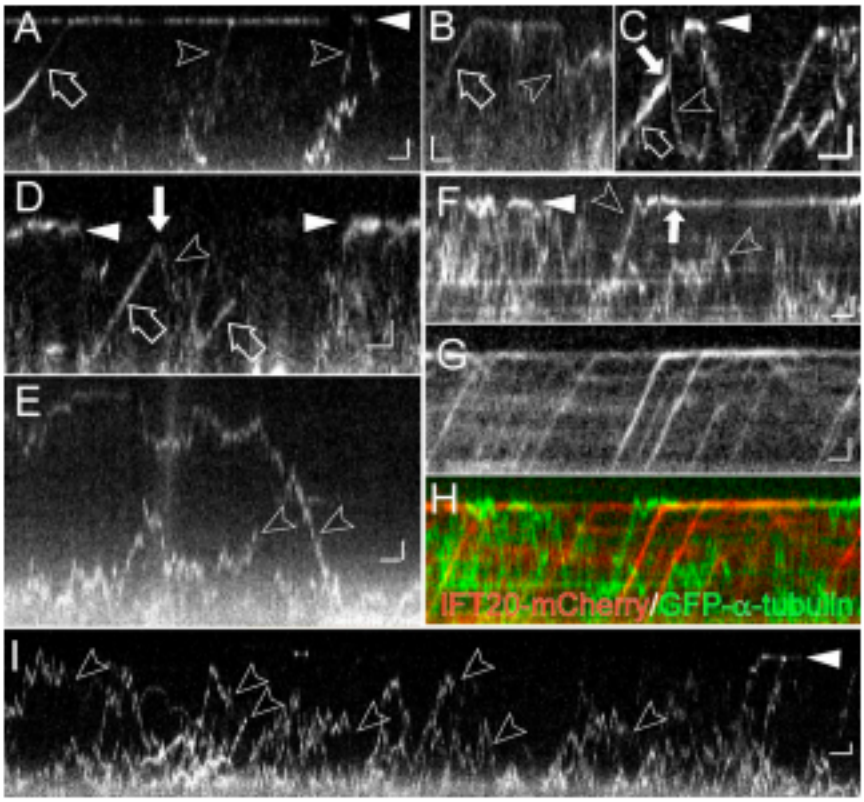

Figure S2. Comparison of active transport and diffusion of fluorescent protein-tagged α-tubulin. Gallery of kymograms showing active transport (open arrows in A–D) and diffusion (open arrowheads in A–E) of GFP–α-tubulin; IFT20-mCherry is shown in G and H (red ; the corresponding GFP-tubulin track is shown in F). Solid arrows in C and D: transition from IFT to diffusion indicative for unloading of GFP–α-tubulin; solid arrow in F: putative docking of GFP–α-tubulin to the ciliary tip. White arrowheads in A, C, D, and I: reduced mobility of diffusing GFP–α-tubulin at the ciliary tip. Open arrowheads in I indicate bleaching events of mNeonGreen–α-tubulin. Bars, 1 µm and 1 s.

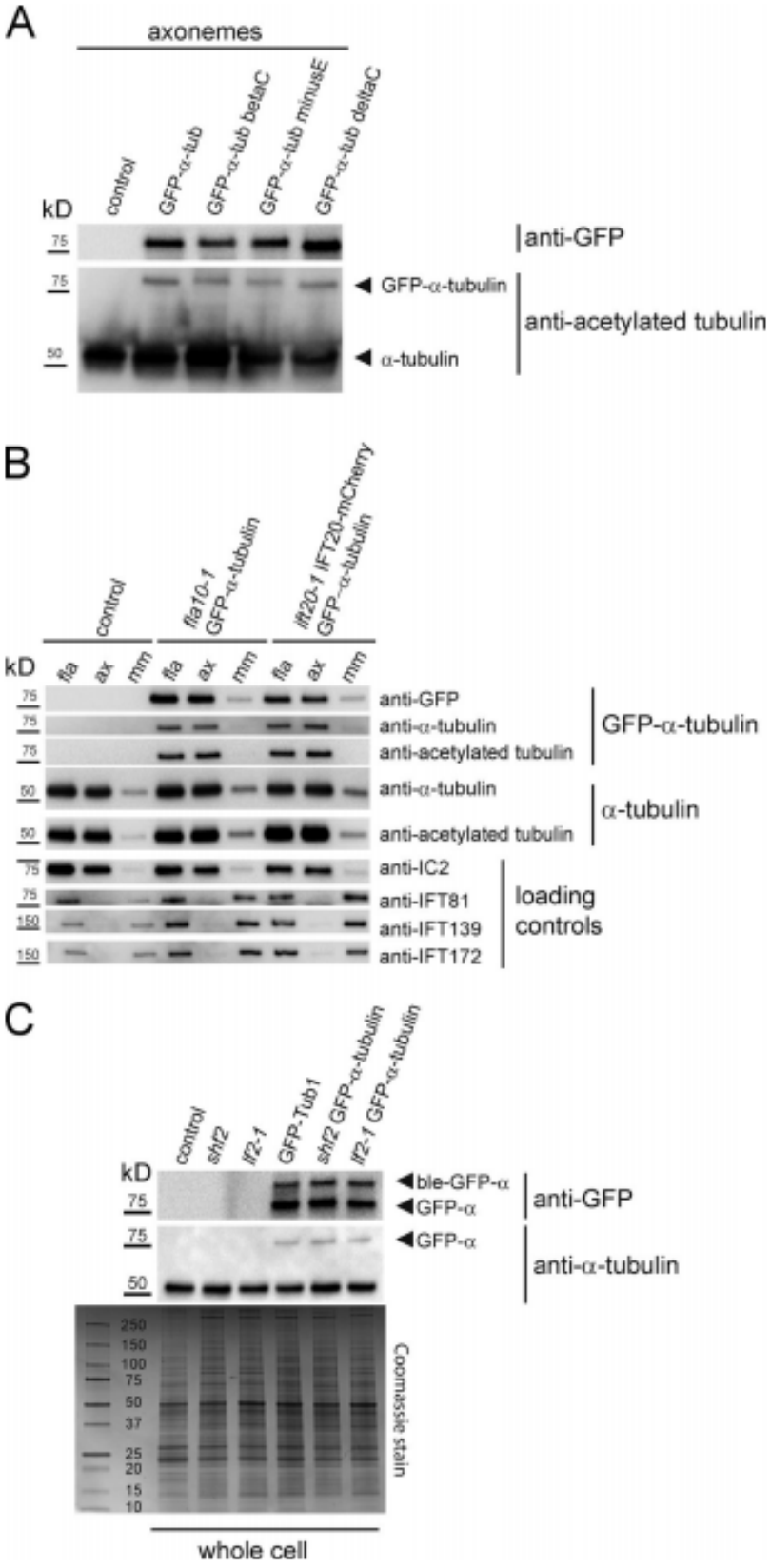
A
axonemes
control
GFP-α-tub
GFP-α-tub betaC
GFP-α-tub minusE
GFP-α-tub deltaC
kD
75
anti-GFP
75
50
GFP-α-tubulin
α-tubulin
anti-acetylated tubulin
B
control
fla10-1 GFP-α-tubulin
ift20-1 IFT20-mCherry GFP-α-tubulin
kD
fla
ax
mm
anti-GFP
anti-α-tubulin
anti-acetylated tubulin
GFP-α-tubulin
α-tubulin
anti-IC2
anti-IFT81
anti-IFT139
anti-IFT172
loading controls
C
control
shf2
ift2-1
GFP-Tub1
shf2 GFP-α-tubulin
ift2-1 GFP-α-tubulin
kD
ble-GFP-α
GFP-α
anti-GFP
anti-α-tubulin
250
150
100
75
50
37
25
20
15
10
Coomassie stain
whole cell

Figure S3. Western blot analysis of strains used in this study. (A) The C-terminal domain of GFP–α-tubulin is not required for incorporation into the axoneme. Western blot analysis of axonemes isolated from a wild-type control strain and strains expressing GFP–α-tubulin and the modified minusE, betaC, and deltaC GFP-tubulins. Modified tubulins were expressed in an *ift20-1* IFT20-mCherry background. See Table S1 for a description of the constructs. (B) Western blot analysis of the *fla10-1* GFP–α-tubulin and the *ift20-1* IFT20-mCherry GFP–α-tubulin strains. Isolated cilia (fla) were fractionated and probed with the antibodies as indicated. (C) Western blot (top) and Coomassie stained gel (bottom) of whole cell extracts from wild type, *shf2*, *lf2-1*, and GFP–α-tubulin expressing version of these strains. Western blots were stained with anti-GFP and anti–α-tubulin.

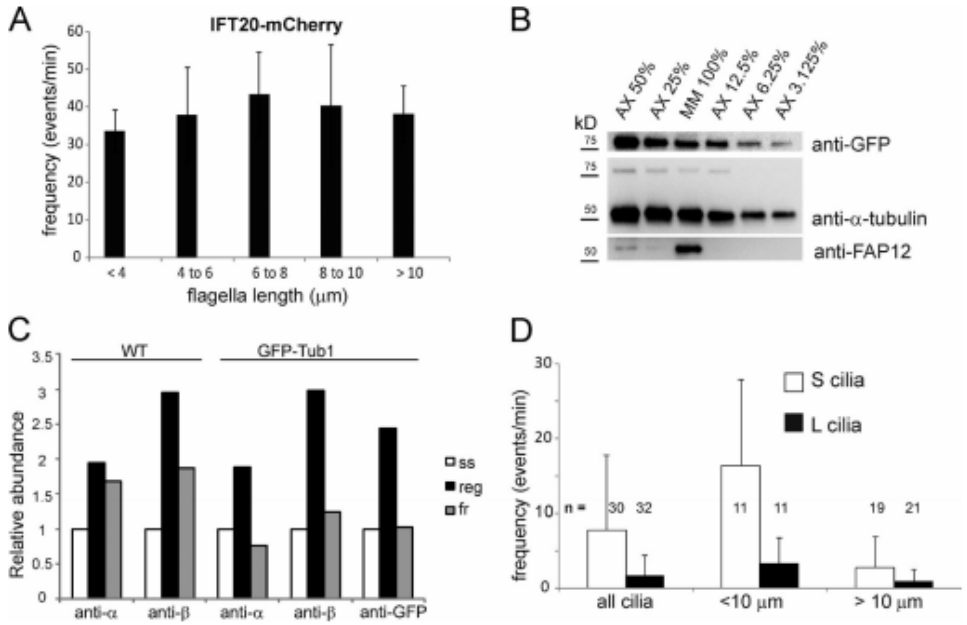
A
IFT20-mCherry
frequency (events/min)
flagella length (μm)
< 4
4 to 6
6 to 8
8 to 10
> 10
B
AX 50%
AX 25%
MM 100%
AX 12.5%
AX 6.25%
AX 3.125%
kD
anti-GFP
anti-α-tubulin
anti-FAP12
C
WT
GFP-Tub1
Relative abundance
ss
reg
fr
anti-α
anti-β
anti-α
anti-β
anti-GFP
D
S cilia
L cilia
frequency (events/min)
n =
30 32
11 11
19 21
all cilia
<10 μm
> 10 μm

Figure S4. Increased concentration of soluble tubulin in growing cilia. (A) Frequency of IFT20-mCherry particles in regenerating and steady-state cilia. The reduced apparent IFT frequency in this strain could be caused, for example, by low expression levels of IFT20-mCherry. Also, some IFT20-mCherry particles could have escaped detection due to their reduced brightness and/or loss of fluorescence. Error bars indicate SEM. (B) Western blot showing a dilution series of the axonemal fraction and the undiluted MM sample from regenerating cilia to determine the ratios of tagged and endogenous tubulin between the two fractions. The blot was probed with anti–α-tubulin, anti-GFP, and, as a control, an antibody to FAP12, the major membrane-associated protein in *C. reinhardtii* cilia. Compare to Fig. 1 D showing a similar blot of steady-state cells. (C) Quantitative analysis of the amount of tubulin in the MM fraction of steady-state (ss), regenerating (reg), and fully regenerated (fr) cilia. Quantifications are based on the blot shown in Fig. 6 A and band intensities were normalized for IC2 loading. This experiment was completed once. Elevated tubulin levels in the matrix of the fully regenerated cilia of the control might indicate that some cells in this sample have not yet completed regeneration. (D) Analysis of the GFP-tubulin transport frequencies in nonregenerating GFP-Tub1–derived L cilia and regenerating wild-type–derived S cilia of long-short zygotes. Error bars indicate SEM.

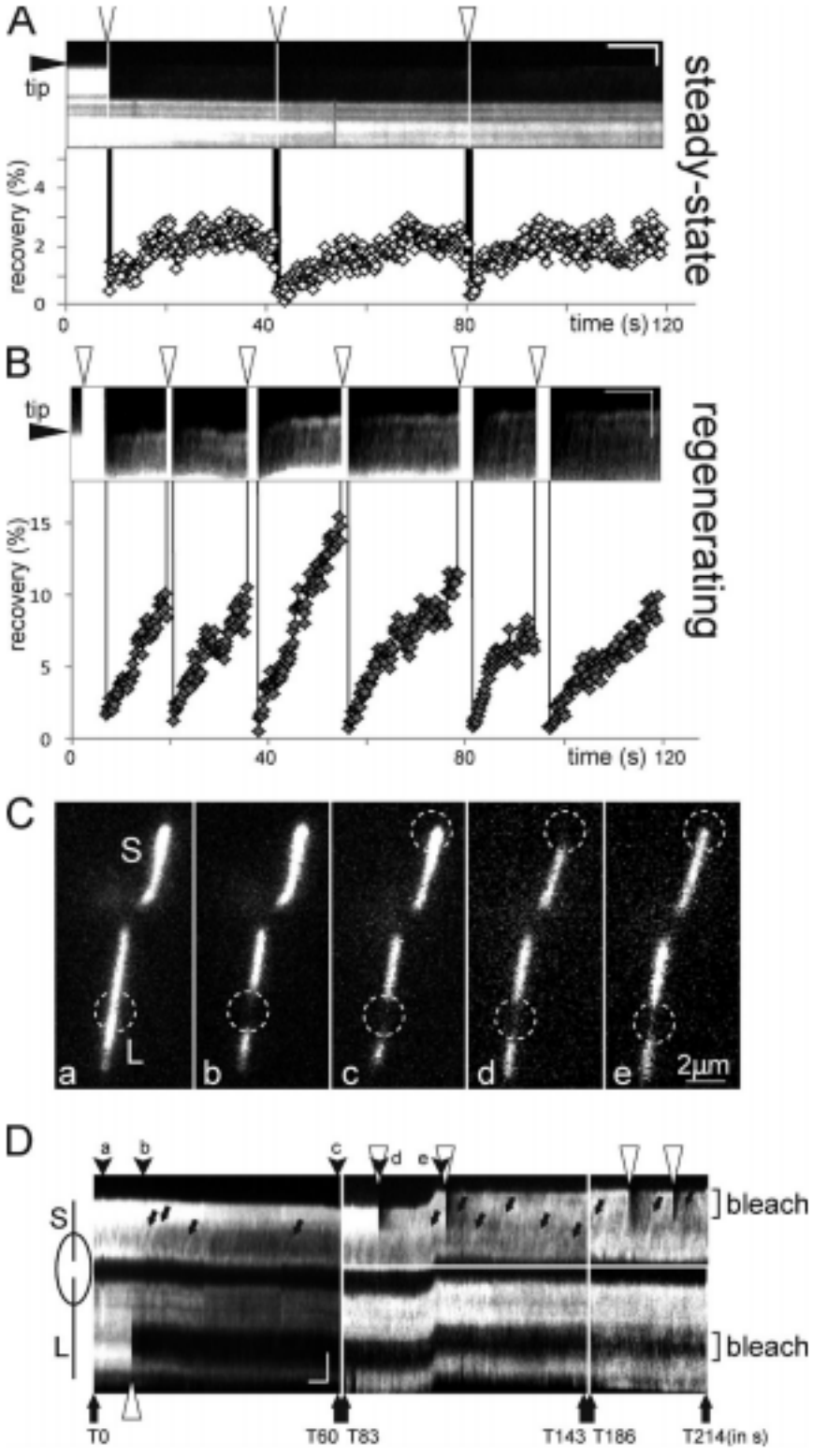
A
tip
recovery (%)
0
2
4
0
40
80
time (s) 120
steady-state
B
tip
recovery (%)
0
5
10
15
0
40
80
time (s) 120
regenerating
C
S
L
a
b
c
d
e
2µm
D
a
b
c
d
e
S
L
bleach
bleach
T0
T60 T83
T143 T186
T214(in s)

Figure S5. Repeated FRAP of growing and nongrowing cilia is followed by similar rates of recovery. (A and B) Segments of a steady-state (A) and a regenerating (B) cilium were repeatedly bleached (indicated by arrowheads). Kymograms (top) and FRAP quantification (bottom) indicate similar rates (in percentage of pre-bleach GFP–α-tubulin fluorescence) of recovery after each bleaching step. (C and D) Individual frames (C) and kymograms (D) of a longshort cell. Bleached areas are marked by dashed circles. The kymogram (D) is a composite of several recordings, and arrowheads labeled a–e indicate the positions of the frames in C. The time (in seconds) for each recording and the position the bleaching laser (Brackets) is indicated; overexposed frames caused by photobleaching were deleted. Arrows in D: GFP–α-tubulin trajectories. Note fast and strong recovery in subsequent bleachings of the short cilium while the initially bleached area in the long cilium remains visible. The extended observation time will also bleach some of the (axonemal) GFP–α-tubulin outside of the spot bleaching area. This loss of fluorescence in the nonbleached areas results in a higher apparent recovery in the bleached areas. Bars: (C) 2 µm; (D) 2 µm and 5 s.

Table I: The E-hook of α-tubulin is not required for transport via IFT. The table shows the C-terminal sequences of wild-type and the modified α-tubulin molecules. Transport velocities by anterograde IFT and qualitative assessment of axonemal incorporation of the strains are listed.

Construct	C-ter (428-451)	IFT transport (μm/s)	Incorporation into the axoneme
sfGFP-Tub1	LEKDFEEVGAAESAEGAGEGEGEEY	2.09 (±0.35, *n* = 114)	Yes
FP-minusE	LEKDFAAVGAQSAQGAGAGAGAEY	1.83 (±0.36, *n* = 32)	Yes
FP-deltaC	LEKDFEEVGAEY	2.04 (±0.43, *n* = 89)	Yes
FP-betaC	LEKDFQQYQDASAEEEGEFEGEEEEAEF	2.29 (±0.57, *n* = 19)	Yes

The table shows the C-terminal sequences of wild-type and the modified α-tubulin molecules. Transport velocities by anterograde IFT and qualitative assessment of axonemal incorporation of the strains are listed.

2.13 Materials and methods

Strains and culture conditions: *C. reinhardtii* cultures were maintained in modified M medium and aerated with 0.5% CO2 at ~21°C with a light/dark cycle of 14:10 h. To generate gametes, cells were grown on M plates for ~7–10 d, placed into dim light for 2 d, and then incubated overnight in constant light in liquid M-N medium to induce gametogenesis. In mating reactions involving gametes with regenerating cilia, cell fusing was facilitated by addition of 15 mM dibutyryl-cAMP (Sigma-Aldrich; Pasquale and Goodenough, 1987).

Generation of transgenic strains: The vector pBR25 encoding mCerulean–α-tubulin downstream of the viral 2A sequence and the *BLE* selectable marker gene was provided by B. Rasala and S. Mayfield (University of California, San Diego, San Diego, CA). The humanized sfGFP gene was amplified by PCR using the primers 5’-CGCGGATCCATGGTGAGCAAGGGC-3’ and 5’-GCGGAATTCTTACTTGTACAGCTCGTCC-3’, digested with XhoI and BamH1 and ligated into pBR25 digested with the same enzymes; the mCerulean will be replaced with the sfGFP in the product. To generate mNeon-Green–

tagged α-tubulin, the gene was synthesized (Genewiz) using the *C. reinhardtii* codon usage and inserted into pBR25 as described above. α-Tubulin derivates were prepared as follows: gene segments encoding the modified C termini of α-tubulin were synthesized by Genewiz, excised with EcoRI and BglII, and ligated into pBR25-sfGFP vector digested with the same enzymes. Plasmids were restricted with KpnI and XbaI, and the gel-purified fragment encompassing the *BLE* and *TUA2* genes was transformed into *C. reinhardtii* by electroporation. Transformants were selected on TAP plates containing 10 µg/ml zeocin in constant light, transferred to liquid medium and analyzed by TIRF microscopy and Western blotting. The *ift20-1* IFT20-mCherry strain was generated by expressing the coding region of *IFT20* fused to mCherry under the control of the *FLA14* promoter in the *ift20-1* deletion mutant (Lechtreck et al., 2009); for double imaging the rescued *ift20-1* IFT20-mCherry strain was transformed again with the pBR-GFP–α-tubulin expression plasmid. The *fla10-1 ift20-1* IFT20-mCherry strain was generated by mating *fla10-1* and *ift20-1* IFT20-mCherry strains, followed by phenotypical and microscopic selection.

Isolation and fractionation of cilia: To isolate cilia for biochemical analysis, a protocol described by Witman (1986) was used. In brief, cells were concentrated and washed with 10 mM Hepes, pH 7.4. Cells were resuspended in HMS (10 mM Hepes, 5 mM MgSO4, and 4% sucrose) and deciliated by adding dibucaine to a final concentration of 4.17 mM (Sigma-Aldrich). Cilia and cell bodies were separated by differential centrifugations and cilia were collected by sedimentation (17,000 *g*, 4°C, 20 min). Isolated cilia were resuspended in HMEK

(30 mM HEPES, 5 mM MgSO4, 0.5 mM EGTA, and 25 mM KCl) plus protease inhibitor (P9599; 1:100; Sigma-Aldrich) and demembranated by addition of 1% NP-40 Alternative (final concentration; EMD Millipore) on ice for 20 min. Axonemes were pelleted by centrifugation (30,000 *g*, 4°C, 20 min) and fractions were analyzed by SDS-PAGE and Western blotting.

Flagellar regeneration and generation of long-short cells: Cells in M were deflagellated by pH shock, transferred to fresh M medium, and allowed to regrow cilia under constant light with agitation (Lefebvre, 1995). To delay the onset on regeneration, cells were kept on wet ice until needed. For long-short experiments, cells were passed 4–6× through a 26G × 1/2 needle using a 1-ml syringe, which resulted in a small percentage of long-zero cells. In experiments involving CHX, 10 µM CHX was added to the cells ~30 min before pH shock and cells were resuspended in fresh M medium supplemented with 10 µM CHX after pH shock. Cells were allowed to regenerate for 20 min at RT or 16°C, and then aliquots were transferred to 32°C for >180 min to inactivate IFT in *fla10-1* strains.

TIRF microscopy: A microscope (Eclipse Ti-U; Nikon) equipped with 60× NA1.49 TIRF objective and through-the-objective TIRF illumination provided by a 40-mW 488-nm and a 75-mW 561-nm diode laser (Spectraphysics) was used for in vivo imaging (Lechtreck, 2013). The excitation lasers were cleaned up with a Nikon GFP/mCherry TIRF filter and the emission was separated using an Image Splitting Device (Photometrics DualView2 with filter cube 11-EM). Observation chambers were assembled by inverting a 22 × 22 mm no. 1.5 cover glass with □10 µl of 5 mM Hepes, pH 7.3, 6.25 mM EGTA onto an equal volume of cells in

M medium on a 24 × 60 mm no. 1.5 cover glass. Cells were imaged through the large cover glass at room temperature or, for temperature-sensitive experiments, at 32°C using a Bioptechs objective heater. Images were recorded at 2–31 fps using an iXON3 (Andor) and the NIS-Elements Advanced Research software (Nikon). ImageJ (National Institutes of Health) with the LOCI plugin (University of Wisconsin, Madison WI) and multiple kymogram plugin (European Molecular Biology Laboratory) were used to generate kymograms as described in Lechtreck (2013). Videos were generated by adjusting image contrast in ImageJ. Images were then cropped, rotated, converted to 8-bit in ImageJ, and exported in AVI format; QuickTime was used for scene selection. Individual frames were copied into Photoshop (Adobe) and adjusted for contrast and brightness; figures were assembled in Illustrator (CS6 version 16.0.3; Adobe). For photobleaching of the entire cilia, the intensity of the 488-nm laser was increased to 10% or more for 4–12 s. Partial bleaching of the cilia was achieved by using a focused 488-nm laser beam in epifluorescence; near complete bleaching of a 3-µm diameter region was accomplished in 50–300 ms.

FRAP analysis: Videos were opened in ImageJ, a region of interest (ROI) encompassing the central part of the bleached region was selected using the *Rectangular* tool, fluorescence intensities in the ROIs were determined using the *Plot z-axis Profile* tool, and the values were exported into Excel. Data of each frame were corrected for background fluorescence. The pre-bleach signal within the bleached ROI was set to 100% and the recovery (in percentage of the pre-bleach signal) was calculated. The distal regions of growing cilia were excluded

from the ROIs used for recovery analysis. GFP–α-tubulin incorporated into the axoneme cannot recover and will lose fluorescence intensity with time. In contrast, soluble tubulin in the matrix will perpetually reenter cilia and the bleached areas. This will lead to an apparent increase of signal intensity in the FRAP areas compared with the unbleached areas. Correction of FRAP data for loss of fluorescence in unbleached control regions was therefore omitted.

Calculation of the diffusion coefficient of GFP-α-tubulin: To determine the diffusion coefficient of GFP–α-tubulin, we followed the method described for DRC4-GFP (Wren et al., 2013). In brief, 10 videos were selected based on their kymograms which showed many trajectories of diffusing particles. Trajectories were then identified from each video using the ImageJ plug-in Mosaic Particle Tracker (Sbalzarini and Koumoutsakos, 2005). The coefficients used in the particle tracker were the following: kernel radius 2, cutoff radius 3.0, percentile 0.2, displacement 5.0, and link range 5. We calculated the mean square displacement versus time for all trajectories longer than 3 s (30 time points) according to the method of Qian et al. (1991). For the time point n, corresponding to a time $t = n\mathrm{D}T$, the mean square displacements in the x and y dimensions are calculated for each trajectory, j, as

$$\rho_{x,j}(n) = \frac{1}{N_{j,n}+1} \sum_{i=0}^{N_{j,n}} (x_{i+n} - x_i)^2$$

and

$$\rho_{y,j}(n) = \frac{1}{N_{j,n}+1}\sum_{i=0}^{N_{j,n}}(y_{i+n}-y_i)^2,$$

Where $N_{j,n}$ is the number of values calculated for the j^{th} trajectory and n^{th} time point; for shorter times, $N_{j,n}$ will be larger because there will be more pairs of points separated by n. The x and y dimensions are defined along the camera axes, not in relation to the cilia. The mean square displacement along the cilia is $\rho_j^{(n)} = \rho_{x,j}^{(n)} + \rho_{y,j}^{(n)}$. The mean square displacements for all the trajectories are then combined:

$$\rho(n) = \frac{1}{1+\sum N_{j,n}}\sum_j (N_{j,n}+1)\rho_j(n).$$

Custom programs were written in Matlab to read the trajectories produced by the Mosaic Particle Tracker and perform the above analysis.

This resulted in 64 trajectories being analyzed. A linear fit to the first six data points (the first 0.5 s) yields a slope of 3.13 ± 0.20 $\mu m^2/s$, corresponding to a 1D diffusion coefficient of 1.76 ± 0.18 $\mu m^2/s$. The uncertainty of each data point is calculated as the standard error of the mean. Similarly, we analyzed GFP–α-tubulin particles diffusing with reduced mobility in the vicinity of the ciliary tip (1D diffusion coefficient 0.2 $\mu m^2/s$ based on 58 trajectories from 12 videos). In detail, an area containing ~1 μm at the tip of the cilia was cut out. Trajectories were then identified as described for diffusion along the cilia body. We calculated

the mean square displacement versus time for all trajectories longer than 1s (corresponding to 10 time points at 10 fps). Trajectories in which the particle's mean movement was <0.1 µm in 100 ms were excluded from further analysis because these might present particles stably incorporated into the axoneme. This resulted in 58 trajectories being analyzed. A linear fit to the first six data points yields a slope of 0.3644 ± 0.044 $\mu m^2/s$, corresponding to a 1D diffusion coefficient of 0.18 ± 0.02 $\mu m^2/s$.

Immunoprecipitation of GFP–α-tubulin: Cilia were isolated from the GFP–α-tubulin–expressing strain GFP-Tub1 and a wild-type control strain, resuspended in HMEK (30 mM Hepes, 5 mM MgSO4, 0.5 mM EGTA, and 25 mM KCl) plus protease inhibitor cocktail and lysed by adding an equal volume of HMEK supplemented with 250 mM NaCl and 0.5% NP-40; axonemes were removed by centrifugation (20,000 *g*, 4°C, 10 min). The MM fractions were incubated for 1 h at 5°C with agitation with anti-GFP agarose beads (GFP-nAb; Allele Biotechnology) pretreated with 5% BSA. After several washes with HMEK supplemented with 250 mM NaCl, the beads were eluted using 1 M glycine, pH 2.5. The eluted proteins were then analyzed by SDS-PAGE followed by silver staining (Bio-Rad Laboratories) and Western blotting.

Western blotting: Flagellar proteins were separated by SDS-PAGE and transferred to PVDF membrane (Immobilon; Millipore) using standard protocols. The following primary antibodies were used: mouse anti-acetylated tubulin (clone 6-11B-1; 1:10,000; Sigma-Aldrich), mouse anti–α-tubulin (clone B-5-1-2; 1:10,000; Sigma-Aldrich), mouse anti-IC2 (1:50; King and Witman, 1990), mouse

anti-IFT81 (1:200; Cole et al., 1998), mouse anti-IFT139 (1:50; Cole et al., 1998), and mouse anti-IFT172 (1:50; Cole et al., 1998), mouse GT335 (anti-glutamylated tubulin; 1:2,000; AdipoGen), rabbit anti–α-tubulin (1:2,000; Silflow and Rosenbaum, 1981), rabbit anti-FAP12 (1:1,000; provided by D. Cole, University of Idaho, Moscow, ID), rabbit anti-GFP (1:500; Invitrogen), and rabbit anti-NAB1 (1:5,000; Agrisera). Western blots were developed using anti–mouse or anti–rabbit secondary antibodies conjugated to horseradish peroxidase (Molecular Probes) and chemiluminescence substrate (SuperSignal West Dura; Thermo Fisher Scientific). A ChemiDoc MP imaging system was used for imaging and Image Lab (both Bio-Rad Laboratories) was used for signal quantification.

Calculation of the concentration of tubulin in the ciliary matrix: The axoneme contains 11 microtubules with 13 protofilaments and 9 B-tubules with 10 protofilaments. The length of an α/β-tubulin dimer is ~8 nm and ~350,000 dimers are required to assemble one axoneme of 12-μm length. Approximately 10% of the total ciliary tubulin is in the MM fraction suggesting a total of ~380,000 tubulin dimers per cilium. Cilia have a diameter of 250 nm and the volume of a cilium of 12-μm length is 0.75 μm^3 or 0.75×10^{-15} liters. Thus, the total tubulin concentration in cilia is around 0.9 mM which is ~40× higher than the 24 μM reported for *Xenopus* egg extracts (Gard and Kirschner, 1987). Based on unstained cross sections through cilia, we estimate that the ciliary axoneme occupies ~50% of the ciliary volume; then, the tubulin concentration in the ciliary matrix is ~160 μM during steady-state. FRAP analysis of GFP-tubulin revealed a

significant increase of free tubulin in the matrix of growing cilia and Western blotting indicated that the concentration of soluble tubulin in growing cilia is about twice as high as that of steady-state cilia corresponding to ~320 μM.

For the ovoid cell bodies of *C. reinhardtii*, we estimated a volume of 251 μm3 or 2.5 × 10^13 liters, using a length of 10 μm, a height of 6 μm, and a width of 8 μm. Ciliary tubulin amounts to ~20% of the total tubulin in whole cells (~4 × 106 tubulin dimers) indicating ~3.2 × 106 dimers corresponding to a concentration of ~20 μM to be present in the cell body. However, this value is misleading because cell bodies, in contrast to most cilia, contain membrane-enclosed spaces (plastids, mitochondria, vesicles etc.) which are not accessible to tubulin. Assuming that 20% of the cellular space in *C. reinhardtii* is accessible to tubulin, the tubulin concentration would increase to 120 μM. In mammalian cells, ~30–50% of the tubulin in the cell body is soluble (Sharma et al., 2011). The microtubular cytoskeleton of *C. reinhardtii* cell bodies consists of the two flagellar-bearing basal bodies of 250-nm length with triplet microtubules, two short nascent basal bodies, 12 rootlet microtubules organized into four bundles, two consisting of 2 and two consisting of 4 microtubules, and an unknown number of socalled secondary cytoplasmic microtubules. Assuming that ~40% of the tubulin in the cell body of *C. reinhardtii* is soluble, the concentration of soluble tubulin in the cell body cytoplasm would be ~50 μM. Even taking into account that during ciliary generation some of the cytoplasmic microtubules are shortened and tubulin expression is up-regulated, we consider it unlikely that the concentration of soluble tubulin in the cell body will exceed a concentration of

320 μM calculated for the matrix of growing cilia. Although there are numerous uncertainties in this estimate, we consider the presence of a gradient in tubulin concentration from the cell body to cilium improbable. Such a gradient would be required for an efficient diffusion driven net influx of tubulin into cilia. In conclusion, active transport in the form of IFT is required to concentrate tubulin in the ciliary matrix.

CHAPTER 3

THE C-TERMINAL E-HOOKS OF α– AND β–TUBULIN ARE DISPENSABLE FOR IFT TRANSPORT[1]

[1] Craft, J.M., and Lechtreck, K.F. 2015. In preparation for publication.

3.1 Abstract

The hallmark of all cilia is the microtubular-based axoneme. Microtubules are polymers of α- and β-tubulin heterodimers. The role of the C-terminal E-hooks of α- and β-tubulin in IFT transport *in vivo* is unknown. In *Chlamydomonas*, we express GFP-tagged E-hook mutants of α- and β-tubulin. Modifications only to β–tubulin E-hook show a significant reduction in IFT transport. β–tubulin E-hook mutants display a reduction in the processivity to the tip of cilia when transported by IFT, indicative of an unstable association with the IFT particle. Expression of β-tubulin wild-type E-hook on an exogenous protein did not result in robust IFT transport. Strains that exhibit near abrogation of transport of GFP-β–tubulin reveal a major role for diffusion tubulin in contributing to axonemal incorporation. We propose that the E-hook of α– and β–tubulin are neither essential nor sufficient for IFT transport, but specifically the β–tubulin E-hook is required for proper transport.

3.2 Background

All cilia and eukaryotic flagella possess a microtubular based structural scaffold called the axoneme (Borisy and Taylor, 1967). In cilia, the microtubules provide the scaffold for axonemal complexes and are the tracks upon which IFT motors move. Axonemal microtubules grow by subunit additions at their distal plus ends and ~350,000 tubulin heterodimers are required at the site of assembly to build one 9 + 2 cilium of ~12 μm length (Euteneur and McIntosh, 1981, Johnson and Rosenbaum, 1992, Witman, 1975). Intraflagellar transport (IFT) is a ubiquitous ciliary protein translocation system and is required for ciliary assembly

(Kozminski et al., 1995, Kozminski et al., 1993). Previous studies revealed that tubulin is transported by IFT (Craft et al., 2015; Bhogaraju et al., 2013; Marshall and Rosenbaum, 2001, Hao et al., 2011).

Recent *in vitro* data revealed that IFT74 and IFT81 form a tubulin-binding module (Bhogaraju et al., 2013). IFT81 binds the globular interface between α- and β-tubulin with high specificity, while the basic N-terminus of IFT74 interacts with the highly acidic E-hook of β-tubulin with 16-fold increase in affinity via a proposed electrostatic interaction (Bhogaraju et al., 2013. To investigate the *in vivo* role of the E-hooks of α- and β-tubulin in IFT, we expressed tubulin with altered E-hooks in wild-type cells.

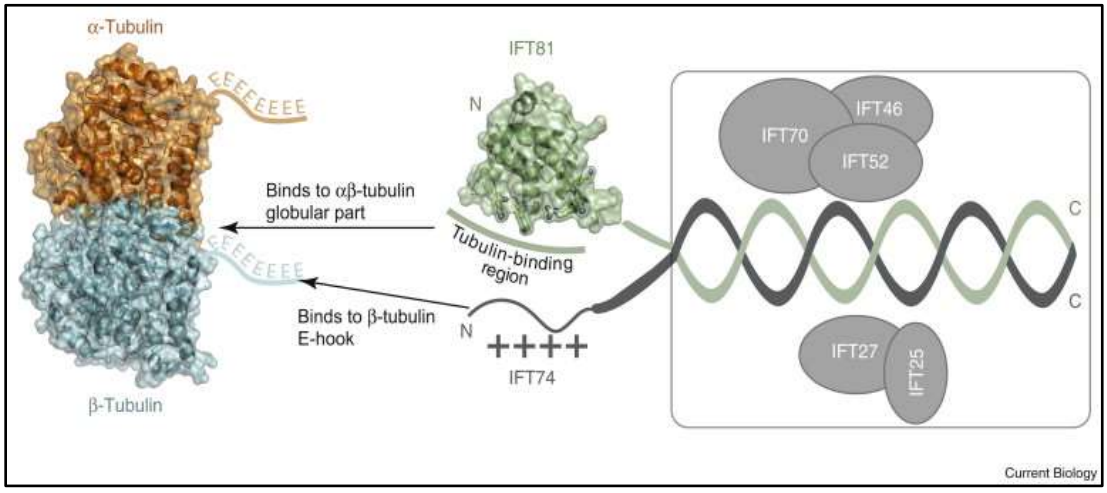

(Scholey, 2013 in reference to (Bhogaraju et al., 2013) *Science*)

3.3 Altered E-hooks of α- or β-tubulin do not perturb localization and tagged-tubulins with altered E-hooks are cargoes of IFT

E-hook modification mutant strains

To further investigate tubulin regulation in cilia, constructs were made which modified the E-hooks of α-tubulin; listed in Table II, modified α-tubulin E-

hooks were still transported by IFT and incorporated into the axoneme. Modification of the α-tubulin E-hook had no significant effect on IFT transport when compared to GFP-α-tubulin-wt-E-hook expressed at similar levels.

To explore the *in vivo* role of β-tubulin E-hook in the binding of heterodimer to the IFT particle, we constructed several β-tubulins with modified E-hooks (Table III). To determine if the specific sequence of β-tubulin E-hook was required, or just the presence of a protruding C-terminus, we constructed GFP-β-tubulin α-E-hook, where the β-tubulin E-hook was replaced with that of α-tubulin. The wild-type β-tubulin E-hook is negatively charged; to determine if this is necessary for IFT transport, we constructed GFP-β-tubulin Minus5-E-hook, where five glutamic acid residues were exchanged for neutral alanines. To investigate the interaction of tagged-tubulin without an E-hook, we constructed GFP-β-tubulin trunc-E-hook that had the 13 terminal amino acid residues removed. GFP-β-tubulin α-E-hook, GFP-β-tubulin Minus5-E-hook, and GFP-β-tubulin trunc-E-hook were expressed in *Chlamydomonas* and further analyzed.

Constructs were made in which *Chlamydomonas* did not express the transgenes. Glutamic acid residues receive post-translational modifications; to determine if these residues impact transport, we constructed GFP-β-tubulin Neg5D-E-hook that has five glutamic acid residues exchanged for aspartic acid residues; this construct retains the negative charge, but lacks glutamic acid residues that receive post-translational modifications. To explore an enhanced electrostatic interaction with IFT, we constructed GFP-β-tubulin Sugerneg4E-E-hook. This construct has 13 terminal glutamic acid residues creating a highly

negative E-hook. To examine a potential electrostatic repulsion between tubulin and IFT, we constructed GFP-β-tubulin Plus5K-E-hook; this construct has five glutamic acid residues exchanged for lysine residues to interject a positive charge on the E-hook. We failed to stably express GFP-β-tubulin Neg5D-E-hook, GFP-β-tubulin Sugerneg4E-E-hook, and GFP-β-tubulin Plus5K-E-hook.

We wondered whether the presence of β-tubulin E-hook mutants in the axoneme interferes with axonemal function and IFT transport. Strains with a mutated β-tubulin did exhibit an overall phenotype that emphasizes the importance of these E-hooks. *Chlamydomonas* with a mutated β-tubulin E-hook displayed an overall reduction in swimming speed (Fig. 13A). Further, IFT20-mCherry velocities were reduced anterogradely and retrogradely in the GFP-β-tubulin-Minus5-E-hook expressing mutant strain (Fig. 13B). We acknowledge that perturbing the E-hook of tubulins can manifest in a larger organismal phenotype, but these implications are outside of this work.

Altered E-hook mutants have similar expression and distribution to GFP-β-tubulin wt E-hook.

To determine expression levels across strains expressing GFP-β-tubulins with wild-type and mutated E-hooks, cells were fractionated and examined by western blot analysis. Anti-GFP antibodies were used in lieu of anti-β-tubulin antibodies as the vast majority recognizes epitopes of the C-terminal E-hooks. Anti-GFP stained a band of ~77kD, the proposed weight of β-tubulin with GFP (Fig.8A). Anti-NAB1 and anti-IC2 signals are used for loading control. Transgenic β-tubulins are present in similar amounts in cells (Fig. 8A).

To determine if distribution was affected in these strains, western blot analysis of dilution series was performed coupled with densitometry (Fig. 8B-C). In the three mutants analyzed, all had a similar distribution of tagged tubulin in flagella versus cell body as gathered from serial dilution of cell body (CB) sample in comparison to undiluted flagella (FLA) sample (Fig. 8 B-C). Likewise to determine if mutant E-hooks were discriminated upon being incorporated into the axoneme after being admitted into the flagellum proper, we performed another dilution series western blot (Fig. 8 D-E). We also found here that the distribution remained aligned with the wild type construct with 6.25-12.5% in the soluble membrane and matrix fraction as compared to tubulin incorporated into the axoneme (Fig. 8 D-E). Taken together, the modified E-hook does not affect the distribution of β-tubulin in cells versus cilia and ciliary matrix versus axoneme.

3.4 E-hook mutants undergo substoichiometric IFT with interruped processivity

E-hook mutants exhibit reduced frequency of anterograde transport.

The modifications to the E-hook of β-tubulin resulted in a significantly reduced frequency of transport by IFT (Fig. 9 B) with the strongest effect observed for a construct in which the terminal 13 amino acids of the E-hook was deleted (GFP-β-tubulin trunc-E-hook). This finding suggests that loading of tubulin onto IFT particles favors a stable interaction generated by the β-tubulin E-hook.

In our strains, the endogenous β-tubulin is still present and in much greater quantities than our tagged β-tubulins. Experiments with exchanging glutamic acids residues in the E-hook of β-tubulin in *Tetrahymena* resulted in

lethality when more than three subsitiutions were made in the entire tubulin pool (Xia et al., 2000). We avoid this consequence with the presence of endogenous β-tubulin. This approach allows for the expression of changes to β-tubulin that would likely be detrimental should the entire pool of tubulin be modified. Further, this provides a situation in which we can change tubulin binding to IFT without affecting ciliary assembly. We can specifically test the effect of the changes to IFT association with our mutated tagged-tubulins.

E-hook mutants undergo retrograde transport at a high frequency.

While GFP-β-tubulin wt E-hook was rarely seen undergoing retrograde transport (three retrograde events per 431 anterograde events), all of the modified E-hook mutants displayed an increased frequency of retrograde transport (Fig. 10). These quantifications were made during regeneration when tubulin is required to build the axoneme.

E-hook mutants are less likely to proceed directly to the ciliary tip.

Our preliminary data indicate that the processivity of tubulin transport by IFT is reduced causing frequent loss of tubulin cargoes from IFT trains before reaching the ciliary tip. GFP-β-tubulin wt E-hook proceeded to the tip in 97% of events. Likewise, GFP-α-tubulin wt E-hook also proceeded directly to the tip in 98% of 1,281 events (Craft et al., 2015). All modified E-hook β-tubulin constructs displayed a reduced percentage of events moving on IFT directly to the tip (Fig.11A). Representative kymograms look to show particles dissociating from IFT tracks and moving into a diffusive motion (Fig. 11B). These results

suggest that the E-hook functions in stabilizing IFT-tubulin interaction as indicated by *in vitro* studies (Bhogaraju et al., 2013).

3.5 β-tubulin E-hook is not sufficient for robust IFT transport of exogenous cargo

Next, we tested if the β-tubulin E-hook is sufficient to establish transport by IFT. To determine this, we constructed fusion constructs of green fluorescent protein with varying parts of the C-terminus of β-tubulin and expressed it in wild-type *Chlamydomonas* (Fig. 12). Our control, free GFP, readily diffused in cilia, but did not undergo IFT transport. The second construct, GFP::β-tubulin wt E-hook was observed being transported with IFT velocity to the tip of a regenerating cilium once during 21.5 minutes of observation (Fig. 12). The third construct crNeon::β-tubulin H11-12 wt E-hook utilized a brighter fluorophore and included the antiparallel helices H11 and H12 of β-tubulin. This construct was observed being transported by IFT velocity once in 17 minutes. These frequencies are ~400x less than GFP-β-tubulin. The β-tubulin E-hook permitted some interactions, but clearly not sufficient for binding to IFT. Should an exogenous cargo of IFT show high transport, that tool could be used to investigate the minimum requirements for binding to IFT and the regulation of binding sites.

3.6 Diffusion plays a major role in supplying unpolymerized tubulin for axonemal incorporation

To investigate the contributions of supplying unpolymerized tubulin to the growing tip by IFT and diffusion, we aimed to create a tubulin construct that could not undergo IFT transport. Since GFP-β-tubulin-trunc-E-hook is still transported,

so we sought to express this construct in a strain with the entire pool of IFT81 mutated in such a way that it no longer binds to the tubulin heterodimer interface. Collaborators created and graciously provided two rescue strains of the IFT81 mutant in *Chlamydomonas*: *ift81* IFT81 wild-type rescue and *ift81*IFT815E (Kubo and Witman, unpublished). *ift81*IFT815E has five glutamic acid substitutions in the conserved, basic binding domain of IFT81 to the tubulin heterodimer to disrupt this interaction (Kubo and Witman, unpublished; Bhogaraju et al., 2013).

We created strains expressing either GFP-β-tubulin- wt-E-hook or GFP-β-tubulin-trunc-E-hook in the wild-type, *ift81* IFT81, and *ift81*IFT815E backgrounds. Frequency of anterograde transport GFP-β-tubulin-trunc-E-hook in *ift81*IFT815E was reduced to 0.04 events per minute during regeneration; this strain represents a severe disruption of the IFT81/74 tubulin-binding domain.

Upon microscopy, qualitative evaluation of strains warranted further inquiry as the strain expressing GFP-β-tubulin-trunc-E-hook in *ift81*IFT815E background that rarely exhibited IFT transport of tagged-tubulin still had high levels of incorporation into the axoneme. To investigate this quantitatively, we isolated and fractionated cilia for western blot analysis (Fig. 15A). Since expression levels were lower in GFP-β-tubulin wt-E-hook in *ift81*IFT81, we evened out loading for GFP expression in whole cells and applied this loading to the remaining cellular fractions. Densitometry of the blot in Fig. 15A revealed an overall reduction in incorporation into the axoneme (Fig. 15B).

We sought to use this information to determine the relative contributions of IFT and diffusion in supplying unpolymerized tubulin to the growing tip for

incorporation into the axoneme. To this end, we factored the reduction of anterograde events in Fig. 14 (and Fig. 15E) versus the reduction of axonemal incorporation when comparing GFP-β-tubulin-wt-E-hook and GFP-β-tubulin-trunc-E-hook in wild-type, *ift81* IFT81, and *ift81* IFT815E background. In the wild-type background, we calculated a ~90% reduction in anterograde frequency resulted in only a ~16% reduction of tagged tubulin incorporated into the axoneme. In the rescue *ift81* IFT81 background, a ~90% reduction in anterograde frequency resulted in a ~25% reduction of tagged tubulin incorporated into the axoneme. In the *ift81* IFT815E background, a ~97% reduction in anterograde transport showed only a ~18% reduction. This approach suggests that diffusion likely accounts for ~80% of tubulin incorporated into the axoneme, while IFT supplements by supplying ~20% of tubulin for incorporation.

3.7 Discussion and Conclusions

The E-hook of α-tubulin or β-tubulin is not required for IFT transport. E-hook truncation mutants of both subunits of the heterodimer individually are still transported by IFT. However, defects in the E-hook of β-tubulin perturb this interaction and do not allow for proper IFT transport. Further, the E-hooks are not required for proper localization or distribution of tubulin in *C. reinhardtii* as mutants displayed near wild-type levels in cellular compartments.

Our data do corroborate *in vitro* data that the β-tubulin E-hook may function to stabilize the association of the tubulin heterodimer to the IFT particle. We observe a lack of processivity of tagged-tubulin to the tip when the β-tubulin

E-hook is mutated; this suggests that the β-tubulin E-hook is likely involved in a similar high affinity electrostatic interaction *in vivo*. However, this electrostatic interaction alone is not sufficient for robust IFT trafficking of an exogenous cargo. The high specificity interaction of IFT81 and the tubulin heterodimer may be needed to bring the β-tubulin E-hook in close proximity to the IFT74 N-terminus.

The observation of increased retrograde transport during regeneration raises the question why IFT would transport tubulin out of a growing cilium (Fig.10A-B). One possible explanation could be that some quality control measure of the axoneme recognizes the defective heterodimer with a faulty β-tubulin E-hook, and via some unknown mechanism, 'edits' the dimer out of the axoneme. Once we obtain a better understanding of the disassembly process of axonemal microtubules, the interaction of tubulin and retrograde IFT should become clearer.

Disruption of the IFT81/74 tubulin-binding module *in vivo* by expressing GFP-β-tubulin-trunc-E-hook in *ift81*IFT815E background resulted in a near complete cessation of IFT transport of tagged-tubulin, with events rarely seen. This provides *in vivo* confirmation of the IFT81/74 bipartite binding domain. However the occurrence of rare events in this strain suggests the presence of an additional tubulin-binding domain elsewhere on the IFT particle. Other plausible explanations include the rare events could have shown tagged-tubulin associating with another cargo that was in direct association with IFT or that the addition of glutamic acid residues in *ift81*IFT815E did not completely destroy the binding site. More probable is an additional tubulin-binding site as IFT54 has a

calponin-homology domain that is implicating in tubulin-binding. These experiments also revealed the unforeseen finding that diffusion is the major contributor to provide unpolymerized tubulin for axonemal incorporation. If IFT were the main contributor in supplying soluble unpolymerized tubulin for axonemal incorporation, we would expect to see a dramatic reduction of tagged tubulin in the axoneme when we disrupt transport so severely. Since we see only a moderate reduction in axonemal incorporation, we propose that diffusion likely supplies the majority of tubulin for axonemal microtubule growth and IFT works to insure this critical concentration is met to simultaneously build these complex microtubules. Diffusion is likely how microtubule assemblies of the cell body polymerize and IFT may be required to supplement this passive accumulation given the small volume of the cilium.

To further explore the interaction of α/β tubulin with the IFT particle, we will use a multipronged approach. 1) Observe our new constructs modulating the overall charge of the β-tubulin E-hook to determine the importance of this proposed electrostatic interaction *in vivo*. These constructs will perturb the interaction as follows: Neg5D will retain a negative charge that cannot undergo proper posttranslational modifications, SuperNeg4E will increase the negative charge of the E-hook, and Plus5K will interject positive charges on the E-hook. 2) We expect to gain further insight by generating double expressing tubulin strains, e.g. mCherry-β-tubulin-wt-E-hook coupled with GFP-β-tubulin-trunc-E-hook. In the context of a single cell, we hope to gain clarity as to the degree and nature of IFT transport discrimination and disruption of processivity.

3) We will proceed examining varying fluorescent protein fusion constructs to try to determine a fragment that is sufficient to drive robust IFT transport of an exogenous protein. This approach will give further understanding to loading and binding of cargoes to IFT particles.

Table II: Modifications of wild type and various mutations on α-tubulin

The table shows the C-terminal sequences of wild-type and the modified α-tubulin molecules. Transport velocities by anterograde IFT and qualitative assessment of axonemal incorporation of the strains are listed.

Table II: Modifications of wild type and various mutations on α-tubulin

Name of variant	Amino acids (positions 428-451)	Axonemal incorporation	IFT velocity(μm/s)
sfGFP-TUA2	LEKDFEEVGAAESAEGAGEGEGEEY	yes	2.09±0.35
sfGFP-minusE	LEKDFAAVGAQSAQGAGAGAGAEY	yes	1.83±0.36
sfGFP-deltaC	LEKDFEEVGAEY	yes	2.04±0.43
sfGFP-betaC	LEKDFQQYQDASAEEEGEFEGEEEEAEF	yes	2.29±0.57

Table III: Modifications of wild type and various mutations on β-tubulin

The table shows the C-terminal sequence of wild-type and the modified β-tubulin molecules. Transport velocities by anterograde IFT and qualitative assessment of axonemal incorporation of the strains are listed.

Table III: Modifications of wild type and various mutations on β-tubulin

Name of variant	Amino acids (positions 429-443)	Axonemal incorporation	IFT velocity (μm/s)
sfGFP-WT	SAEEEGEFEGEEEEA	yes	2.11 ± 0.46
sfGFP-α-end	SAEGAGEGEGEEY	yes	2.13 ± 0.44*
sfGFP-Minus5	SAEEEGAFAGAAAEA	yes	1.95 ± 0.49*
sfGFP-trunc-end	SA	yes	2.29 ± 0.45*
sfGFP-Neg5D	SAEEEGDFDGDDDEA		
sfGFP-Superneg4E	SAEEEEEEEEEEEEE		
sfGFP-Plus5K φ	SAEEEGKFKGKKKEA		

*denotes atypical transport
φ unstable expression

acidic basic

3.8 Figures

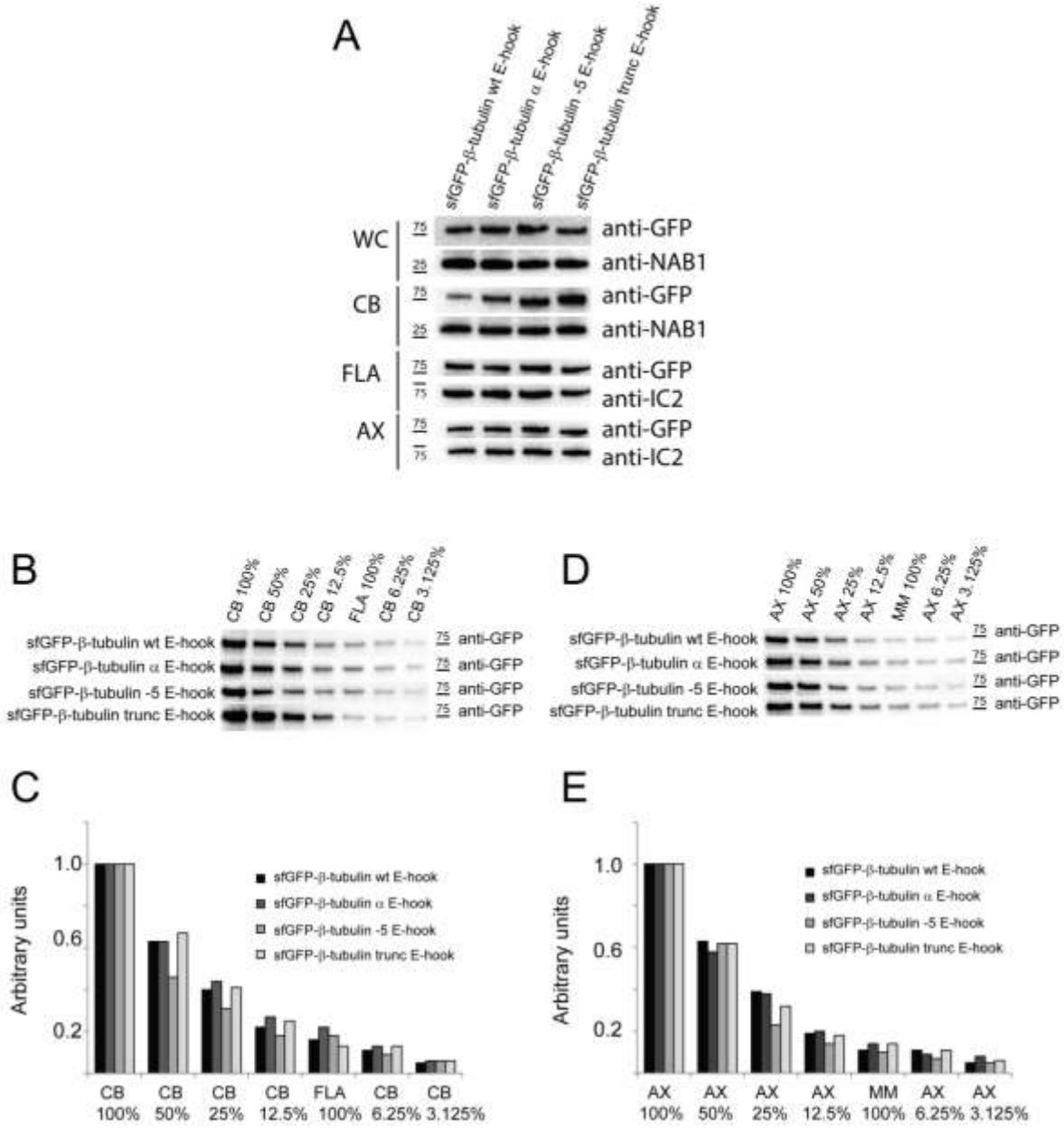
A
sfGFP-β-tubulin wt E-hook
sfGFP-β-tubulin α E-hook
sfGFP-β-tubulin -5 E-hook
sfGFP-β-tubulin trunc E-hook
WC
CB
FLA
AX
anti-GFP
anti-NAB1
anti-IC2
75
25
B
CB 100%
CB 50%
CB 25%
CB 12.5%
FLA 100%
CB 6.25%
CB 3.125%
D
AX 100%
AX 50%
AX 25%
AX 12.5%
MM 100%
AX 6.25%
AX 3.125%
C
E
Arbitrary units
1.0
0.6
0.2
CB 100%
CB 50%
CB 25%
CB 12.5%
FLA 100%
CB 6.25%
CB 3.125%
AX 100%
AX 50%
AX 25%
AX 12.5%
MM 100%
AX 6.25%
AX 3.125%

Figure 8: β–tubulin E-hook mutants show similar expression and distribution to tagged β-tubulin wt E-hook (A) Western blot analysis of β-tubulin wt E-hook and three E-hook mutants, all expressing sfGFP. Whole cells (WC), cell bodies (CB), isolated cilia (FLA), and axonemes (AX) were loaded and probed with antibodies to GFP. NAB1 and IC2 signals were used as loading controls. (B) Western blots probed with anti-GFP showing different dilutions of the cell body (CB) sample in comparison to the undiluted cilia sample (FLA). (C) Densitometry from blot in B. (D) Western blot showing a dilution series of axonemes (AX) and undiluted MM of β-tubulin wt E-hook and three E-hook mutants to determine the distribution of tagged tubulins inside cilia. The blot was probed with antibodies to GFP. (E) Densitometry from blot in D.

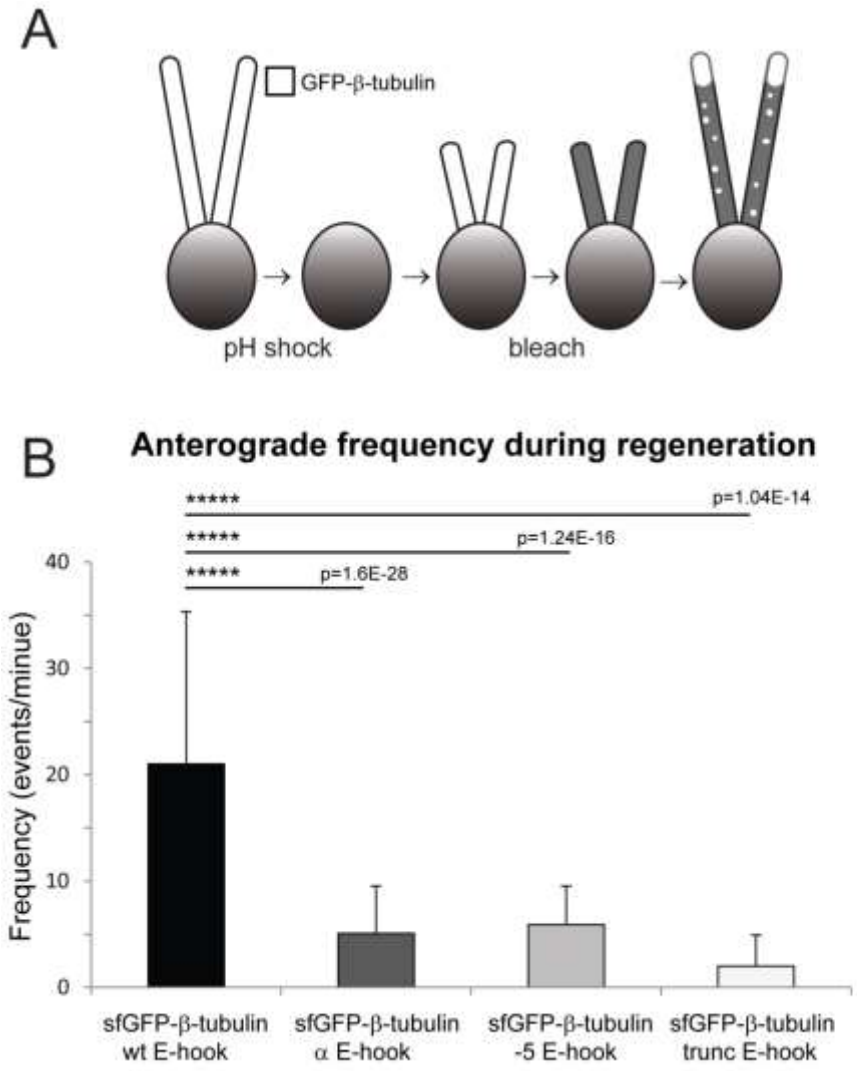

Figure 9: Anterograde frequency is substoichmetric in E-hook mutants. (A) Schematic presentation of the experimental design. Cells were deciliated via pH shock and then allowed to partially regenerate their cilia. Next, cilia were bleached completely to allow for observation of unbleached tagged β-tubulin entering cilia. (B) Mean frequency of GFP-β-tubulin wt E-hook and three tagged E-hook mutants transport events by anterograde IFT during regeneration. Error bars indicate SEM.

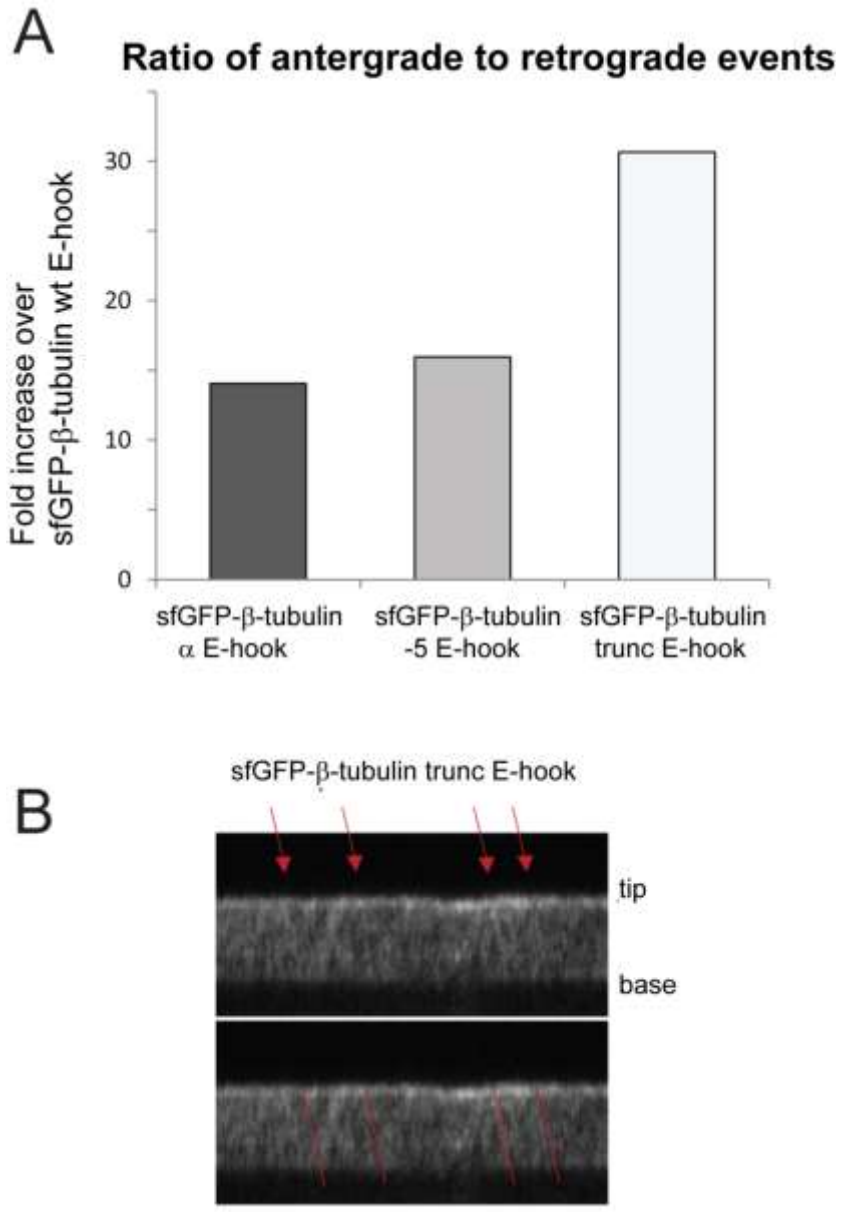

Figure 10: β-tubulin E-hook mutants undergo more retrograde transport. (A) Ratios of anterograde to retrograde movements were made for wild type E-hook and each E-hook mutant. Graph in A shows fold increase for each E-hook mutant over wt E-hook. (B) Representative kymogram of GFP-β-tubulin-trunc E-hook during regeneration. Retrograde tracks are indicated by red arrows in top kymogram and trajectories are traced in red in duplicate kymogram below.

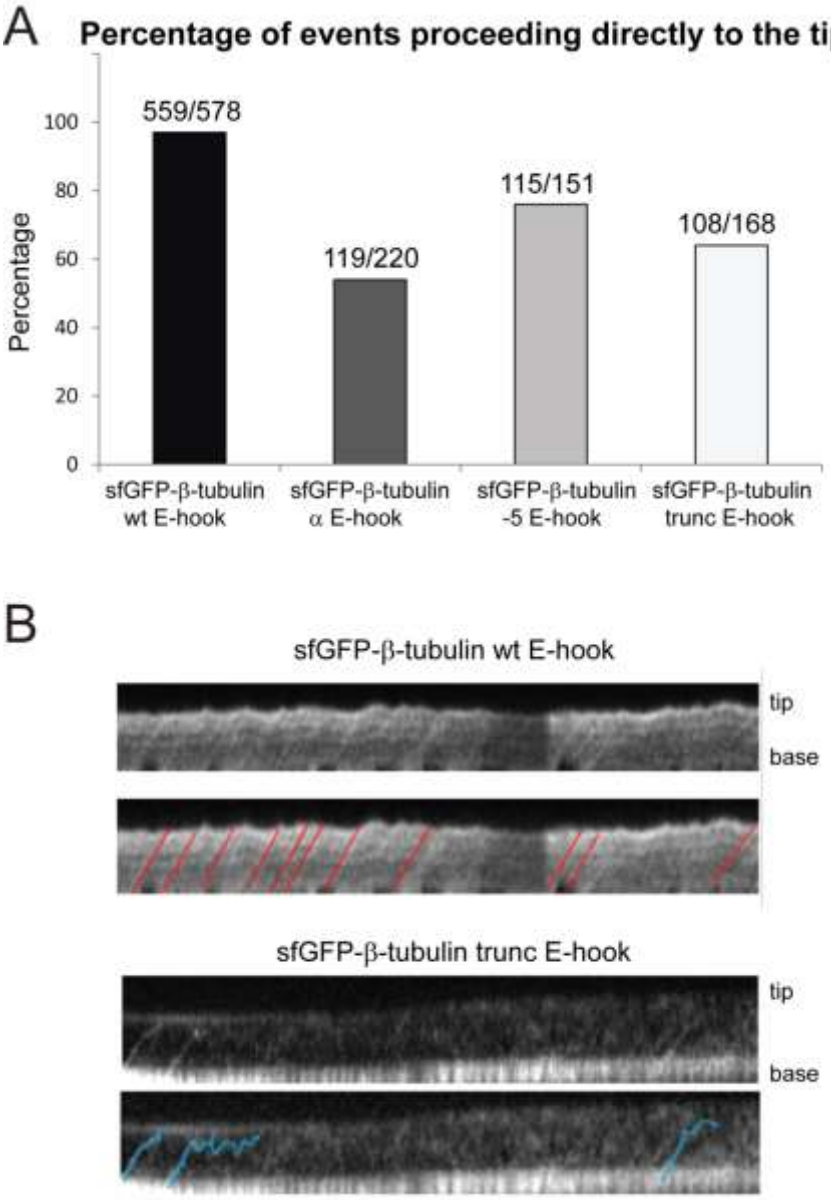

Figure 11: E-hook mutants display reduced processivity to the tip. (A) Quantification of trajectories moving directly to the tip displayed in percentages. Raw numbers for each strain are above the bars. (B) Representative kymograms from GFP-β-tubulin wt E-hook depicting events proceeding to the tip. Trajectories are outlined in red below. In the representative kymogram below,

GFP-β-tubulin trunc E-hook is shown dissociating from IFT-like trajectories before reaching the tip. Trajectories are outline in blue at bottom.

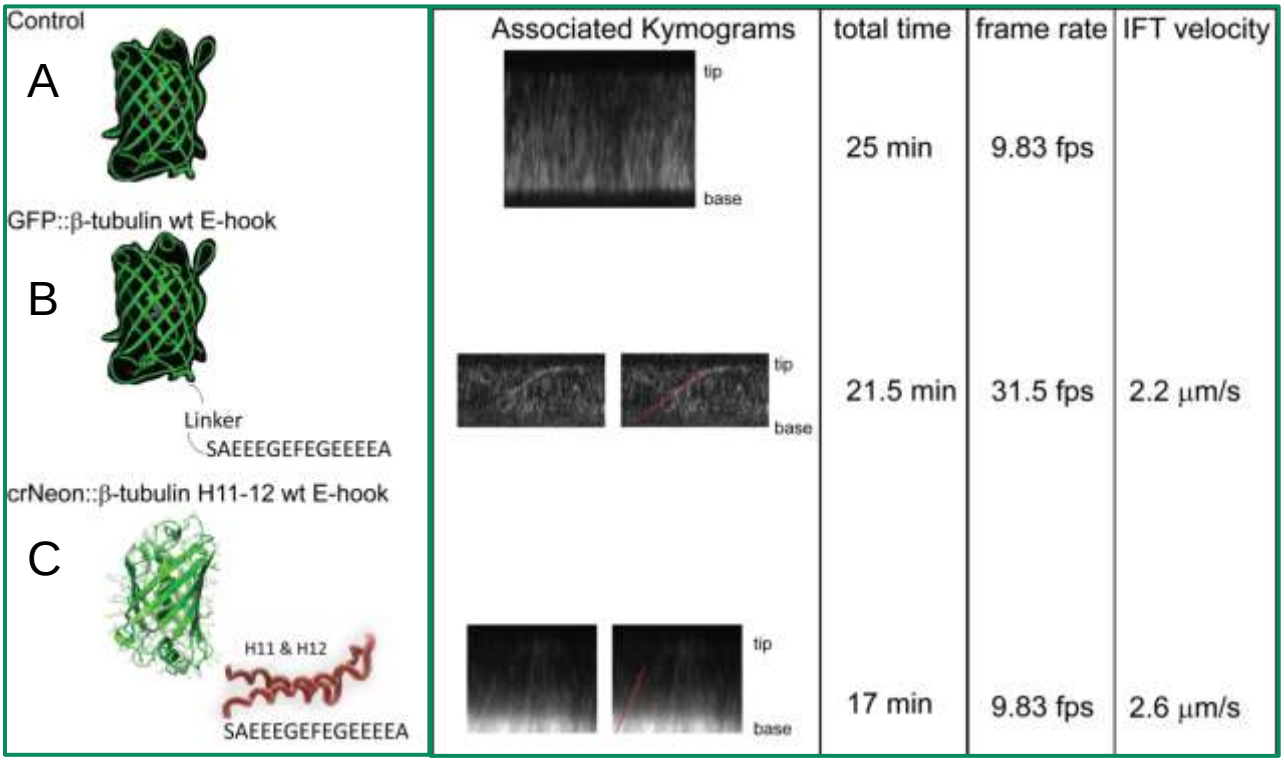

Figure 12: β-tubulin E-hook is not sufficient to drive robust IFT transport of an exogenous cargo. (A) Control GFP diffuses into cilia and does not undergo IFT transport. (B) Construct one introduced the wildtype β-tubulin E-hook to GFP and was observed in cilia. Kymogram depicts one trajectory with IFT-like velocity. (C) Construct two introduced anti-parallel helices H11 and H12 with wild type β-tubulin E-hook wildtype β-tubulin E-hook to crNeon. Kymogram depicts one trajectory with IFT velocity.

A

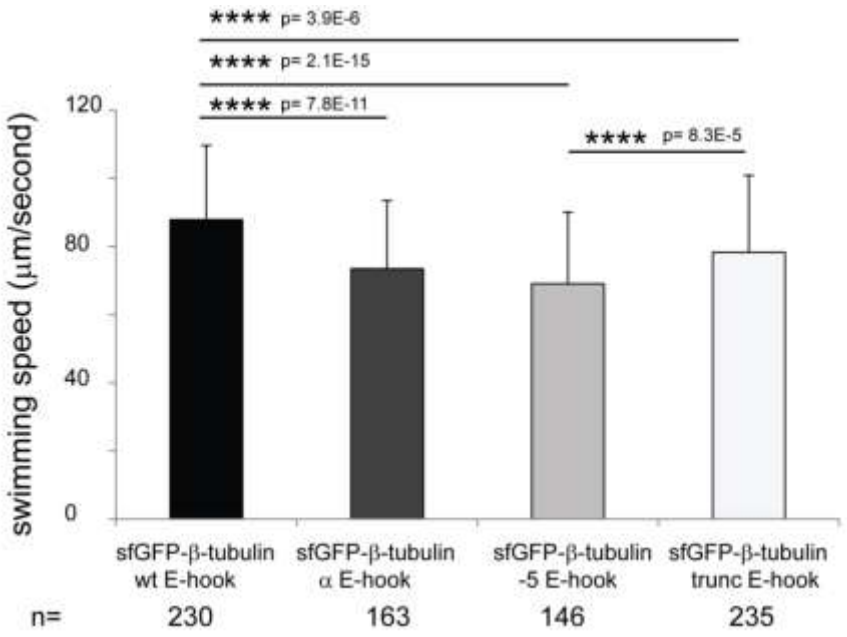
**** p= 3.9E-6
**** p= 2.1E-15
**** p= 7.8E-11
**** p= 8.3E-5
swimming speed (µm/second)
120
80
40
0
sfGFP-β-tubulin wt E-hook
sfGFP-β-tubulin α E-hook
sfGFP-β-tubulin -5 E-hook
sfGFP-β-tubulin trunc E-hook
n=
230
163
146
235

B

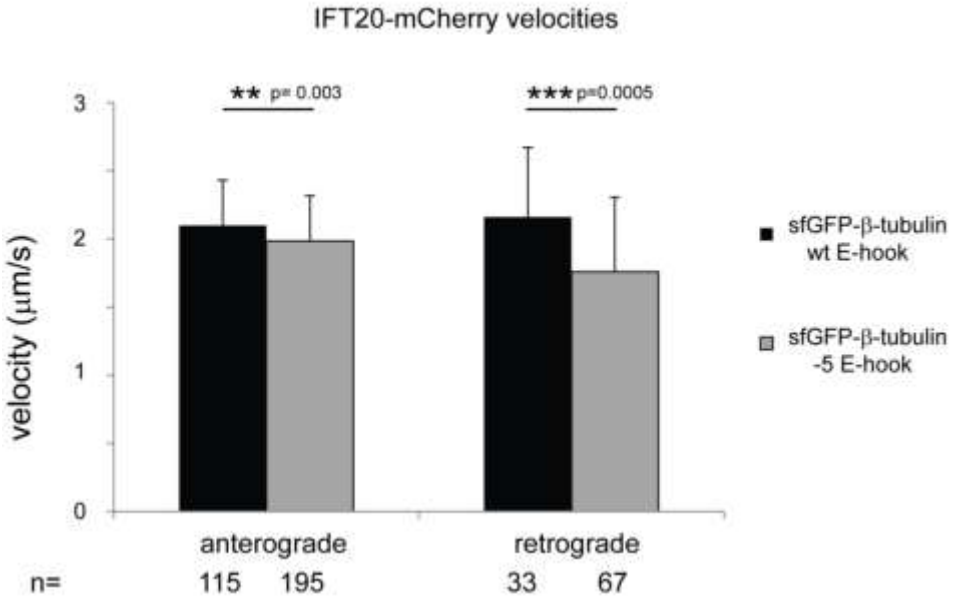
IFT20-mCherry velocities
** p= 0.003
*** p=0.0005
velocity (µm/s)
3
2
1
0
anterograde
retrograde
n=
115
195
33
67
sfGFP-β-tubulin wt E-hook
sfGFP-β-tubulin -5 E-hook

Figure 13: E-hook mutants display reduced swimming speed and IFT velocity.

(A) Overall swimming speed for each strain was calculated and compared to GFP-β-tubulin-wt-E-hook. All E-hook mutants had a statistically significant reduction of overall *Chlamydomonas* swimming speed. (B) The most severe disruption in (A) was then examined for IFT velocities in two-color expressing strains: GFP-β-tubulin- wt-E-hook *ift20* IFT20-mCherry and GFP-β-tubulin-trunc-E-hook *ift20* IFT20-mCherry. A significant reduction of IFT velocity was seen for anterograde and retrograde movements.

A

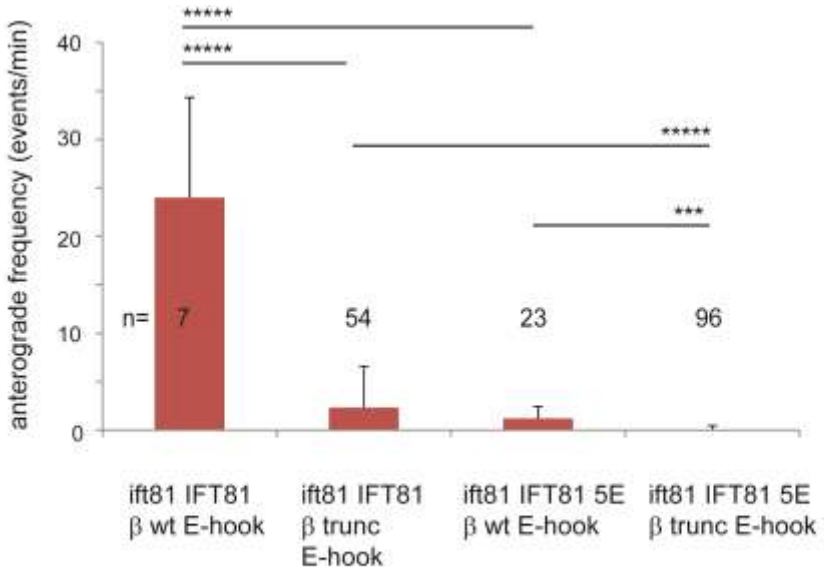
*****
*****
*****
***
anterograde frequency (events/min)
40
30
20
10
0
n=
7
54
23
96
ift81 IFT81
β wt E-hook
ift81 IFT81
β trunc
E-hook
ift81 IFT81 5E
β wt E-hook
ift81 IFT81 5E
β trunc E-hook

B

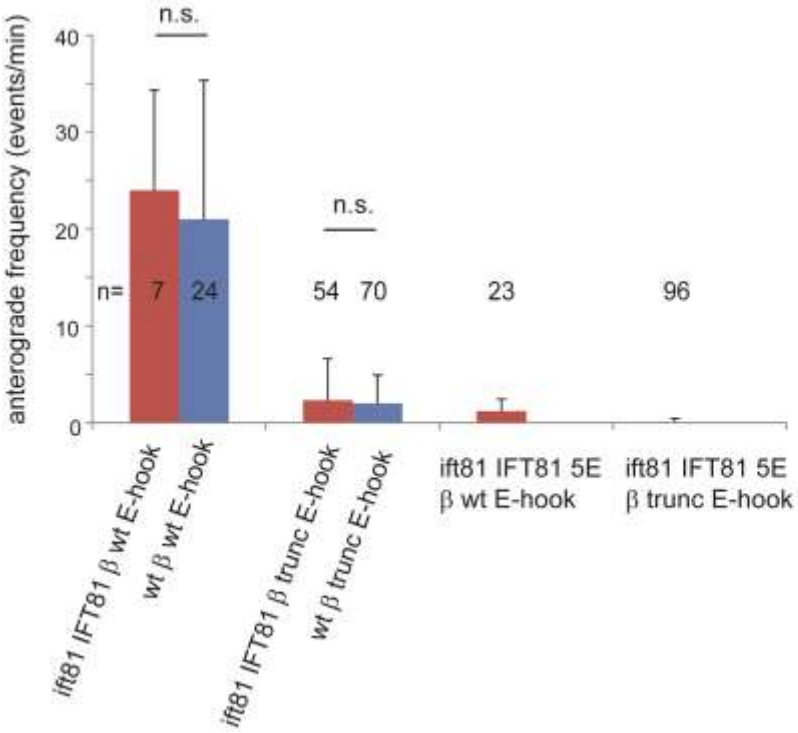
n.s.
n.s.
anterograde frequency (events/min)
40
30
20
10
0
n=
7
24
54
70
23
96
ift81 IFT81 β wt E-hook
wt β wt E-hook
ift81 IFT81 β trunc E-hook
wt β trunc E-hook
ift81 IFT81 5E
β wt E-hook
ift81 IFT81 5E
β trunc E-hook

Figure 14: Anterograde transport frequency is near abrogation in absence of IFT81/74 tubulin-binding module. (A) Mean frequency of GFP-β-tubulin wt E-hook and GFP-β-tubulin trunc-E-hook transport events by anterograde IFT during regeneration. Error bars indicate SEM. (B) Same data with inclusion of GFP-β-tubulin wt-E-hook and GFP-β-tubulin-trunc-E-hook transport events by anterograde IFT during regeneration in wild-type backgrounds for comparison.

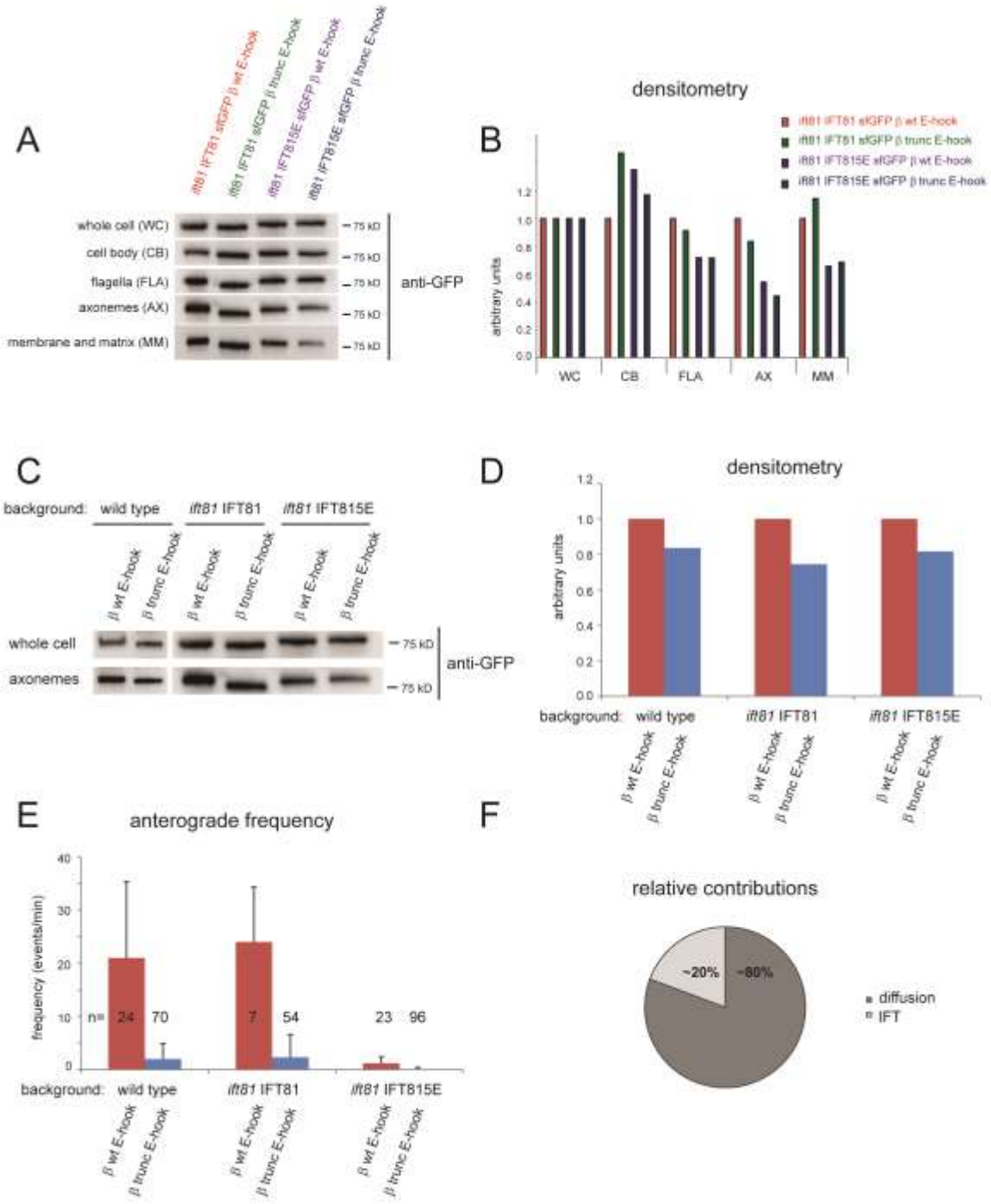
A
ift81 IFT81 sfGFP β wt E-hook
ift81 IFT81 sfGFP β trunc E-hook
ift81 IFT815E sfGFP β wt E-hook
ift81 IFT815E sfGFP β trunc E-hook
whole cell (WC)
cell body (CB)
flagella (FLA)
axonemes (AX)
membrane and matrix (MM)
75 kD
anti-GFP
B
densitometry
arbitrary units
WC
CB
FLA
AX
MM
C
background: wild type
ift81 IFT81
ift81 IFT815E
β wt E-hook
β trunc E-hook
whole cell
axonemes
anti-GFP
D
densitometry
arbitrary units
E
anterograde frequency
frequency (events/min)
n=
24
70
7
54
23
96
F
relative contributions
~20%
~80%
diffusion
IFT

Figure 15: Diffusion contributes the majority of unpolymerized tagged-β-tubulin incorporated into the axoneme.

(A) Western blot comparing distribution of tagged-β-tubulin in various cellular compartments. Whole cells (WC), cell bodies (CB), isolated cilia (FLA), axonemes (AX), and membrane and matrix (MM) fractions were loaded and probed with antibodies to GFP. The bands correspond to tagged-β-tubulin. Loading was adjusted for equal amounts of GFP expression in whole cells based on anti-GFP staining. (B) Quantitative analysis via densitometry of the amount of tagged-β-tubulin in cellular fractions based on the blot shown in A and band intensities were normalized for whole cell GFP loading. (C) Western blot comparing distribution of tagged-β-tubulin wt E-hook versus tagged-β-tubulin trunc E-hook in three different genetic backgrounds, including the two backgrounds shown in A; fractions of whole cell and axonemes were probed with antibodies to GFP. The bands correspond to tagged-β-tubulin. Loading was adjusted for equal amounts of GFP expression per pair in whole cells based on anti-GFP staining. (D) Quantitative analysis via densitometry of the amount of tagged-β-tubulin in axonemes based on the blot shown in C to determine reduced amounts of tagged β-tubulin trunc E-hook in each background as compared to tagged β-tubulin wt E-hook. (E) Anterograde frequency of tagged-β-tubulin transport per each pair of tagged β-tubulins in three genetic backgrounds. (F) Approximate contributions of IFT and diffusion in supplying unpolymerized tagged-β-tubulin for axonemal incorporation. Relative contributions were determined by factoring the reduction of anterograde events in

E and Fig.14 versus the reduction of axonemal incorporation when comparing GFP-β-tubulin wild-type-E-hook and GFP-β-tubulin trunc-E-hook in both three genetic backgrounds in D. See Material and Methods for calculations.

3.9 Material and Methods

Strains and culture conditions: *C. reinhardtii* cultures were maintained in modified M medium and aerated at room temperature with 0.5% CO_2 with a light/dark cycle of 14:10 h.

Generation of transgenic strains: The vector pBR25 encoding sfGFP–α-tubulin (Craft et al, 2015) was used to generate β-tubulin constructs. β-tubulin gene was synthesized (Genewiz); α-tubulin was then replaced with β-tubulin. β-tubulin E-hook mutant constructs were prepared as follows: gene segments encoding the modified C termini of β-tubulin were synthesized by Genewiz, excised with EcoRI and EcoRV, and ligated into pBR25-sfGFP vector digested with the same enzymes. Plasmids were restricted with KpnI and XbaI, and the gel-purified fragment encompassing the functional cassette was transformed into *C. reinhardtii* by electroporation. TAP plates 10 μg/ml zeocin were used to select transformants. Transformant colonies were picked and cultivated in a 96-well plate in liquid media. Positive transformants were assessed via TIRF microscopy for fluorescence. The *ift20-1* IFT20-mCherry strain was generated by expressing the coding region of *IFT20* fused to mCherry under the control of the *FLA14* promoter in the *ift20-1* deletion mutant (Lechtreck et al., 2009); for IFT velocity

analysis the rescued *ift20-1* IFT20-mCherry strain was transformed again with the pBR-GFP–β-tubulin expression plasmid.

Isolation and fractionation of cilia: To biochemical analyze cilia, a protocol for cilia isolation described by Witman (1986) was used. In brief, various strains were concentrated and washed with 10 mM Hepes, pH 7.4. Cells were resuspended in HMS (10 mM Hepes, 5 mM MgSO4, and 4% sucrose) and deciliated via of addition dibucaine to a final concentration of 4.17 mM (Sigma-Aldrich). Cilia and cell bodies were separated by differential centrifugations and cilia were collected by sedimentation (17,000 *g*, 4°C, 20 min). Isolated cilia were resuspended in a microtubule-stabilizing buffer, HMEK (30 mM HEPES, 5 mM MgSO4, 0.5 mM EGTA, and 25 mM KCl) plus protease inhibitor (P9599; 1:100; Sigma-Aldrich) and demembranated by addition of 1% NP-40 Alternative (final concentration; EMD Millipore) on ice for 20 min. Axonemes were pelleted from membrane/matrix fraction by centrifugation (30,000 *g*, 4°C, 20 min) and fractions were analyzed by SDS-PAGE and Western blotting.

Ciliary regeneration: Cells were washed and resuspended in M media, then deflagellated by pH shock, transferred to fresh M medium, and allowed to regrow cilia under constant light with agitation (Lefebvre, 1995). To delay the onset on regeneration, cells were kept on ice until needed. To initiate regeneration, cells were then washed into room temperature M media.

TIRF microscopy*:* A microscope (Eclipse Ti-U; Nikon) equipped with 60× NA1.49 TIRF objective and through-the-objective TIRF illumination provided by a 40-mW 488-nm and a 75-mW 561-nm diode laser (Spectraphysics) was used for

real-time *in vivo* imaging (Lechtreck, 2013). The excitation lasers were cleaned up with a Nikon GFP/mCherry TIRF filter and the emission was separated using an Image Splitting Device (Photometrics DualView2 with filter cube 11-EM). Observation chambers were constructed by drawing a ring of vacuum grease on a 24 x 60 mm no. 1.5 coverslip; cells were seeded inside this circle. To close the chamber a 22 × 22 mm no. 1.5 cover glass with ~10 µl of 5 mM Hepes, pH 7.3, 6.25 mM EGTA was inverted onto the larger coverslip. Cells were imaged through the large cover glass at room temperature. Images were recorded at 10–31 fps using an iXON3 (Andor) and the NIS-Elements Advanced Research software (Nikon). ImageJ (National Institutes of Health) with the LOCI plugin (University of Wisconsin, Madison WI) and multiple kymogram plugin (European Molecular Biology Laboratory) were used to generate kymograms as described in Lechtreck (2013). For photobleaching of the entire cilia, the intensity of the 488-nm laser was increased to 10% or more for 4–12 s. Partial bleaching of the cilia was achieved by using a focused 488-nm laser beam in epifluorescence; near complete bleaching of a 3-µm diameter region was accomplished in 50–300 ms.

Western blotting: Ciliary proteins were separated by SDS-PAGE and transferred to PVDF membrane (Immobilon; Millipore) using standard protocols. The following primary antibodies were used: mouse anti-IC2 (1:50; King and Witman, 1990), rabbit anti-GFP (1:500; Invitrogen), and rabbit anti-NAB1 (1:5,000; Agrisera). Western blots were developed using anti–mouse or anti–rabbit secondary antibodies conjugated to horseradish peroxidase (Molecular Probes) and chemiluminescence substrate (SuperSignal West Dura; Thermo

Fisher Scientific). A ChemiDoc MP imaging system was used for imaging and Image Lab (both Bio-Rad Laboratories) was used for signal quantification via densitometry.

Calculation of IFT and diffusion contribution to axonemal incorporation:

		Frequency (events/min)	% reduction in freq (vs wt)		Densitometry Axonemes	% reduction in incorporation (vs wt)
wt/βwt		21			1	
wt/βtrunc		2.01	=100-(2.01/21*100)= -90.43		0.8365	=100-(0.8365/1*100)= -16.35
81R/βwt		24			1	
81R/βtrunc		2.33	=100-(2.33/24*100)= -90.28		0.745	=100-(.745/1*100)= -25.5
5E/βwt		1.22			1	
5E/βtrunc		0.04	=100-(0.04/1.22)= -96.72		0.8171	=100-(.8171/1*100)= -18.29
			Theoretic 100% reduction in IFT transport			=(100*16.35/90.43)=18.08 =(100*25.5/90.28)=28.245 =(100*18.29/96.72)=18.91 =(18.08+28.245+18.91)/3= 21.813 ~22% from IFT ~78% from diffusion

CHAPTER 4

CONCLUSION AND FUTURE DIRECTIONS

In my graduate work, I have analyzed how tubulin, the major protein of cilia and flagella, is transported into and inside cilia. I provide direct evidence that α-tubulin is a cargo of IFT and cells regulate the amount of tubulin entering cilia in a length dependent manner. Two color *in vivo* imaging showed that IFT trains were largely occupied with tubulin during growth and ran essentially empty, with respect to tubulin during non-growth states. This observation suggests the presence of a mechanism that can modulate the amount of cargo transported by IFT trains. In addition, we showed that this regulation of loading occurs in a cilium-autonomous manner, i.e., when growing and non-growing cilia are present on the same cell tubulin transport by IFT will be only elevated in the growing cilium. Hitherto, a great source of debate in the field has centered around the concept of if the cell "knows" when they have cilia and if they are growing or non-growing. These data corroborate the notion that cells can "sense" the state of their cilia and actively regulate cargo transport by IFT into one cilium or the other, all without the use of a traditional localization signal. We posit this regulation could be achieved by either an increased permeability in the transition zone, which is the barrier between the cell body and cilium proper, or perhaps more

likely an increased loading of IFT particles with ciliary cargoes specifically at basal bodies with a cilium that is too short.

4.1 Cilia assembly: logistics of building a cellular high-rise

Abstract

Cilia and eukaryotic flagella are devoid of ribosomes and a dedicated protein shuttle, intraflagellar transport (IFT), supplies them with proteins. Recent direct imaging of cargo flux inside cilia revealed that the amount of structural proteins carried by IFT is regulated in response to changes in ciliary length. A correct length is critical for the motile and sensory functions of cilia and deviant length has been linked to cilia-related disease. Here we discuss how cells might regulate the amount of protein transport by IFT to ensure the desired length of cilia.

Cilia and flagella: cellular high-rises

Any building project requires a supply of precursor materials. The construction of a high-rise presents extra challenges because materials not only have to be brought to the building site but also be moved up to the ever more distant end of growth, requiring special equipment. Cilia and flagella (interchangeable terms) are cellular ‘high-rises’, thin projections with a diameter of 200 nm extending several microns from the cell surface. The ciliary membrane is continuous with the plasma membrane. While not membrane-bound organelles, cilia still are partially isolated from the cell body by the transition zone (TZ), an ultrastructural region at the base of the cilium, which is thought to function as a barrier limiting access of proteins into the organelle

(Czarnecki and Shah, 2012). Because cilia are devoid of ribosomes, ~600-1000 distinct ciliary proteins must be transported into the organelle during assembly; many of these proteins are highly enriched in cilia compared to the cell body (Pazour et al., 2005). The axoneme, the microtubular scaffold of cilia, grows by addition of subunits to its distal end (Witman, 1975). Thus, cilia assembly requires logistics for selecting proteins for admission into the organelle and transporting them to the distal growing end. A major role in this feat is played by intraflagellar transport (IFT), which picks-up ciliary precursors in the cell body and delivers them to the ciliary tip (Rosenbaum and Witman, 2002). So when building a cilium, how does the cell manage the logistics of what proteins, when, and how much of them to transport?

IFT – the ciliary freight elevator

IFT is the bidirectional movement of multi-megadalton protein arrays (=IFT trains) along the axonemal microtubules (Kozminkski et al., 1993). IFT trains, composed of IFT A and B, sub-complexes composed of 6 and 16 specific particle proteins, are the primary cargo of IFT motors. (Cole and Snell, 2009). The IFT trains serve as adaptors for proteins that require transport into and out of cilia. IFT is thought to have evolved from coatomer-like progenitors; some IFT particles structurally resemble COPI, COPII, and clathrin coats and, further, have some degree of sequence homology (Jekely and Arendt, 2006). In the first leg of the journey, anterograde IFT trains move from the ciliary base to the tip using the molecular motor kinesin-2; in the second leg, retrograde IFT trains return to the cell body pulled by IFT dynein. Genetic analyses indicate that anterograde IFT is

generally required for the assembly of cilia. Direct imaging revealed that IFT trains transport axonemal proteins from the cell body to the ciliary tip, where most cargoes are released presumably because the anterograde trains dissolve and reorganize into retrograde trains (Buisson et al., 2012; Wren et al., 2013). Among the confirmed cargoes of IFT is tubulin, the major structural protein of cilia (Craft et al., 2015; Hao et al., 2011). IFT is a novel type of tubulin interactor functioning in dimer transport. IFT does not only deliver building materials during cilia growth, but also is required for ciliary maintenance, signaling, and protein export.

Size matters: regulation of protein delivery and ciliary length

Having established that IFT functions as a protein shuttle, the question arises how this transport is regulated. Conceivably, reduced protein supply could result in shorter cilia; conversely, too much material might cause cilia to exceed their set length. Ciliary length is typically tightly regulated depending on the cell type, and the length is important for ciliary function: Mutations that affect ciliary length reduce swimming speed in protists and cause disease in mammals (Barsel et al., 1988; Ko et al., 2010).

How cells regulate ciliary length is a field of intense discussion. Cells could employ more or faster IFT trains, each carrying a fixed load while cilia grow, and downsize the system once cilia have reached their usual length (Fig. 8A). However, the amount and velocity of IFT trains in cilia are largely constant and independent of cilia length (Marshall et al., 2005). Still, cells could establish cilia of a fixed length without regulating the load carried by IFT trains (Marshall

and Rosenbaum, 2001). Returning to the high rise analogy, consider a situation in which the number and velocity of freight elevators is fixed and each car carries the same amount of building material. The larger the structure gets, the more time the cars will spend in transit causing the rate at which material reaches the tip to decrease and therefore, an overall reduction in the rate at which the structure elongates. Biological structures are seldom static and axonemes will continually lose material from the distal end. Assuming that the disassembly is constant and length independent, cilia assembly and disassembly will be equal at one point, the balance point (Fig. 16B). Thus, ciliary length could be maintained simply by fixing the number of IFT trains and their velocity without changing the cargo load or measuring the length of the organelle. *In vivo* imaging, however, showed that IFT trains are highly loaded with tubulin and other axonemal cargoes while cilia grow but largely devoid of these proteins once cilia reach their steady state length (Craft et al., 2015; Wren et al., 2013). Cells apparently regulate the amount of cargo present on a given IFT train in a ciliary-length dependent manner. Together with other factors (e.g. ciliary disassembly), differential cargo loading of IFT likely contributes to ciliary length regulation.

Does the size of the stockpile regulate what is transported into cilia?

The observation that the degree of cargo occupation of IFT trains varies raises the question how cells regulate IFT load. This could be achieved by regulating cargo supply in the cell body (Chan and Marshall, 2012; Goehring and Hyman, 2012). Revisiting the high-rise example, as long as plenty of building material is available at its base, the elevators will be fully loaded but when the

material is used up they will run empty and elongation of the structure will cease (Fig. 16C). Cells, however, still maintain a decent-sized pool of ciliary precursors even after cilia are fully grown raising the question why this material is not used to further elongate the cilia (Rosenbaum et al., 1969). Notably, the precursors pool will be used to assemble new cilia of about half-length when cilia are lost and new protein synthesis is prevented (Lefebvre et al., 1978).

We generated cells possessing both growing and non-growing cilia either by amputating just one of the two cilia from *Chlamydomonas* cells or by fusing cells with full-length cilia to cells possessing short growing cilia. Despite originating from the same cell body with a given concentration of cargo, trains entering the growing cilia were highly loaded with tubulin while those moving inside the non-growing cilia were essentially devoid of tubulin (Craft et al., 2015). This observation has far-reaching implications: First, cells must have a sensory system to identify cilia that are too short, and second, this information must be processed so that trains entering the short cilia are highly loaded with building material while those entering the neighboring non-growing cilia are not. Thus, cilium length impacts how much cargo is entering via IFT, generating a feedback loop (Fig. 16D).

Who is the architect?

Now we know there is an architect on site who knows the desired size of the structure and accordingly regulates the loading of the elevators. Numerous models of how cells could measure ciliary length exist (Ludington et al., 2013). Particularly valuable are mutations that affect ciliary length to elucidate the

molecular mechanism. These include defects in MAP (LF4p/DYF-5/MOK/ICK) and CDK-related protein kinases (LF2p/DYF-18/CCRK, LF5p/CDKL5) which in various systems result in abnormally long cilia (Bengs et al., 2005; Berman et al., 2003; Broekhuis et al., 2014; Burghoorn et al., 2010; Tam et al., 2013; Tam et al., 2007). *Chlamydomonas lf2* mutants are unable to down-regulate tubulin transport frequency after their cilia have exceeded wild-type length (Craft et al., 2015). IFT kinesin-2 is phosphorylated by intestinal cell kinase (ICK) establishing a direct link between length regulating kinases and the protein-transporting IFT (Broekhuis et al., 2014; Chaya et al., 2014). A calcium-dependent kinase apparently regulates the binding of kinesin-2 motors to IFT particles, which could kick-start train assembly and cargo loading or regulate the dwell time of trains at the ciliary base (Liang et al., 2014). Hypothetically, length-regulating kinases could function as biochemical timers: Kinase activity might be regulated proportional to the time they spend passing via IFT through cilia, i.e., because they encounter regulatory phosphatases or kinases distributed along the cilium; since IFT velocity is essentially constant, the activity of kinases returning to the cell body would reflect ciliary length. Indeed, the phosphorylation state of the aurora protein kinase CALK, which is located in the cell body and functions in ciliary shortening, varies depending on ciliary length and growth state (Pan et al., 2004).

And how does the loading dock work?

Various molecular mechanisms could regulate the amount of cargo bound to IFT trains entering cilia. These include ciliary-length dependent changes in the

environment of the basal body to increase cargo loading or in the TZ to facilitate cargo admission. Also, the cargo binding capacity of IFT trains could be modulated. Many IFT proteins undergo phosphorylation, the function of which is unclear, but could alter their affinity for cargoes (Boesger et al., 2009; Wang et al., 2014). Electron microscopy has identified at least two ultrastructurally distinct types of IFT trains in cilia, short and long trains with 16-nm and 40-nm repeats, respectively (Pigino et al., 2009). While the functional significance of train architecture is unknown, it could conceivably impact loading capacity, e.g., binding sites could be exposed or hidden depending on train architecture. Recently, the binding sites for tubulin, the BBSome (a small protein complex which cycles in association with IFT trains through cilia), and outer dynein arms have been identified (Ahmed et al., 2008; Bhogaraju et al., 2013; Brown et al., 2015; Eguether et al., 2014; Hou et al., 2007; Liew et al., 2014).

Concluding remarks

The role of IFT in transporting structural proteins into cilia during assembly has been firmly established. While some aspects of the cellular circuits regulating the amount of protein shuttled via IFT into cilia are emerging, it remains unclear how cells measure the length of their cilia and use this information to adjust the amount of cargo carried by IFT trains. The structural analysis of IFT proteins, particles, and trains and the identification of cargo binding sites should further our understanding of how cells assemble cilia and regulate the length.

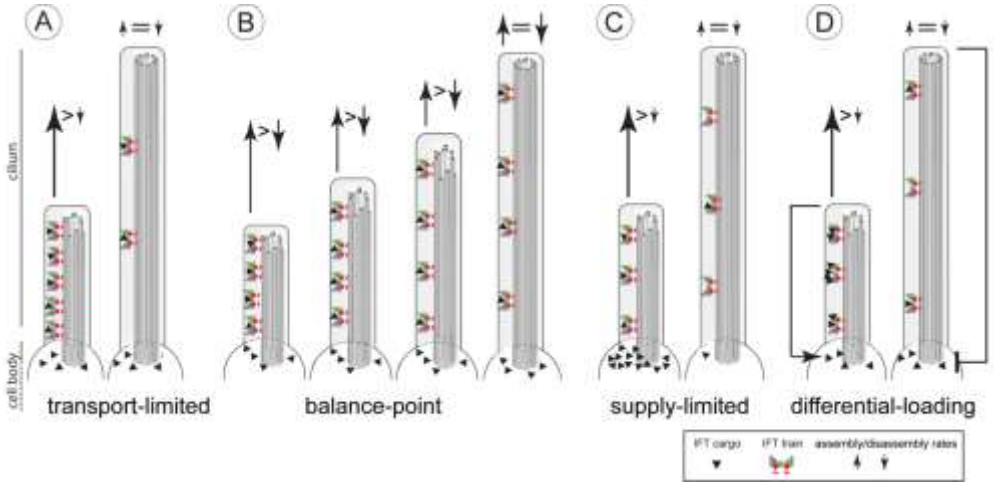
A
B
C
D
cilium
cell body
transport-limited
balance-point
supply-limited
differential-loading
IFT cargo
IFT train
assembly/disassembly rates

Figure 16. Cargo transport and ciliary length

A) The transport-limitation model suggests that cells will employ many IFT trains while cilia grow and reduce the number of trains in fully grown cilia. The cargo load per train is constant.

B) In the balance-point model, the ciliary assembly rate will decrease with increasing ciliary length because the transit time of IFT trains increases. Neither the number of IFT trains nor the cargo load/train is regulated. To achieve ciliary assembly in a physiological time frame, this model requires a high disassembly rate of cilia.

C) The supply-limitation model predicts that cilia will grow until the cell body pool of precursors is exhausted. IFT cargo load is regulated passively by the presence or absence of cargoes.

D) The differential-loading model suggests that cell regulate the amount of cargo/train in response to changes in ciliary length. The extra capacity of trains in steady-state cilia enables the cells to quickly adjust ciliary length and composition. In contrast to the models described in A-C, the differential-loading model postulates a feedback of ciliary length onto IFT.

4.2 Insufficient diffusion begets constitutively active molecular motors: A ciliary system poised on high alert

Abstract

Cilia and eukaryotic flagella are widely distributed cellular organelles in the human body and their assembly requires a dedicated protein shuttle, intraflagellar transport (IFT). This active transport sets them apart from many other cytoskeletal assemblies, such as the mitotic spindle, that are likely to obtain their precursors via diffusion from the surrounding cytoplasm. Given the high surface to volume ratio that makes cilia prime locations for signaling, this attribute also constrains diffusion's efficiency to supply precursors at the needed rate; therefore, active transport is required for assembly and maintenance of this organelle. IFT particles consist of ~22 distinct proteins forming complexes that translocate via kinesin-II and IFT dynein. IFT particles are the primary cargoes in constant association with the IFT motors during transport, thus ensuring the continuous engagement of the motors. Recent direct imaging of cargo flux inside cilia revealed that the amount of structural proteins carried by IFT is adjusted drastically according to the ciliary growth status, with IFT under heavy load during regeneration and running lightly loaded during non-growth. Why does the cell continually run IFT, an ATP-dependent process, after the organelle is built? Here we discuss the far-reaching implications of a system poised on high alert to enable rapid responsiveness.

Cilia and disease: Why is this organelle so important?

In mammals, cilia are found in two forms: motile and non-motile or primary cilia. Motile cilia function to facilitate fluid flow, e.g., in aiding mucociliary clearance of the airways and sperm locomotion. Most differentiated cells possess a single primary cilium used for sensing diverse cues ranging from light and odorants to mechanical stimuli. Primary cilia are found on diverse cells (e.g., kidney tubule epithelial cells, photoreceptors cells, taste receptor cells, cochlear hair cells, bile duct epithelial cells, follicular cells, neurons, fibroblasts, myocytes, chondrocytes, ependymal cells, pituitary cells, hepatocytes, uterine, and Schwann cells) (Satir and Christensen, 2007). Cilia dysfunction results in a variety of disorders collectively called ciliopathies (Brown and Witman, 2014). Defects in ciliary assembly will impact many cell types and tissues generating multi-organ phenotypes. The features of ciliopathies range from male infertility and congenital heart defects to blindness, cystic kidneys and obesity. Mutations in the IFT pathway have been liked to several such conditions (Huber and Cormier-Daire, 2012). Parallel with the rising awareness of the important role of cilia in human health and disease, the interest in how cilia are assembled and how IFT works has increased.

Soluble protein accumulation against a concentration gradient

Ciliary microtubules grow by additions of tubulin at their distal plus tip (Johnson and Rosenbaum, 1992; Marshall and Rosenbaum, 2001). Given the small volume of the ciliary matrix, we predict ~15 fold increase in soluble tubulin concentration in the growing organelle is required to simultaneously build all

axonemal microtubules (i.e., ~20 μM in the cell body versus a predicted ~320 □M at the tip of a growing cilium: see Craft et al., 2015 for calculations). While in parts based on assumption, the data strongly indicate that the tubulin concentration in cilia is higher than that of the cell body rendering diffusion incapable. Diffusion by definition cannot concentrate a soluble protein against a concentration gradient. Therefore, IFT functions as a tubulin pump ensuring that the critical concentration of tubulin is met and the axoneme extends. Further to this end, using a temperature sensitive mutant of the anterograde motor (*fla10* in Chlamydomonas), it is known that cilia will not grow in the absence of IFT (Walther et al., 1994;Kozminski et al., 1995). Inasmuch, once cilia are in a steady state and IFT is "switched off," the cilia cannot be maintained and will slowly resorb. Taken together, diffusion alone is not sufficient for building or maintaining this organelle.

Molecular motors in overdrive

Molecular motors, kinesin-II and IFT dynein, generate the force required for IFT train translocation along a cilium. Heterotrimeric kinesin-II is a plus-end directed motor which moves from the ciliary base to the distal tip. Kinesin moves in 8 nm steps as it hydrolyzes 1 ATP (Visscher et al., 1999). A special form of cytoplasmic dynein, dynein 1b, is an AAA-type ATPase which moves from the distal plus end of the axonemal microtubules in a retrograde fashion back to the cell body. Dynein has a more variable step size (8-24 nm) and also requires 1 ATP per step (Reck-Peterson et al., 2006). A *Chlamydomonas* cilium of 12 microns exhibits ~40 IFT tracks per minute without respect to growth state. In a

conservative estimation assuming only one motor per train, IFT would consume 80,000-120,000 ATP molecules per min and ATP is produced in cilia to support high ATP consumption (Mitchell et al., 2005). Intracellularly, motors are inactive without cargo to limit wasteful ATP consumption as molecular motors undergo multiple levels of complex and specific regulation (reviewed in Verhey and Hammond, 2009); unifyingly, in the absence of cargo, kinesin is autoinhibited and dynein is also not singularly progressive (reviewed in Verhey et al., 2011; Kardon and Vale, 2009; Schroer, 2004; Schlager et al., 2014; McKenney et al., 2014). Intracellularly, functionality of dynein critically depends upon dynactin, which serves as an adaptor, targets dynein, and regulates processive movement; dynein coupled with dynactin and a cargo adaptor is sufficient for motor processivity (Kardon et al., 2009; Schroer, 2004). Differential phosphorylation of kinesin-2's Fla8/Kif3b subunit acts as a molecular switch. Dephosphorylation of this subunit activates kinesin and promotes association with IFT complexes, while phosphorylation disrupts this interaction and allows for complex remodeling at the tip (Lian et al., 2014). Upon kinesin-2 activation, it has been further shown that kinesin-2 carries IFT dynein to the tip; once at the tip, it is available for minus-end directed retrograde transport (Pedersen et al, 2006). Why does this cooperative motor transport continually cycle? How does this change in the context of a cilium?

Are ciliary motors inactivated without cargo?

To begin to address this question, we must first explore the motor-adaptor (IFT)-cargo association. While most structural components are believed to be

cargoes of this transport system, firm data exist for only a few proteins. Among the confirmed cargoes of IFT is tubulin, the major structural protein of cilia (Craft et al., 2015; Hao et al., 2011). *In vivo* two color imaging showed that IFT trains are highly loaded with tubulin and other axonemal cargoes while cilia grow but largely devoid of these proteins once cilia reach their steady state length (Craft et al, 2015; Wren et al., 2013). IFT trains (particles in association with motors) run at a largely constant frequency and velocity without dependence on length. Simply put, IFT continually moves somewhat akin to a conveyor belt and materials are loaded onto the belt predominately only when they are required. This finding is the basis for the differential cargo loading model: Cells apparently regulate the amount of cargo present on a given IFT train in a ciliary-length dependent manner. This model poses important cellular questions that we will now discuss. 1) How can these cargo adaptors (IFT particles) differentially bind cargo? 2) Why continually run an ATP-expensive system during stages of non-growth?

How to adapters bind variable amounts of cargo?

There is a lack of precise knowledge on how IFT particles bind various amounts of cargoes. Here we consider feasible mechanisms. First, IFT particles could have a variable affinity for cargoes achieved by post-translational modifications or an allosteric regulation mechanism (Fig. 9B). It is known that specific IFT particles undergo phosphorylation, but the purpose remains unclear (Wang et al., 2014). Second, little is known about the microenvironment of cilia and basal bodies. In our IFT-conveyor belt metaphor, gravity is the acting force

that facilitates the interaction of the cargo to the belt; however intracellular proteins are outside the confines of this force. Perhaps a permissive microenvironment of ions or other small molecules in efflux from the cilium could drive cargo association to IFT localized at the base of a growing cilium (Fig. 9C). This would allow for quick manipulation of cargo loading as ciliary membranes are rich in ion transporters. This concept is supported by work in axonal transport, where literature details a mechanism for changes in local calcium concentrations directly regulating cargo trafficking by modulating association with motors (Wang et al., 2009; Macaskill et al., 2009). Last, it is unknown if this cargo loading is self-governed or if proteins facilitate cargo-IFT interaction, i.e. involves non-IFT proteins which chaperone IFT-cargo association. One could imagine a spatially regulated scaffolding protein or other loading-assistive protein situated at the specific cilium-basal body entity that tether cargoes locally (Fig. 9D).

Further, it is known that cells can regulate how much cargo binds in a cilium-autonomous manner (Craft et al., 2015). So in the context of the same cell, the cell can ‘sense’ which cilium is growing and directs transport accordingly. Control of transport per cargo makes sense biologically as it is inherently judicious; likely only needed precursors are transported in quantities that reflect the ciliary requirements. This ability to respond per cilium with needed precursors enables the cell to react to ciliary needs while maintaining overall efficiency.

Why continually run an ATP-expensive system during stages of non-growth?

The role of IFT during non-growth, or maintenance, is currently unclear. The vast ATP consumption required for running IFT continuously leads one to ponder the precise role of IFT in non-growing cilia, when the trains are largely running empty with respect to structural cargo proteins, which probably represent the predominant cargo class during growth. Do the IFT trains themselves participate in the critical sensing length of this organelle? Do the cells use continuous IFT to preemptively poise themselves to quickly respond to ciliary needs? Axonemal precursor turnover in cilia has been described, so could the primary purpose of IFT during non-growth lie in removal of materials? We posit that IFT functions, as a primary cargo, to keep kinesin and IFT dynein engaged and constantly cycling to and fro in the cilium. So why does the cell constantly engage IFT motors, but cytoplasmic motors are engaged only when specifically needed? Evolutionarily, it must be advantageous, for currently unelucidated reasons, to have this constitutively active system.

Concluding Remarks

We posit that the continual cycling of IFT leads to the cell being poised to quickly respond to signals and adjust ciliary protein content. It has recently been depicted that primary cilia on neurons are much more dynamic than previously thought, with live-imaging detailing primary cilia that readily change shape and extend and retract (Higginbotham et al., 2013). This challenges our current

notions that primary cilia are structurally static. IFT continually running during maintenance could function to poise the system on high alert for action; this also implies that cilia are inherently dynamic and robustly interactive, continually fine-tuning their protein composition.

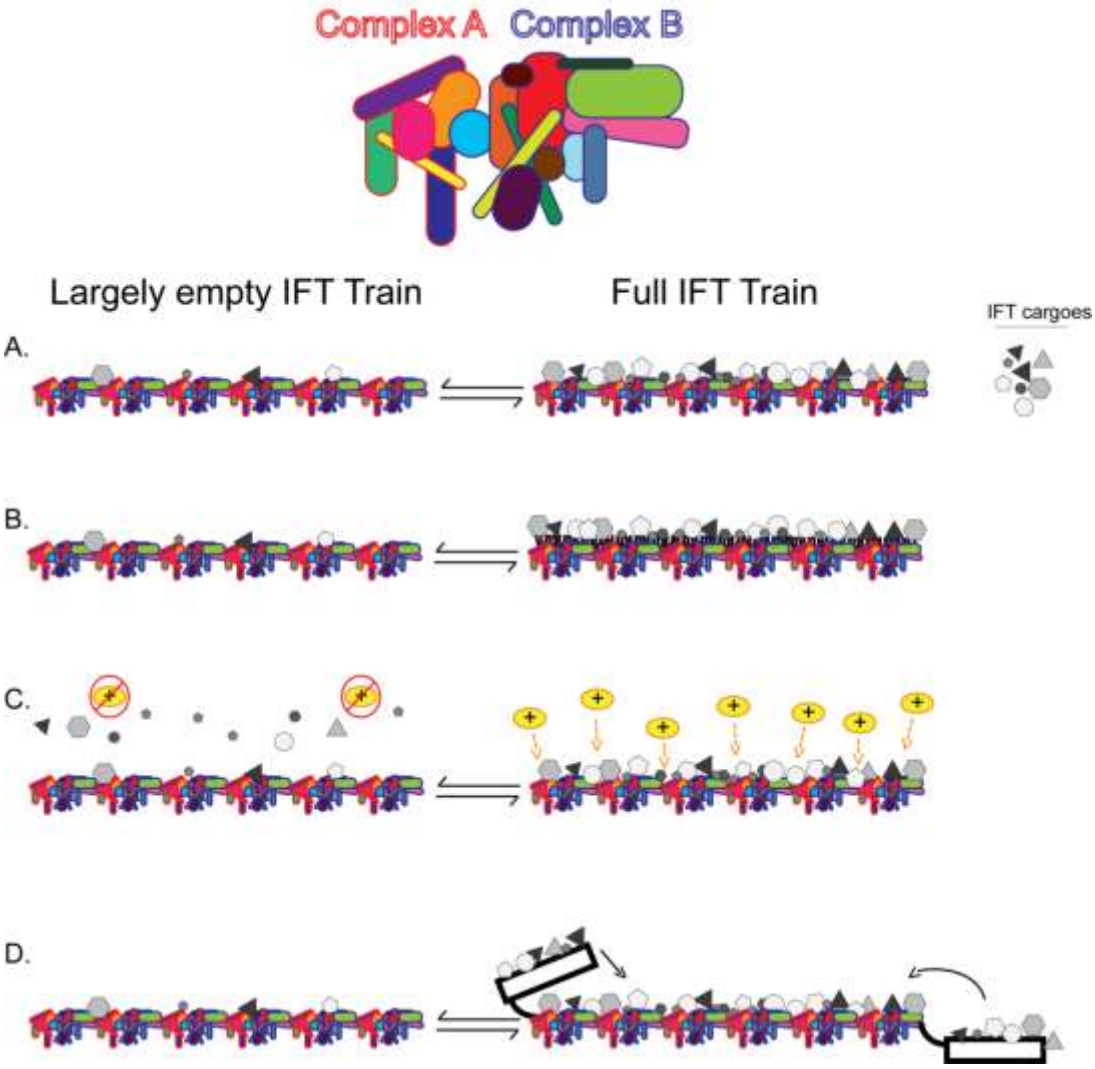

Figure 17. Feasible mechanisms for differential cargo loading.

A) IFT trains are able to modulate between low-load states where they are largely empty and high-load states where they are largely full of cargo.

B) IFT trains could be modified to have increased affinity for cargoes via post-translational modifications or allosteric regulation.

C) The microenvironment of a cilium could facilitate heavy loading by ion concentration.

D) Non-IFT proteins could aid in heavy cargo loading by tethering cargoes locally.

4.3 Future Directions

Now that GFP-α-tubulin is established as a good tool to study ciliary tubulin dynamics in *Chlamydomonas*, many experimental areas are quite accessible. Here I discuss avenues for future research.

Disassembly and tubulin turnover

The dynamics of disassembly of the axoneme are not characterized, whether complete disassembly or the disassembly that occurs with microtubule turnover. To isolate and observe tubulin that is being disassembled at the distal tip, the GFP could be easily exchanged for a photoactivatable or photo-convertible fluorophore. A spot bleaching laser could be adjusted to drive photo-activation or conversion of the tubulin spatially restricted at the tip. This experimental setup would allow for clear observation of this subset of tagged tubulin, while being able to differentiate from the diffusing tubulin that often obscures retrograde movements. This approach would further allow for the investigation of the role of IFT in the breakdown of the axoneme. Is IFT required for tubulin exit from cilia, or is diffusion alone sufficient? In the context of long-short cells, a photoconvertible fluorophore could be used to see if tubulin is recycled from the shortening long cilium into the growing short cilium.

Central pair assembly

How the central pair microtubules assemble is largely unknown. No obvious nucleation site exists and the fast-growing plus ends of the microtubules are occupied with an elaborate capping structure (Dentler, 1980). It is known that upon fusing a central pair-deficient mutant to wild-type cells the *de novo*

formation of the central pair will occur (Lechtreck, 2013B). High level expression of GFP-tubulin would likely allow one to observe *in vivo* assembly of the central pair.

***In vitro* reconstitution of axonemal microtubule doublets**.

Based on this work, we performed calculations to estimate the concentration of soluble tubulin required to simultaneously build the axonemal microtubules. We posit that a concentration of upwards of 320 μM is required at the distal tip for this process to occur in a timely manner. All efforts to reconstitute doublet microtubules of the axoneme *in vitro* have failed, perhaps due to a potential requirement for such a high concentration of tubulin. Utilizing a protocol to purify tubulin (Widlund et al, 2012), one could isolate tubulin from *Chlamydomonas* axonemes; this would ensure that the heterodimers purified would be axonemal assembly competent. One could readily imagine that other non-tubulin factors are pivotal to axonemal assembly; extract from ciliary matrix of regenerating *Chlamydomonas* could supplement the high concentration of competent tubulin with a purified nucleation site.

Polymerization state of transported tubulin

It is a contentious point if tubulin is transported by IFT in a short polymerized form or in the heterodimeric form, with little data to support either claim. Utilizing our tagged tubulin, we performed immunoprecipitations in which endogenous β-tubulin was the sole protein detectable that co-precipitated with GFP-α-tubulin. In such experiments after optimization, a high concentration of salt (250 mM NaCl) was used to ensure there would be no non-specific binding

of tubulin to beads. Should this experiment be revisited with incremental decreases in salt concentration to the limit of still retaining clean control beads, perhaps other proteins would co-precipitate. Pull-down of endogenous untagged α-tubulin from the soluble ciliary fraction with GFP-α-tubulin, for example would suggest an interaction of GFP-α-tubulin with α-tubulin indicative for the presence of at least tubulin tetramers.

Chapter 3: Differential Cargo Loading Model

The cell achieves heavy loading on some IFT particles, while others are largely without cargo. Here I discuss potential routes to begin to unravel the governing molecular mechanism of differential cargo loading.

Are non-IFT proteins involved in loading of cargoes onto IFT?

To determine if non-IFT proteins may facilitate cargo loading, it would be of interest to identify proteins that are close to IFT trains during assembly and loading. One approach could include proximity labeling of IFT trains in the cell body. The use of a promiscuous biotinylation protein, BirA, has been verified in *Chlamydomonas* (Roux et al, 2012; Lechtreck, not published). Tagging an IFT protein would be ideal as they are known to cycle throughout cilia and back through the proximal cell body area near basal bodies. Tagging an IFT protein with BirA, then through the use of biotin, anything within ~10 nm radius from the tagged protein will become biotinylated facilitating affinity purification and mass spectrometry for identification. Cells could then be fractionated to determine proteins interacting with an IFT protein in the cell body. Steady state and

regenerating cells could be used to examine any differential biotinylation dependent on the ciliary growth state.

Identification of facilitative ion microenvironment for cargo loading

To determine if the microenvironment of cilia could facilitate heavy loading, varying sensors could be used coupled with live cell imaging during steady state, regeneration, and long-short cells. If a measurable difference is seen, small molecule inhibitors could then be used to block ion transport to halt heavy loading. Tagged tubulin could be used in conjunction with such sensors, as the frequency of transport over stages of growth is now known.

Identification of players involved in regulating cargo loading

Cells with one amputated cilium or uni mutants with only one cilium spin due to their inability to swim properly, a phenotype that can be readily identified by low magnification light microscopy. This occurence could be used to screen for mutagenized cells that have lost the ability to equally load cargo between both cilia; this would result in a transient inability to phototax and a spinning phenotype.

Chapter 4: The role of β-tubulin E-hooks

The E-hooks of α- and β-tubulin are not essential for IFT transport, but the β-tubulin E-hook does play a role *in vivo* to stabilize the IFT-tubulin interaction and to enable proper IFT transport.

Characterization of β-tubulin E-hook mutants

To report solidly upon the tubulin interaction with the IFT particle, a continuation of the work described here is needed. We need to see a clear fate

of tagged β–tubulin that appears to dissociate from the IFT particle. The use of a brighter fluorophore may result in prolongued observation of singly-tagged tubulins, but the diffusing tubulin would still be a hindrance. For single molecule imaging, the vast amount of tubulin diffusing in the cytoplasm of the cilia is seemingly unavoidable. Further, should there become available means of curtailing the background of diffusing fluorescent tubulin, quantitative photobleaching could shed light upon how many copies of the fluorescent molecule is carried per train. It would be of interest to gain knowledge on the stoichiometry of cargoes and IFT train in such a manner.

To aid in determination of any defect of β-tubulin E-hook mutants, it would be of some benefit to create strains with fluorescently tagged β–tubulin wildtype E-hook and a different color fluorescently tagged β–tubulin mutant E-hook. In the context of the same cell, one could elegantly show defects in IFT transport.

Interaction of tubulin heterodimer with IFT particle

Preliminary experiments are underway to further tease apart the interaction of the tubulin heterodimer with the IFT particle, IFT81 and IFT74 specifically. In collaboration with the George Witman lab of the University of Massachusetts Medical School, we have obtained strains with a disruption of the proposed IFT81/74 tubulin-binding module. A continuation of the work examining various β-tubulin E-hook mutants in the the IFT81 and IFT74 rescue mutants separately should reveal more clearly the interaction of the heterodimer with the IFT trains. Further, incorporation of IFT54 mutants rescued with a partial deletion

of calponin-homology domain should inform is this IFT protein binds tubulin *in vivo*.

Taken together, the work herein this dissertation has advanced the collective knowledge on the terrifyingly complex process of building a cell organelle. By investigating the most abundant protein of cilia, we disentangle some obscure regulations governing precursor logistics. We have uncovered the presence of intracellular soluble protein sorting without known localization signals. The field will benefit as more IFT cargoes are identified and characterized. From the few cargoes we have seen thus far, it has exposed IFT as a constantly trafficking system, yet highly adaptable and responsive to the overall state of the cilia.

REFERENCES

Ahmed, N.T., C. Gao, B.F. Lucker, D.G. Cole, and D.R. Mitchell. 2008. ODA16 aids axonemal outer row dynein assembly through an interaction with the intraflagellar transport machinery. *J. Cell Biol.* 183:313–322. http://dx .doi.org/10.1083/jcb.200802025

Adair, W.S. (1985) Characterization of *Chlamydomonas* sexual agglutinins. *J Cell Sci Suppl.* 2:223-60.

Al-Bassam, J., and F. Chang. (2011) Regulation of microtubule dynamics by TOG-domain proteins XMAP215/Dis1 and CLASP. *Trends Cell Biol.* 21:604–614. http://dx.doi.org/10.1016/j.tcb.2011.06.007

Allen, C. and G.G. Borisy. (1974) Structural polarity and directional growth of microtubules of *Chlamydomonas* flagella*. J Mol Biol.* 90(2):381-402.

Barsel, S.E., D.E. Wexler, and P.A. Lefebvre. (1988) Genetic analysis of Long flagella mutants of *Chlamydomonas reinhardtii*. *Genetics*. 118:637 –648.

Belzile, O., C.I. Hernandez-Lara, Q. Wang, and W.J. Snell. (2013) Regulated Membrane protein entry into flagella is facilitated by cytoplasmic Microtubules and does not require IFT. *Curr. Biol.* 23:1460–1465. http://dx.doi.org/10.1016/j.cub.2013.06.025

Bengs, F., A. Scholz, D. Kuhn, and M. Wiese. (2005). LmxMPK9, a mitogen-activated protein kinase homologue affects flagellar length in Leishmania mexicana. *Molecular microbiology*. 55:1606-1615.

Berbari, N.F., et al. (2008) Bardet-Biedl syndrome proteins are required for the localization of G protein-coupled receptors to primary cilia. *PNAS*. 105, 4242-4246.

Berman, S.A., N.F. Wilson, N.A. Haas, and P.A. Lefebvre. (2003) A novel MAP kinase regulates flagellar length in *Chlamydomonas*. *Curr. Biol.* 13:1145–1149. http://dx.doi.org/10.1016/S0960-9822(03)00415-9

Bhogaraju, S., L. Cajanek, C. Fort, T. Blisnick, K. Weber, M. Taschner, Mizuno, S. Lamla, P. Bastin, E.A. Nigg, and E. Lorentzen. (2013). Molecular Basis of tubulin transport within the cilium by IFT74 and IFT81. *Science*. 341:1009–1012. http://dx.doi.org/10.1126/science.1240985

Bhogaraju, S., K. Weber, B.D. Engel, K.F. Lechtreck, and E. Lorentzen. (2014) Getting tubulin to the tip of the cilium: one IFT train, many different tubulin cargo-binding sites? *BioEssays*. 36:463–467. http://dx.doi.org/10.1002/bies.201400007

Blacque, O.E., M.J. Reardon, C. Li, J. McCarthy, M.R. Mahjoub, S.J. Ansley, J.L. Badano, A.K. Mah, P.L. Beales, W.S. Davidson, et al. (2004) Loss of *C. elegans* BBS-7 and BBS-8 protein function results in cilia defects and compromised intraflagellar transport. *Genes Dev.* 18:1630–1642. http://dx.doi.org/10.1101/gad.1194004

Boesger, J., V. Wagner, W. Weisheit, and M. Mittag. (2009). Analysis of flagellar phosphoproteins from Chlamydomonas reinhardtii. *Eukaryotic cell*. 8:922-932.

Borisy, G.G., and E.W. Taylor. (1967) The mechanism of action of colchicine. Binding of colchincine-3H to cellular protein. *J. Cell Biol.* 34:525–533. http://dx.doi.org/10.1083/jcb.34.2.525

Borisy, G.G. (1978) Polarity of microtubules of the mitotic spindle. *J Mol Biol*. 124(3):565-70.

Breslow, D.K., E.F. Koslover, F. Seydel, A.J. Spakowitz, and M.V. Nachury. (2013) An in vitro assay for entry into cilia reveals unique properties of the soluble diffusion barrier. *J. Cell Biol.* 203:129–147. http://dx.doi.org/10.1083/jcb.201212024

Broekhuis, J.R., K.J. Verhey, and G. Jansen. (2014). Regulation of cilium length and intraflagellar transport by the RCK-kinases ICK and MOK in renal epithelial cells. *PloS one*. 9:e108470.

Brown, J.M., D.A. Cochran, B. Craige, T. Kubo, and G.B. Witman. (2015). Assembly of IFT Trains at the Ciliary Base Depends on IFT74. *Current biology : CB*. 25:1583-1593.

Brown, J.M., and G.B. Witman. (2014). Cilia and Diseases. *Bioscience*. 64:1126-1137.

Brust-Mascher, I., G. Ou, and J.M. Scholey. (2013) Measuring rates of Intraflagellar transport along *Caenorhabditis elegans* sensory cilia using Fluorescence microscopy. *Methods Enzymol.* 524:285–304. http://dx.doi.org/10.1016/B978-0-12-397945-2.00016-0

Buisson, J., N. Chenouard, T. Lagache, T. Blisnick, J.C. Olivo-Marin, and P. Bastin. (2012). Intraflagellar transport proteins cycle between the flagellum and its base. *Journal of cell science*.

Burghoorn, J., M.P. Dekkers, S. Rademakers, T. de Jong, R. Willemsen, P. Swoboda, and G. Jansen. (2010). Dauer pheromone and G-protein signaling modulate the coordination of intraflagellar transport kinesin motor proteins in C. elegans. *Journal of cell science*. 123:2077-2084.

Cao, M., D. Meng, L. Wang, S. Bei, W.J. Snell, and J. Pan. (2013) Activation loop phosphorylation of a protein kinase is a molecular marker of organelle size that dynamically reports flagellar length. *Proc. Natl. Acad. Sci. USA*. 110:12337–12342. http://dx.doi.org/10.1073/pnas.1302364110

Chan, Y.H., and W.F. Marshall. (2012) How cells know the size of their organelles. *Science*. 337:1186–1189. http://dx.doi.org/10.1126/science.1223539

Chaya, T., Y. Omori, R. Kuwahara, and T. Furukawa. (2014). ICK is essential for cell type-specific ciliogenesis and the regulation of ciliary transport. *The EMBO journal*. 33:1227-1242.

Chih B, et al. (2011) A ciliopathy complex at the transition zone protects the cilia as a privileged membrane domain. *Nature Cell Biology*. 14:61–72.

The Chlamydomonas Sourcebook 2nd ed. (2009) Volume 1: Introduction to Chlamydomonas and Its Laboratory Use, ed. E.H. Harris. Vol. 1. San Diego, CA: Academic Press.

Cole, D.G., and W.J. Snell. (2009). SnapShot: Intraflagellar transport. *Cell*. 137:784-784 e781.

Cole, D.G., et al. (2003) The intraflagellar transport machinery of *Chlamydomonas reinhardtii. Traffic*. 4(7):435-42.

Cole, D.G., D.R. Diener, A.L. Himelblau, P.L. Beech, J.C. Fuster, and J.L. Rosenbaum. (1998) *Chlamydomonas* kinesin-II-dependent intraflagellar transport (IFT): IFT particles contain proteins required for ciliary assembly in *Caenorhabditis elegans* sensory neurons. *J. Cell Biol.* 141:993–1008. http://dx.doi.org/10.1083/jcb.141.4.993

Collingridge, P., C. Brownlee, and G.L. Wheeler. (2013) Compartmentalized calcium signaling in cilia regulates intraflagellar transport. *Curr. Biol.* 23:2311–2318. http://dx.doi.org/10.1016/j.cub.2013.09.059

Craft, J.M., J.A. Harris, S. Hyman, P. Kner, and K.F. Lechtreck. (2015). Tubulin transport by IFT is upregulated during ciliary growth by a cilium-autonomous mechanism. *The Journal of cell biology*. 208:223-237.

Craige, B., C.C. Tsao, D.R. Diener, Y. Hou, K.F. Lechtreck, J.L. Rosenbaum, and G.B. Witman. (2010) CEP290 tethers flagellar transition zone microtubules to the membrane and regulates flagellar protein content. *J. Cell Biol.* 190:927–940. http://dx.doi.org/10.1083/jcb.201006105

Czarnecki, P.G., and J.V. Shah. (2012). The ciliary transition zone: from morphology and molecules to medicine. *Trends in cell biology*. 22:201-210.

Deane, J.A., D.G. Cole, E.S. Seeley, D.R. Diener, and J.L. Rosenbaum. (2001) Localization of intraflagellar transport protein IFT52 identifies basal body transitional fibers as the docking site for IFT particles. *Curr. Biol.* 11:1586–1590. http://dx.doi.org/10.1016/S0960-9822(01)00484-5

Dentler, W.L.,, et al. (1974) Directionality of brain microtubule assembly *in vitro. PNAS.* 71 (5)1710-4.

Dentler, W.L., and J.L. Rosenbaum. (1977). Flagellar elongation and shortening in *Chlamydomonas*. III. structures attached to the tips of flagellar microtubules and their relationship to the directionality of flagellar microtubule assembly. *JCB* 74(3);747-59.

Dentler, W.L. (1980). Structures Linking the tips of ciliary and flagellar microtubules to the membrane. *J Cell Science*. 42:207-220.

Dentler, W. L. (1984) Attachment of the cap to the central microtubules of *Tetrahymena* cilia. *J Cell Science.* 66:167-173.

Dentler, W. (2005) Intraflagellar transport (IFT) during assembly and disassembly of *Chlamydomonas flagella*. *J. Cell Biol.* 170:649–659.

Desai, A., and T.J. Mitchison. (1997) Microtubule polymerization dynamics. *Annu. Rev. Cell Dev. Biol.* 13:83–117. http://dx.doi.org/10.1146/annurev.cellbio.13.1.83

Dobell C: Anthony van Leeuwenhoek and his 'Little Animals.' Harcourt, Brace and Co, New York; 1932 https://archive.org/details/antonyvanleeuwen00dobe

Duan, J., and M.A. Gorovsky. (2002) Both carboxy-terminal tails of alpha- and beta-tubulin are essential, but either one will suffice. *Curr. Biol.* 12:313–316. http://dx.doi.org/10.1016/S0960-9822(02)00651-6

Eguether, T., J.T. San Agustin, B.T. Keady, J.A. Jonassen, Y. Liang, R. Francis, K. Tobita, C.A. Johnson, Z.A. Abdelhamed, C.W. Lo, and G.J. Pazour. (2014). IFT27 links the BBSome to IFT for maintenance of the ciliary signaling compartment. *Developmental cell*. 31:279-290.

Engel, B.D., et al. (2009) Total internal reflection fluorescence (TIRF) microscopy of *Chlamydomonas flagella. Methods Cell Bio.* 93:157-77.

Engel, B.D., W.B. Ludington, and W.F. Marshall. (2009) Intraflagellar transport particle size scales inversely with flagellar length: revisiting the balance point length control model. *J. Cell Biol.* 187:81–89. http://dx.doi.org/10.1083/jcb.200812084

Escudier, E., et al. (2009). Ciliary defects and genetics of primary ciliary dyskinesia*. Paediatr Respir Rev*. 10(2):51-4.

Euteneuer, U. and J.R. McIntosh. (1981) Polarity of some motility-related microtubules. *PNAS.* 78(1):372-6.

Follit, J.A., et al. (2009) Characterization of mouse IFT complex B. *Cell Motil Cytoskeleton*. (8):457-68.

Gaertig, J., and D. Wloga. (2008) Ciliary tubulin and its post-translational modifications. *Curr. Top. Dev. Biol.* 85:83–113. http://dx.doi.org/10.1016/S0070-2153(08)00804-1

Garcia-Gonzalo FR, et al. (2011) A transition zone complex regulates mammalian ciliogenesis and ciliary membrane composition. *Nature genetics*. 43:776–784.

Gard, D.L., and M.W. Kirschner. (1987) Microtubule assembly in cytoplasmic extracts of *Xenopus* oocytes and eggs. *J. Cell Biol.* 105:2191–2201. http://dx.doi.org/10.1083/jcb.105.5.2191

Geimer, S., and M. Melkonian. (2004). The ultrastructure of the *Chlamydomonas reinhardtii* basal apparatus: identification of an early marker of radial asymmetry inherent in the basal body. *J Cell Science.* 117:2663-2674.

Goehring, N.W., and A.A. Hyman. (2012) Organelle growth control through Limiting pools of cytoplasmic components. *Curr. Biol.* 22:R330–R339. http://dx.doi.org/10.1016/j.cub.2012.03.046

Graser S, Stierhof Y-D, Lavoie SB, Gassner OS, Lamla S, Le Clech M, Nigg EA. (2007) Cep164, a novel centriole appendage protein required for primary cilium formation. *J Cell Biol.*179:321-330.

Hao, L., M. Thein, I. Brust-Mascher, G. Civelekoglu-Scholey, Y. Lu, S. Acar, B. Prevo, S. Shaham, and J.M. Scholey. (2011) Intraflagellar transport delivers tubulin isotypes to sensory cilium middle and distal segments. *Nat Cell Biol.* 13:790–798. http://dx.doi.org/10.1038/ncb2268

Higginbotham, H., Guo, J., et al. (2013). Arl13b-regulated activities of primary cilia are essential for the formation of the polarized radial glial scaffold. *Nature Neuroscience*. 16(8): 1000-1007.

Hilton, L.K., K. Gunawardane, J.W. Kim, M.C. Schwarz, and L.M. Quarmby. (2013). The kinases LF4 and CNK2 control ciliary length by feedback regulation of assembly and disassembly rates. *Curr. Biol.* 23:2208–2214.

Hou, Y., H. Qin, J.A. Follit, G.J. Pazour, J.L. Rosenbaum, and G.B. Witman. (2007). Functional analysis of an individual IFT protein: IFT46 is required for transport of outer dynein arms into flagella. *J. Cell Biol.* 176:653–665. http://dx.doi.org/10.1083/jcb.200608041

Howard, J. 2001. Mechanics of motor proteins and the cytoskeleton. Sinauer Associates, Publishers, Sunderland, Mass. 67 pp.

Hu, Qicong and W. J. Nelson. (2011) Ciliary diffusion barrier: The gatekeeper for the primary cilium compartment. *Cytoskeleton*. 68(6): 313-324.

Huang, K., D.R. Diener, A. Mitchell, G.J. Pazour, G.B. Witman, and J.L. Rosenbaum. 2007. Function and dynamics of PKD2 in *Chlamydomonas reinhardtii* flagella. *J. Cell Biol.* 179:501–514. http://dx.doi.org/10.1083/jcb.200704069

Huber, C., and V. Cormier-Daire. (2012). Ciliary disorder of the skeleton. *American journal of medical genetics. Part C, Seminars in medical genetics*. 160C:165-174.

Ibanez-Tallon, I., N. Heintz, et al. (2003). To beat or not to beat: roles of cilia in development and disease. *Hum Mol Genet*. 12 Spec No 1:R27-35.

Iomini, C., et al. (2001) *Protein particles in Chlamydomonas* flagella undergo a transport cycle consisting of four phases*. J Cell Biol.* 153(1):13-24.

Ishikawa H, Kubo A, Tsukita S, Tsukita S. (2005) Odf2-deficient mother centrioles lack distal/subdistal appendages and the ability to generate primary cilia. *Nat Cell Biol.* 7**:**517-524.

Jekely, G. and. Arendt. (2006) Evolution of intraflagellar transport from coated vesicles and autogenous origin of the eukaryotic cilium. *Bioessays*. 28:191.198.

Jin, H. et al. (2010) The conserved Bardet-Biedl syndrome proteins assemble a coat that traffics membrane proteins to cilia. *Cell*. 141(7);1208-19.

Johnson, K.A., and J.L. Rosenbaum. (1992) Polarity of flagellar assembly in *Chlamydomonas*. *J. Cell Biol.* 119:1605–1611. http://dx.doi.org/10.1083/jcb.119.6.1605

Kardon, J.R., and R.D. Vale. (2009). Regulators of the cytoplasmic dynein motor. *Nat Rev Mol Cell Biol.* 10(12):854-65.

Kee, H.L., and K.J. Verhey. (2013) Molecular connections between nuclear and ciliary import processes. *Cilia*. 2:11. http://dx.doi.org/10.1186/2046-2530-2-11

Kee, H.L., J.F. Dishinger, T.L. Blasius, C.J. Liu, B. Margolis, and K.J. Verhey. (2012) A size-exclusion permeability barrier and nucleoporins characterize a ciliary pore complex that regulates transport into cilia. *Nat. Cell Biol.* 14:431–437. http://dx.doi.org/10.1038/ncb2450

King, S.M., and G.B. Witman. (1990) Localization of an intermediate chain of outer arm dynein by immunoelectron microscopy. *J. Biol. Chem.* 265: 19807–19811.

Ko, H.W., R.X. Norman, J. Tran, K.P. Fuller, M. Fukuda, and J.T. Eggenschwiler. (2010) Broad-minded links cell cycle-related kinase to cilia assembly and hedgehog signal transduction. *Dev. Cell*. 18:237–247.

Kozminski, K.G., K.A. Johnson, P. Forscher, and J.L. Rosenbaum. (1993) A Motility in the eukaryotic flagellum unrelated to flagellar beating. *Proc. Natl. Acad.Sci. USA*. 90:5519–5523. http://dx.doi.org/10.1073/pnas.90.12.5519

Kozminski, K.G., P.L. Beech, and J.L. Rosenbaum. (1995) The *Chlamydomonas* kinesin-like protein FLA10 is involved in motility associated with the flagellar membrane. *J. Cell Biol.* 131:1517–1527. http://dx.doi.org/10.1083/jcb.131.6.1517

Kuchka, M.R., and J.W. Jarvik. (1987) Short-Flagella Mutants of *Chlamydomonas reinhardtii*. *Genetics*. 115:685–691.

Lechtreck, K.F. (2013) In vivo imaging of IFT in *Chlamydomonas* flagella. *Methods Enzymol.* 524:265–284. http://dx.doi.org/10.1016/B978-0-12-397945-2.00015-9

Lechtreck, K.F., E.C. Johnson, T. Sakai, D. Cochran, B.A. Ballif, J. Rush, G.J. Pazour, M. Ikebe, and G.B. Witman. (2009) The *Chlamydomonas reinhardtii* BBSome is an IFT cargo required for export of specific signaling proteins from flagella. *J. Cell Biol.* 187:1117–1132. http://dx.doi.org/10.1083/jcb.200909183

Lechtreck, K.F., J.M. Brown, J.L. Sampaio, J.M. Craft, A. Shevchenko, J.E. Evans, and G.B. Witman. (2013A) Cycling of the signaling protein phospholipase D through cilia requires the BBSome only for the export phase. *J. Cell Biol.* 201:249–261. http://dx.doi.org/10.1083/jcb.201207139

Lechtreck, K. F., Gould, T.J., and G. B. Witman. (2013B). Flagellar central pair assembly in *Chlamydomonas reinhardtii*. *Cilia*. 2:15.

Lee, L., (2011). Mechanisms of mammalian ciliary motility: Insights from primary ciliary dyskinesia genetics. *Gene*. 473(2):57-66.

Lefebvre, P.A., Nordstrom, S.A., Moulder, J.E., and Rosenbaum, J.L. (1978) Flagellar elongation and shortening in *Chlamydomonas*. IV. Effects of Flagellar detachment, regeneration, and resorption on the induction of flagellar protein synthesis. *JCB*. 78(1):8-27.

Lefebvre, P.A. (1995) Flagellar amputation and regeneration in *Chlamydomonas*. *Methods Cell Biol.* 47:3–7. http://dx.doi.org/10.1016/S0091-679X(08)60782-7

Lefebvre, P.A. (2009) Flagellar length control. *In* The *Chlamydomonas* sourcebook, Vol. 3: Cell motility and behavior. E.H. Harris and G.B. Witmann, editors. Elsevier, Amsterdam, 115–129.

Liang, Y., Y. Pang, Q. Wu, Z. Hu, X. Han, Y. Xu, H. Deng, and J. Pan. (2014). FLA8/KIF3B phosphorylation regulates kinesin-II interaction with IFT-B to control IFT entry and turnaround. *Developmental cell*. 30:585-597.

Liew, G.M., F. Ye, A.R. et al. (2014). The intraflagellar transport protein IFT27 promotes BBSome exit from cilia through the GTPase ARL6/BBS3. *Developmental cell*. 31:265-278.

Lin, Y.C., P. Niewiadomski, B. Lin, H. Nakamura, S.C. Phua, J. Jiao, A. Levchenko, T. Inoue, R. Rohatgi, and T. Inoue. (2013) Chemically inducible diffusion trap at cilia reveals molecular sieve-like barrier. *Nat. Chem.Biol.* 9:437–443. http://dx.doi.org/10.1038/nchembio.1252

Lohret, T.A., F.J. McNally, and L.M. Quarmby. (1998) A role for katanin-mediated axonemal severing during *Chlamydomonas* deflagellation. *Mol Biol Cell*. **9**(5): p. 1195-207.

Lu, Q., Insinna, C., Ott, C., Stauffer, J., Pintado, P.A., Rahajeng, J., et al. (2015) Early steps in primary cilium assembly require EHD1/EHD3-dependent ciliary vesicle formation. *Nature Cell Biology*. 17:228-240.

Ludington, W.B., L.Z. Shi, Q. Zhu, M.W. Berns, and W.F. Marshall. (2012) Organelle size equalization by a constitutive process. *Curr. Biol.* 22:2173–2179. http://dx.doi.org/10.1016/j.cub.2012.09.040

Ludington, W.B., K.A. Wemmer, K.F. Lechtreck, G.B. Witman, and W.F. Marshall. (2013) Avalanche-like behavior in ciliary import. *Proc. Natl. Acad. Sci. USA*. 110:3925–3930. http://dx.doi.org/10.1073/pnas.1217354110

Luo, M., M. Cao, Y. Kan, G. Li, W. Snell, and J. Pan. (2011) The phosphorylation state of an aurora-like kinase marks the length of growing flagella in Chlamydomonas. *Curr. Biol.* 21:586–591. http://dx.doi.org/10.1016/j.cub.2011.02.046

Mahjoub, M.R., and T. Stearns. (2012) Supernumerary centrosomes nucleate extra cilia and compromise primary cilium signaling. *Curr. Biol.* 22:1628–1634. http://dx.doi.org/10.1016/j.cub.2012.06.057

Mahjoub, M.R., M.L. Trapp, and L.M. Quarmby. (2005) NIMA-related kinases defective in murine models of polycystic kidney diseases localize to primary cilia and centrosomes. *J. Am. Soc. Nephrol.* 16:3485–3489. http://dx.doi.org/10.1681/ASN.2005080824

Macaskill, A. F., Rinholm, J. E., Twelvetrees, A. E., Arancibia-Carcamo, I. L., Muir, J., Fransson, A., Aspenstrom, P., Attwell, D., & Kittler, J. T. (2009). Miro1 is a calcium sensor for glutamate receptor-dependent localization of mitochondria at synapses. *Neuron.* 61, 541–555.

Marshall, W.F., and J.L. Rosenbaum. (2001) Intraflagellar transport balances continuous turnover of outer doublet microtubules: implications for flagellar length control. *J. Cell Biol.* 155:405–414. http://dx.doi.org/10.1083/jcb.200106141

Marshall, W.F., H. Qin, M. Rodrigo Brenni, and J.L. Rosenbaum. (2005) Flagellar length control system: testing a simple model based on intraflagellar transport and turnover. *Mol. Biol. Cell*. 16:270–278. http://dx.doi.org/10.1091/mbc.E04-07-0586

Marshall, W.F. (2008). Chapter 1 Basal Bodies: Platforms for Building Cilia. *Current Topics in Developmental Biology* 85:1-22.

Mitchell, B.F., Pedersen, L.B., Feely, M., Rosenbaum, J.L., and D. R. Mitchell. (2005). ATP Production in *Chlamydomonas reinhardtii* Flagella by Glycolytic Enzymes. *Mol Biol Cell.* 16(10):4509-4518.

Mueller, J., C.A. Perrone, R. Bower, D.G. Cole, and M.E. Porter. (2005) The FLA3 KAP subunit is required for localization of kinesin-2 to the site of flagellar assembly and processive anterograde intraflagellar transport. *Mol. Biol. Cell*. 16:1341–1354. http://dx.doi.org/10.1091/mbc.E04-10-0931

Nachury, M.V., et al. (2007) A core complex of BBS proteins cooperates with the GTPase Rab8 to promote ciliary membrane biogenesis. *Cell.* 129

Nonaka, S., Tanaka, Y., Okada, Y., Takeda, S., Harada, A., Kanai, Y., Kido, M., and Hirokawa, N. (1998) Randomization of Left-right assemetry due to loss of nodal cilia generating leftward flow of extraembryonic fluid in mice lacking KIP3B motor protein. *Cell.* 95(6):829-837.

Oda, T., Yanagisawa, H., Yagi, T., and M. Kikkawa. (2014a) Mechanosignaling Between central apparatus and radial spokes controls axonemal dynein activity. *JCB*. 204(5):807-819.

Oda, T., Yanagisawa, H., Kamiya, R., and M. Kikkawa. (2014b) A molecular ruler determines the repeat length in eukaryotic cilia and flagella. *Science.* 345(6211): 857-60.

Okada, Y., Nonaka, S., Tanaka, Y., Saijoh Y., Hamada, H., and Hirokawa, N. (1999) Abnormal nodal flow precedes situs inversus in iv and inv mice. *Mol Cell*. 4:459-68.

Omran, H. (2010) NPHP proteins: gatekeepers of the ciliary compartment. *J. Cell Biol.* 190:715–717. http://dx.doi.org/10.1083/jcb.201008080

Özgül, R.K., A.M. Siemiatkowska, D. Yücel, C.A. Myers, R.W. Collin, M.N. Zonneveld, A. Beryozkin, E. Banin, C.B. Hoyng, L.I. van den Born, et al. European Retinal Disease Consortium. (2011) Exome sequencing and cis-regulatory mapping identify mutations in MAK, a gene encoding a regulator of ciliary length, as a cause of retinitis pigmentosa. *Am. J. Hum. Genet.* 89:253–264. http://dx.doi.org/10.1016/j.ajhg.2011.07.005

O'Toole ET, Giddings TH Jr, Dutcher SK. (2007) Understanding Microtubule Organizing Centers by Comparing Mutant and Wild-Type Structures with Electron Tomography. In *Methods in Cell Biology*. Edited by McIntosh JR. Academic Press, Waltham, MS :125-143.

Pan, J., and Snell, W. (2007) The primary cilium: keeper of the ke to cell division. *Cell.* 7(29):1255-1257.

Pan, J., Q. Wang, and W.J. Snell. (2004). An aurora kinase is essential for flagellar disassembly in Chlamydomonas. *Developmental cell*. 6:445-451.

Pasquale, S.M., and U.W. Goodenough. (1987) Cyclic AMP functions as a Primary sexual signal in gametes of *Chlamydomonas reinhardtii*. *J. Cell Biol.* 105:2279–2292. http://dx.doi.org/10.1083/jcb.105.5.2279

Pazour, G.J., C.G. Wilkerson, and G.B. Witman. (1998) A dynein light chain is essential for the retrograde particle movement of intraflagellar transport (IFT). *J Cell Biol*. 141(4):979-92.

Pazour, G.J., B.L. Dickert, and G.B. Witman. (1999) The DHC1b (DHC2) isoform of cytoplasmic dynein is required for flagellar assembly. *J Cell Biol*. 144(3): p. 473-81.

Pazour, G.J. and J.L. Rosenbaum. (2002). Intraflagellar transport and cilia-dependent diseases. *Trends Cell Biol*. 12(12):551-5.

Pazour, G.J., N. Agrin, J. Leszyk, and G.B. Witman. (2005). Proteomic analysis of a eukaryotic cilium. *The Journal of cell biology*. 170:103-113.

Pedersen, L.B., Geimer, S., and Rosenbaum, J.L. (2006). Dissecting the molecular Mechanisms of intraflagellar transport in chlamydomonas. Current biology : CB *16*, 450-459.

Pedigo, S., and R.C. Williams Jr. (2002) Concentration dependence of variability in growth rates of microtubules. *Biophys. J.* 83:1809–1819. http://dx.doi.org/10.1016/S0006-3495(02)73946-5

Phirke, P., E. Efimenko, S. Mohan, J. et al .(2011) Transcriptional profiling of *C. elegans* DAF-19 uncovers a ciliary base associated protein and a CDK/CCRK/LF2p-related kinase required for intraflagellar transport. *Dev. Biol.* 357:235–247.

Pigino, G., Geimer, S., et al. (2009) Electron-tomographic analysis of intraflagellar transport particle trains *in situ. JCB.* 187:135-148.

Porter, K.R., Claude, A., and Fullam, E.F. (1945) *J. Exp. Med*. 81, 233-246.

Praetorius HA, Spring KR. (2005) A physiological view of the primary cilium. *Annu Rev Physiol.* 67:515-529.

Preitner, N., J. Quan, D.W. Nowakowski, M.L. Hancock, J. Shi, J. Tcherkezian, T.L. Young-Pearse, and J.G. Flanagan. (2014) APC is an RNA-binding protein, and its interactome provides a link to neural development and microtubule assembly. *Cell*. 158:368–382. http://dx.doi.org/10.1016/j.cell.2014.05.042

Pugacheva, E.N., Jablonski, S.A., Hartman, T.R., Henske, E.P., and Golemis, E.A. (2007) HEF1-dependent Aurora A activation induces disassembly of the primary cilium. *Cell*. 129(7):1351-1363.

Qian, H., M.P. Sheetz, and E.L. Elson. (1991) Single particle tracking. Analysis of diffusion and flow in two-dimensional systems. *Biophys. J.* 60:910–921. http://dx.doi.org/10.1016/S0006-3495(91)82125-7

Qin, H., D.R. Diener, S. Geimer, D.G. Cole, and J.L. Rosenbaum. (2004) Intraflagellar transport (IFT) cargo: IFT transports flagellar precursors to the tip and turnover products to the cell body. *J. Cell Biol.* 164:255–266. http://dx.doi.org/10.1083/jcb.200308132

Rasala, B.A., D.J. Barrera, J. Ng, T.M. Plucinak, J.N. Rosenberg, D.P. Weeks, G.A. Oyler, T.C. Peterson, F. Haerizadeh, and S.P. Mayfield. (2013) Expanding the spectral palette of fluorescent proteins for the green microalga *Chlamydomonas reinhardtii*. *Plant J.* 74:545–556. http://dx.doi.org/10.1111/tpj.12165

Reck-Peterson, S.L., Yildiz, A., Carter, A.P., Gennerich, A., Zhang, N., and R. D. Vale (2010). Single-Molecule Analysis of Dynein Processivity and Stepping Behavior. *Cell.* 126(2):335-348.

Ringo, D.L. (1967). Flagellar motion and fine structure of the flagellar apparatus in *Chlamydomonas*. *JCB* 33:543-571.

Roll-Mecak A. 2015. Intrinsically disordered tubulin tails: complex tuners of microtubule functions? *Seminars in Cell & Devo Biology*. 37:11-19.

Rosenbaum, J.L. and F. M. Child. (1967) Flagellar Regeneration in Protozoan Flagellates. *JCB*. 34(1): 345-364.

Rosenbaum, J.L., J.E. Moulder, and D.L. Ringo. (1969) Flagellar elongation and shortening in *Chlamydomonas*. The use of cycloheximide and colchicine to study the synthesis and assembly of flagellar proteins. *J. Cell Biol.* 41:600–619. http://dx.doi.org/10.1083/jcb.41.2.600

Rosenbaum, J.L., and G.B. Witman. (2002) Intraflagellar transport. *Nat. Rev. Mol. Cell Biol.* 3:813–825. http://dx.doi.org/10.1038/nrm952

Roux, K.J., Kim, D.I., Raida, M., and B. Burke. (2012) A promiscuous biotin ligase fusion protein identifies proximal and interacting proteins in mammalian cells. *JCB.* 196(6):801-810.

Sale, W. S., and Satir, P. (1977). The termination of the central microtubules from the cilia of *Tetrahymena pyriformis*. *Cell Biology International Reports*. 1;45-49.

San Agustin, J.T., Pazour, G.J., and G.B. Witman. (2015) Intraflagellar Transport is Essential for Mammalian Spermiogenesis but is Absent in mature Sperm. *Mol. Bio. Cell.* [Epub ahead of print]

Sang L, Miller Julie J, Corbit Kevin C, Giles Rachel H, Brauer Matthew J, and et al. (2011) Mapping the NPHP-JBTS-MKS Protein Network Reveals Ciliopathy Disease Genes and Pathways. *Cell.* 145**:**513-528.

Satir, Peter. (1999) The cilium as a biological nanomachine. *FASEB .* S236(13)

Satir, P., and S Christensen. (2007). Overview of structure and function of mammalian cilia. *Annu Rev Physiol.* 69: 377-400.

Sbalzarini, I.F., and P. Koumoutsakos. (2005) Feature point tracking and Trajectory analysis for video imaging in cell biology. *J. Struct. Biol.* 151:182–195. http://dx.doi.org/10.1016/j.jsb.2005.06.002

Scholey, JM. (2013) Cilium Assembly: delivery of tubulin by kinesin-2 powered trains. *Curr Biol.* 23(21)R956-9.

Schroer, T. A. (2004). Dynactin*. Annual Review of Cell and Developmental Biology*. 20: 759–779.

Schlager, M.A., oang, H.T., Urnavicius, L., Bullock, S.L., and A.P. Carter. (2014). In Vitro reconstitution of a highly processive recombinant human dynein complex. *EMBO J.* 33(17):1855-68.

Sedar, A. W., and K. R. Porter. (1955) The fine structure of cortical components of Paramecium multimicronucleatum. *JCB*. 1(6) 583-604.

Shaner, N.C., G.G. Lambert, A. Chammas, Y. Ni, P.J. Cranfill, M.A. Baird, B.R. Sell, J.R. Allen, R.N. Day, M. Israelsson, et al. (2013) A bright monomeric green fluorescent protein derived from *Branchiostoma lanceolatum*. *Nat. Methods*. 10:407–409. http://dx.doi.org/10.1038/nmeth.2413

Sharma, N., Z.A. Kosan, J.E. Stallworth, N.F. Berbari, and B.K. Yoder. (2011) Soluble levels of cytosolic tubulin regulate ciliary length control. *Mol. Biol. Cell*. 22:806–816. http://dx.doi.org/10.1091/mbc.E10-03-0269

Shiba D, Manning DK, Koga H, Beier DR, Yokoyama T. (2010) Inv acts as a molecular anchor for Nphp3 and Nek8 in the proximal segment of primary cilia. *Cytoskeleton* 2010, 67:112-119.

Shih, S.M., B.D. Engel, F. Kocabas, T. Bilyard, A. Gennerich, W.F. Marshall, and A. Yildiz. (2013) Intraflagellar transport drives flagellar surface motility. *eLife*. 2:e00744. http://dx.doi.org/10.7554/eLife.00744

Signor, D., et al. (1999) Role of a class DHC1b dynein in retrograde transport of IFT motors and IFT raft particles along cilia, but not dendrites, in chemosensory neurons of living *Caenorhabditis elegans*. *Mol. Biol. Cell.* 10, 693-712.

Silflow, C.D., and J.L. Rosenbaum. (1981) Multiple α- and β-tubulin genes in *Chlamydomonas* and regulation of tubulin mRNA levels after deflagellation. *Cell*. 24:81–88. http://dx.doi.org/10.1016/0092-8674(81)90503-1

Snell, W.J., J. Pan, and Q. Wang. (2004) Cilia and flagella revealed: from flagellar assembly in *Chlamydomonas* to human obesity disorders. *Cell*. 117(6):693-7.

Sorokin, SP. (1968). Reconstruction of centriole formation and ciliogenesis in mammalian lungs. *J Cell Science*. 3:207-230.

Smith, E.F., and P. Yang. (2004) The radial spokes and central apparatus: Mechano-Chemical Transducers that regulate flagellar motility. *Cell Motil Cytoskeleton.* 57(1):8-17.

Srayko, M., A. Kaya, J. Stamford, and A.A. Hyman. (2005) Identification and characterization of factors required for microtubule growth and nucleation in the early *C. elegans* embryo. *Dev. Cell*. 9:223–236. http://dx.doi.org/10.1016/j.devcel.2005.07.003

Summers, K., and M. W. Kirschner. (1979) Characteristics of the polar assembly and disassembly of microtubules observed *in vitro* by darkfield light microscopy. *JCB*. 83(1):205-217.

Supp. D.M., et al. (1997) Mutation of an axonemal dynein affects left-right asymmetry in inversus viscerum mice. *Nature*. 389:963-966.

Tam, L.W., N.F. Wilson, and P.A. Lefebvre. (2007) A CDK-related kinase Regulates the length and assembly of flagella in *Chlamydomonas*. *J. Cell Biol.* 176:819–829. http://dx.doi.org/10.1083/jcb.200610022

Tam, L.W., P.T. Ranum, and P.A. Lefebvre. (2013) CDKL5 regulates flagellar length and localizes to the base of the flagella in *Chlamydomonas*. *Mol. Biol. Cell*. 24:588–600. http://dx.doi.org/10.1091/mbc.E12-10-0718

Tammachote, R., C.J. et al. (2009) Ciliary and centrosomal defects associated with mutation and depletion of the Meckel syndrome genes MKS1 and MKS3. *Hum. Mol. Genet.* 18:3311–3323.

Verhey, K.J., and JW Hammond. (2009). Traffic control: regulation of kinesin motors. *Nat Rev Mol Cell Bio.* 10(11): 765-77.

Verhey KJ, Kaul N, and Soppina V. (2011). Kinesin Assembly and Movement in Cells. *Ann Rev Biophysics* 40: 267-288.

Visscher, K., Schnitzer, M.J., and S.M. Block. (1999). Single kinesin molecules studied with a molecular force clamp. *Nature.* 400:184-189.

Walther, Z., M. et al. (1994) The *Chlamydomonas* FLA10 gene encodes a novel kinesin-homologous protein. *J Cell Biol* 126(1):175-88.

Wang, H., Gau, B., Slade, W.O., Juergens, M., Li, P., and Hicks, L.M. (2014). The Global phosphoproteome of *Chlamydomonas reinhardtii* reveals complex organellar phosphorylation in the flagella and thylakoid membrane. Molecular & cellular proteomics : MCP *13*, 2337-2353.

Wang, L., T. et al. (2013) Flagellar regeneration requires cytoplasmic microtubule Depolymerization and kinesin-13. *J. Cell Sci.* 126:1531–1540.

Wang, X., and Schwarz, T. L. (2009). The mechanism of Ca2+-dependent regulation Of Kinesin mediated mitochondrial motility. *Cell.* 136;163–174.

Weeks, D.P., and P.S. Collis. (1976) Induction of microtubule protein synthesis in *Chlamydomonas reinhardi* during flagellar regeneration. *Cell*. 9(1):15 -27.

Widlund, P.O., Podolski, M., Reber, S., Alper, J., et al (2012) One-step purification of assembly-competent tubulin from diverse eukaryotic sources. *Mol Biol Cell.* 23(22):4393-401.

Williams, C.L., C. et al. (2011) MKS and NPHP modules cooperate to establish basal body/transition zone membrane associations and ciliary gate function during ciliogenesis. *J. Cell Biol.*192:1023–1041.

Witman, G.B. (1975) The site of in vivo assembly of flagellar microtubules. *Ann. N. Y. Acad. Sci.* 253:178–191.

Witman, G.B. (1986) Isolation of *Chlamydomonas* flagella and flagellar axonemes. *Methods Enzymol.* 134:280–290. http://dx.doi.org/10.1016/0076-6879(86)34096-5

Wren, K.N., J.M. Craft, D. Tritschler, A. Schauer, D.K. Patel, E.F. Smith, M.E. Porter, P. Kner, and K.F. Lechtreck. (2013) A differential cargo-loading model of ciliary length regulation by IFT. *Curr. Biol.* 23:2463–2471. http://dx.doi.org/10.1016/j.cub.2013.10.044

Xia, L., et al., (2000) Polyglycylation of tubulin is essential and affects cell motility and division in *Tetrahymena thermophila*. *JCB*. 149 (5):1097-106.

Ye, F., D.K. Breslow, E.F. Koslover, A.J. Spakowitz, W.J. Nelson, and M.V. Nachury. (2013) Single molecule imaging reveals a major role for diffusion in the exploration of ciliary space by signaling receptors. *eLife*. 2:e00654. http://dx.doi.org/10.7554/eLife.00654

Appendix 1: Ciliary Homolog Compendium

	C. reinhardtii	*T. brucei*	*D. rerio*	*C. elegans*	*H. sapiens*
Kinesin motor					
	Kinesin-II motor subunit *FLA8 gene* [61]	KIF3A/ FLA8		KLP11 [1]	
	Kinesin-II Motor subunit *FLA10 gene* [50]	KIP3B/ FLA10 [2]		KLP20	
	KAP non-motor subunit *FLA3 gene* [51]	KAP/FLA3		KAP1 [1]	
				OSM-3, caf-1, klp-2 [3]	
Dynein motor					
	Dhc1b [59]	DHC2.2/DHC2 [4]		CHE3 [5]	
	Dhc1b [59]	DHC2.1/DHC2 [4]		CHE3 [6]	
	Dynein motor-intermediate chain *FAP133* [54]	LC8/FLA14/FAP133 Blisnick unpub			WD34 [54]
	D1bLIC [60]	D1bLIC/D2LIC Blisnick unpub		XBX1 [7]	
				Int chain DYCI-1	
				Light chain XBX-2 [8]	
IFT Complex A					
	IFT43 [56]	IFT43			IFT43 *C14orf179 gene* [63]
	IFT122A (IFT122) [57]	IFT122A		DAF10 OSM-4 [9]	WDR10 [10]
	IFT122B (IFT121) [56]	IFT122B/ OSEG4[11]		IFTA1 (IFT121) [12]	WDR35 [10]
	IFT139 *FLA17* [53,57]	THM1			TTC21B/ THM1 [13]
	IFT140 [57]	IFT140 [11]		CHE11 [14]	
	IFT144 *FLA15* [53,57]	PIFTF6 [11]		DYF2 [8]	WDR19 [15]

	C. reinhardtii	*T. brucei*	*D. rerio*	*C. elegans*	*H. sapiens*
IFT Complex B	IFT20 [58]	IFT20 [11]			
	IFT25 [55]				C1orf41 [55]
	IFT27 [58]				
	IFT46 [58]	IFT46		DYF6 [9]	
	IFT52 [58]	IFT52 [11]		OSM6 [18]	NGD5[10]
	IFT54/*FAP116* [55]	MIP-T3	Elipsa [19,20,21]	DYF11 [22,62]	MIP-T3 TRAF3IP1 [62]
	IFT57	Hippi [11]	Curly [23]	CHE13 (che-9) [24]	Hippi (mammals)[10]
	IFT70/ *FAP259*	PIFB2 [11]	Fleer [25]	DYF1 [26]	
	IFT74 [58]			IFT74 (72/74) [27]	Cmg1
	IFT80 [58]	IFT80 [11, 28]		CHE2 [29]	WDR56
	IFT81 [58]	IFT81	Larry [23]	IFT81 [27]	
	IFT88 [58]	Tg737 [4]	Oval [30,31]	OSM5 [32]	Gene TG737/ Polaris
	IFT172/ *FLA11* [52,58]	IFT172 [11]	Moe [23]	OSM1 [9]	Wimple (mammals) [10]
	TTC26/ *FAP22*	PIFTC3 [11]	Qilin [26,23]	DYF13 (DYF3) [33,34]	
BBS					
	BBS1 (core) [68]	BBS1	BBS1	BBS1 [35]	BBS1 [reviewed in 71]
	BBS2 (core)	BBS2	BBS2	BBS2 [35]	BBS2 [71]
	BBS3	ARL-6	ARL-6	ARL-6 [36]	ARL-6 [71]
	BBS4 (core)[68]	BBS4	BBS4	BBS4	BBS4 [71]
	BBS5 (core)[68]	BBS5	BBS5	BBS5	BBS5 [71]
	BBS6		BBS6		BBS6 [71]
	BBS7 (core)[68]	BBS7	BBS7	OSM-12 [35]	BBS7 [71]
	BBS8 (core)[68]	BBS8	BBS8	BBS8 [35]	BBS8 [71]
	BBS9 (core)	BBS9	BBS9	BBS9	BBS9 [71]
	BBS10		BBS10		BBS10 [69,71]
	BBS11		TRIM32		TRIM32 [71]
	CCDC28B		CCDC28B		CCDC28B
					BBS12 [70]

	C. reinhardtii	*T. brucei*	*D. rerio*	*C. elegans*	*H. sapiens*
Central pair	Pf6 [37,38,39,40]				SPAG17 (mammals) [64]
	Pf16 [37,41]				SPAG6 (mammals) [65]
	Pf20 [39,42]				SPAG16L (mammals) [66]
	Cpc1 [43,44]				rnKPL2
	KLP1-KD [45,46]				KIF9 (mammals)
	Hydin [47]				MmHydin
Other					
	Trpv channel			OSM-9 [48]	
	Trpv channel			OCR-2 [49]	
	Arl13b				Arl13b [67]
	Oda7p		Switch hitter		

REFERENCES FOR CILIARY HOMOLOG COMPENDIUM

1. Snow, J.J., G. Ou, A.L. Gunnarson, M.R. Walker, H.M. Zhou, I. Brust-Mascher, and J.M. Scholey. (2004). Two anterograde intraflagellar transport motors cooperate to build sensory cilia on C. elegans neurons. *Nat. Cell Biol*. 6:1109–1113.

2. Kohl, L. and Bastin, P. (2005). The Flagellum of Trypanosomes. In International Review of Cytology,vol. 244, pp. 227-285. *New York: Academic Press*.

3. Shakir, MA, Fukushige T, Yasuda H, Miwa J, Siddiqui SS. (1993). C. elegans osm-3 Gene Mediating osmotic avoidance behavior encodes a kinesin-like protein. *Neuroreport* Jul;4(7)891-4.

4. Kohl L, Robinson D, Bastin P (2003). Novel roles for the flagellum in cell morphogenesis and cytokinesis of trypanosomes. *EMBO J* 22, 5336–5346

5. Signor D, Wedaman K, Orozco J, Dwyer N, Bargmann C, Rose L, Scholey J. (1999). Role of a class Dhc1b dynein in retrograde transport of ift motors and ift raft particles along cilia, but not dendrites, in chemosensory neurons of living *C. elegans. JCB.* 147(3): 519-530.

6. Wicks SR, de Vries CJ, van Luenen HG, Plasterk RH. (2000). CHE-3, a cytosolic Dynein heavy chain, is required for sensory cilia structure and function in C. elegans. *Dev Biol.* 211(2):295-307.

7. Schafer JC, Haycraft CJ, Thomas JH, Yoder BK, Swoboda P. (2003). XBX-1 encodes A dynein light intermediate chain required for retrograde intraflagellar transport and cilia assembly in C. elegans. 14(5):2057-70.

8. Efimenko E, Bubb K, Mak HY, Holzman T, Leroux MR, Ruvkun G, Thomas JH, Swoboda P. (2005). Analysis of xbx genes in C. elegans. *Development.* Apr;132(8):1923-34.

9. Bell LR, Stone S, Yochem J, Shaw HE, Herman Rk. (2006). The molecular identities of the C.elegans intraflagellar transport genes, dyf-6, daf-10, and osm-1. *Genetics*. July;173(3):1275-86.

10. Taschner M, Bhogaraju S, Lorentzen E. (2012). Architecture and function of IFT Complex proteins in ciliogenesis*. Differentiation*. Feb; 83(2):S12-S22.

11. Absalon, S., Blisnick, T., et al. (2008). Intraflagellar transport and functional analysis of genes required for flagellum formation in trypanosomes. *Mol. Biol. Cell 19*, 929-944.

12.Blacque O, Li C, Inglis P, Esmail M, Ou G, Mah A, Baillie D, Scholey J, Leroux M. (2006). The WD repeat-containing protein IFTA-1 is required for retrograde intraflagellar transport. *Mol Biol Cell.* Dec; 17(12):5053-5062.

13. Goetz SC, Anderson KV. (2010). The primary cilium: a signalling centre during Vertebrate development. *Nature Reviews Genetics*. 11:331–344.

14.Qin H, Rosenbaum JL, Marr MM. (2001). An autosomal recessive polycystic kidney Disease gene homolog is involved in intraflagellar transport in C. elegans ciliated sensory neurons. *Curr Biol.* Mar20;11(6):457-61.

15. Lin B, White JT, Utleg AG, et al. (2003). Isolation and characterization of human and mouse WDR19,a novel WD-repeat protein exhibiting androgen-regulated expression in prostate epithelium. *Genomics. 2003 Sep; 82(3):331-42.*

16. Adhiambo C, Blisnick T, Toutirais G, Delannoy E, Bastin P. (2009) A novel function for the Atypical small G protein Rab-like 5 in the assembly of the trypanosome flagellum. *J Cell Sci*.122:834–841.

17. Schafer JC, Winkelbauer ME< Williams CL, Haycraft CJ, Desmond RA, Yoder BK. (2006). *JCell Sci*. Oct 1:1119(pt19):4088-100

18. Collet J, Spike CA, Lundquist EA, Shaw JE, Herman RK. (1998). Analysis of osm-6, a gene that affects sensory cilium structure and sensory neuron function in *C. elegans*. *Genetics*. Jan;148(1):187-200.

19. Drummond IA, Majumdar A, et al. (1998) Early development of the zebrafish pronephros and analysis of mutations affecting pronephric function. *Development* 125:4655–4667.

20. Malicki J, Schier AF, Solnica-Krezel L, et al. (1996) Mutations affecting development of the zebrafish ear.. *Development,* 123, 275-283.

21. Omori Y, Zhao C, Saras A, et al. (2008). Elipsa is an early determinant of ciliogenesis that links the IFT particle to membrane-associated small GTPase Rab8. *Nat CellBiol*. 10:437–44.

22. Bacaj T, Lu Y, Shaham S. (2008). The conserved proteins CHE-12 and DYF-11 are Required for sensory cilium function in C. elegans. *Genetics.* Feb;178(2):989-1002.

23. Sun, Z., A. Amsterdam, G.J. Pazour, D.G. Cole, M.S. Miller, N. Hopkins. (2004). A genetic screen in zebrafish identifies cilia genes as a principal cause of cystic kidney. *Development*.131:4085–4093.

24. Haycraft CJ, Schafer JC, Zhang Q, Taulman PD, Yoder BK. (2003). Identification of CHE-13, a novel intraflagellar transport required for cilia formation. *Exp Cell Res* 284(2):251-63.

25. 0Pathak N, Obara T, manos S, Liu Y, Drummond I. (2007). The Zebrafish fleer gene encodes an essential regulator of cilia tubulin polyglutamylation. *Mol Bio Cell*. (11):4353-4364.

26. Ou G, Qin H, Rosenbaum J, Scholey J. (2005). The PKD protein qilin undergoes intraflagellar transport. *Current Biology*. 15;11. R4100-411.

27. Kobayashi T, Gengyo-Ando K, Ishihara T, Katsura I, Mitani S. (2007). IFT-81 and IFT-74 are required for intraflagellar transport in *C. elegans. Genes Cells.* 12(5):593-602.

28. Davidge JA, Chambers E, et al. (2006). Trypanosome IFT mutants provide insight into the motor location for mobility of the flagella connector and flagellar membrane formation*. J Cell Science*. 119(pt19):3935-43.

29. Fujiwara M, Ishihara I, Katsura I. (1999). A novel WD40 protien, CHE-2, acts cell-autonomously in the formation of C. elegans sensory cilia*. Development*. 126:4839-4848.

30. Brand M, HeisenbergCP, et al. (1996). Mutations in zebrafish genes affecting the formation fo the boundary between midbrain and hindbrain. *Development*. 123:179-90.

31. Tsujikawa M, Milicki J. (2004). Intraflagellar transport genes are essential for Differentiation and survival of vertebrate sensory neurons*. Neuron.* 42(5):703-16.

32. Haycraft CJ, Swoboda P., Taulman PD, Thomas JH, Yoder BK. (2001). The *C. Elegans* homology of the murine cystic kidney disease gene TG737 functions in a ciliogeneic pathway and is disrupted in OSM-5 mutant worms. *Development*. 128(9):1496.505.

33. Blacque O. E., et al. (2005). Functional genomics of the cilium, a sensory organelle. *Curr.Biol*. 15:935–941.

34. Murayama T, Toh Y, Ohshima Y, Koga M. (2005). The dyf-3 gene encodes a novel Protein required for sensory cilium formation in *C. elegans. J Mol Biol.* 346(3):677-87.

35. Blacque O. E., et al. (2004). Loss of *C. elegans* BBS-7 and BBS-8 protein function results in Cilia defects and compromised intraflagellar transport. *Genes Dev.* 18:1630–1642.

36. Fan Y, Esmail MA, Ansley SJ, Blacque OE, Boroevich K, Ross AJ, Moore SJ, Badano JL, May-Simera H, et al. (2004). Mutations in a member of the Ras superfamily of small GTP-binding proteins causes Bardet-Biedl syndrome. *Nat Genet*, 36(9):989-93.

37. Dutcher, S. K., Huang, B. and Luck, D. L. (1984). Genetic dissection of the central Pair microtubules of the flagella of Chlamydomonas reinhardtii. *J. Cell Biol*. 98, 229-236.

38. Rupp, G., O'Toole, E. and Porter, M. E. (2001). The *Chlamydomonas* PF6 locus encodes a large alanine/proline-rich polypeptide that is required for assembly of a central pair projection and regulates flagellar motility. *Mol. Biol. Cell.* 12, 739-751.

39. Starling D, Randall J. (1971). The flagella of temporary dikaryons of *Chlamydomonas reinhartii. Genetical Research*, Cambridge. 18:107–113.

40. Witman, G. B., Plummer, J. and Sander, G. (1978). *Chlamydomonas* flagellar Mutants lacking radial spokes and central tubules. Structure, composition, and function of specific axonemal components. *J. Cell Biol*. 76, 729-747.

41. Smith EF, Lefebvre PA. (1996). PF16 encodes a protein with armadillo repeats and localizes to a single microtubule of the central apparatus in *Chlamydomonas* flagella*. J Cell Biol*.132:359–370.

42. Adams GM, Huang B, Piperno G, Luck DJ. (1981). Central-pair microtubular complex of *Chlamydomonas* flagella: polypeptide composition as revealed by analysis of mutants. *J Cell Biol*. 91:69–76.

43. Mitchell, D. R. and Sale, W. S. (1999). Characterization of a *Chlamydomonas* Insertional mutant that disrupts flagellar central pair microtubule-associated structures. *J. Cell Biol*. 144, 293-304.

44. Zhang, H. and Mitchell, D. R. (2004). Cpc1, a *Chlamydomonas* central pair protein with an adenylate kinase domain. *J. Cell Sci*. 117, 4179-4188.

45. Bernstein M, Beech PL, Katz SG, Rosenbaum JL. (1994). A new kinesin -like Protein (KLP1) localized to a single microtubule of the *Chlamydomonas* flagellum. *JCB* 125 (6);1313.

46. Yokoyama R, O'Toole E, Ghosh S, Mitchell D. (2004).Regulation of flagellar dynein Activity by a central pair kinesin. *PNAS.* 101 (50);17398-17403.

47. Lechtreck KF, Witman GB. (2007) *Chlamydomonas reinhardtii* hydin is a central pair Protein required for flagellar motility.*J Cell Biol*. 176:473–482.

48. Colbert HA, Smith TL, Bargmann CI. (1997) OSM-9, a novel protein with structural Similarity to channels, is required for olfaction, mechanosensation, and olfactory adaptation in *Caenorhabditis elegans*. *J Neurosci*.1997;17(21):8259–69.

49. Tobin D, Madsen D, Kahn-Kirby A, Peckol E, Moulder G, Barstead R, Maricq A, Bargmann C. (2002) Combinatorial expression of TRPV channel proteins defines their sensory functions and subcellular localization in *C.elegans* neurons. *Neuron.* 35:307–18.

50. Walther, Z., M. Vashishtha, and J.L. Hall. (1994) The *Chlamydomonas* FLA10 gene encodes a novel kinesin-homologous protein. *J Cell Biol* 126(1):175-88.

51. Mueller, J., Perrone, CA, Bower, R, Cole, D.G., and Porter, M. E. (2005) The FLA3 KAP subunit is required for localization of kinesin-2 to the site of flagellar assembly and processive anterograde intraflagellar transport. *Mol. Biol. Cell.* 16(3):1341-54.

52. Pedersen, L.B., Miller, M.S., Geimer, S., Leitch, J.M, Rosenbaum, J.L., and Cole, D.G. (2005) *Chlamydomonas* IFT172 is encoded by FLA11, interacts with CrEB1, and regulates IFT at the flagellar tip. *Curr Biol.* 15(3)262-6.

53. Iomini, C., Esparza, J.M, and Dutcher, S.K. (2009) Retrograde intraflagellar Transport mutants identify complex A proteins with multiple genetic interactions in *Chlamydomonas reinhardtii. Genetics*. (3):885-96.

54. Rompolas, P., Pedersen, L.B., et al. (2007). *Chlamydomonas* FAP133 is a dynein intermediate chain associated with the retrograde intraflagellar transport motor. *J Cell Sci.* 120)Pt 20):3653-65.

55. Follit, J.A., Xu, F., Keady, B.T., and Pazour, G.J. (2009). Characterization of mouse IFT complex B. *Cell Motil Cytoskeleton.* (8):457-68.

56. Cole, D.G. (2003) The intraflagellar transport machinery of *Chlamydomonas reinhardtii. Traffic.* 4:435-442.

57. Piperno, G., and Mead, K. (1997) Transport of a novel complex in the cytoplasmic Matrix of *Chlamydomonas* flagella. *PNAS* 94:4457-4462.

58. Cole, D.G., Diener, D.R., Himelblau, A.L., Beech, P.L., Fuster, J.C., and Rosenbaum, J.L. (1998). *Chlamydomonas* kinesin-II-dependent intraflagellar transport (IFT): IFT particles contain proteins required for ciliary assembly in *Caenorhabditis elegans* sensory neurons. *JCB*. 141:993-1008.

59. Pazour, G.J., Dickert, B.L., Witman, G.B. (1999) The DHC1b (DHC2) isoform of cytoplasmic dynein is required for flagellar assembly. *JCB*. 144(3):473-81.

60. Hou, Y., Pazour, G.J., and Witman, G.B. (2004) A dynein light intermediate chain, D1bLIC, is required for retrograde intraflagellar transport. *Mol. Biol. Cell.* 15(10):4382-94.

61. Miller, M.S., Esparza, J.M., LIppa, A.M., Lux 3rd, F.G., Cole, D.R., and Dutcher, S.K. (2005). Mutant kinesin-2 motor subunits increase chromosome loss. *Mol. Biol.Cell.* 16(8):3810-20.

62. Kunitomo, H., and Iino, Y. (2008). *Caenorhabditis elegans* DYF-11, an orthologue of mammalian/ Traf3ip1/MIP-T3, is required for sensory cilia formation. *Genes Cells.* 13(1):13-25.

63. Arts, H.H., Bongers, E.M., Mans, D.A., van Beersum, S.E., and et al. (2011). C14orf179 encoding IFT43 is mutated in Sensenbrenner syndrome. *J Med Genet.* 48(6)390-5.

64. Zhang, Z., et al., (2005). Dissecting the axoneme interactome: the mammalian orthologue of *Chlamydomonas* PF6 interacts with sperm-associated antigen 6, the mammalian orthologue of *Chlamydomonas* PF16. *Mol Cell Proteomics*. 4(7): 914-23.

65. Sapiro, R., et al., (2002). Male infertility, impaired sperm motility, and hydrocephalus in mice deficient in sperm-associated antigen 6. *Mol Cell Biol,* 22(17):6298-305.

66. Lesich, K.A., Zhang, Z., Kelsch, C.B., Ponichter, K.L., Strauss III, J.F., and Lindemann, C.B. (2009). Functional Deficiencies and a reduced response to calcium in the flagellum of mouse sperm lacking SPAG16L. *Biol Reprod.* 82(4):736-744.

67. Cantagrel, V., Silhavy, J. L., Bielas, S. L., Swistun, D., Marsh, S. E., Bertrand, J. Y., Audollent, S., Attie-Bitach, T., Holden, K. R., Dobyns, W. B., et al. (2008). Mutations in the cilia gene ARL13B lead to the classical form of Joubert syndrome. *Am J Hum Genet* 83, 170-179.

68. Lechtreck, K.F., Johnson, E. C., Sakai, T., Cochran, D., Ballif, B.A., Rush, J., Pazour, G.J., Ikebe, M., and Witman, G.B. (2009). The *Chlamydomonas reinhardtii* BBSome is an IFT cargo required for export of specific signaling proteins from flagella. *JCB*. 187(7)1117-1132.

69. Stoetzel, C., Laurier, V., Davis, E.E., Muller, J., et al (2006). *BBS10* encodes a Vertebrate -specific chaperonin-like protein and is a major BBS locus. *Nat. Genet.* 38:521–524.

70. Stoetzel, C., Muller, J., Laurier, V., Davis, E.E., Zaghloul, Z.A., et al. (2007) Identification of a novel BBS gene (*BBS12*) highlights the major role of a vertebrate-specific branch of chaperonin-related proteins in Bardet-Biedl syndrome. *Am. J. Hum. Genet.* 80:1–11.

71. Blacque, O.E., and Leroux, M.R. (2006) Bardet-Biedl syndrome: an emerging pathomechanism of intracellular transport. *Cellular and Molecular Life Science.* 63:2145-2161.

Appendix 2: Causative Genes of Ciliopathies

Ciliopathy	Causative genes and ciliary localization			
	Basal Bodies	**Transition zone**	**Inversin compartment**	**Cilioplasm/axoneme**
Alström syndrome	ALMS1[1]			
Bardet-Biedl syndrome	MGC1203[85]	MKS1/ BBS13[2]		BBS1[3], BBS2[4] BBS3 (Arl13b) [5,6] BBS4[7], BBS5[8], BBS6/MKKS[9] BBS7[10] BBS8/TRIM32[11] BBS9/PTHB1[12] BBS10[13] BBS11/TRIM32[14] BBS12[15] TMEM67[84]
Jeune asphyxiating thoracic dystrophy	CEP120[16] CSPP1[17] WDR34[18] WDR60[19]			TCTEX1D2[20] IFT72[21], IFT80[22] IFT144/WDR19[23] DYNC2H1[16] IFT40[24] IFT139/TTC21B[25]
Joubert syndrome	AHI1[26,27] CEP41[28] RPGRIP1L/ MKS5[29] CSPP1[30], SCLT1[31]	NPHP1[32] CEP290/ NPHP6/MKS4 [33,79,83] CCDC2A/ MKS6[34] MKS3/ TMEM67[80]		BBS3/ARL13b[35] TMEM67/MKS3[36] INPP5E[115] KIAA0586 [117]
Leber congenital amaurosis	AIPL1[37] CRX[38] RDH12[39]	CEP290/ NPHP6/MKS4 [40] RPGRIP1[86]		CRB1[41,42], GUCY2D[39] RPE65[43], LCA5[44] IMPDH1[81] RDH12[82]
Mainzer-Saldino syndrome				IFT72[21] IFT140[24,119]
Meckel-Gruber syndrome	MKS1/ BBS13[2]	TMEM67/ MKS3[45] CC2D2A/ MKS6[46] MKSR-1,-2[47] TMEM231[48] RPGRIP1L/ MKS5[50]	NPHP3[51]	TMEM67/MKS3[48] BBS2[52] BBS4[52] BBS6/MKKS[52]
MORM syndrome				INPP5E[116]

	Basal Bodies	**Transition zone**	**Inversin compartment**	**Cilioplasm/axoneme**
Nephronophthisis	CEP83[53] CEP164/ NPHP15[54] SCLT1[31]	NPHP4[55,56] NPHP1[57] NPHP5[58] GLIS2[59] RPGRIP1L/ MKS5[60]	INVS/ NPHP2[61] NPHP3[62] NEK8[63] ANKS6/ NPHP16[64]	IFT81[118]
Orofaciodigital syndrome	OFD1[65,66] C2CD3[67,68] SCLT1[31]	TMEM231[69]		
Polycystic Kidney Disease				PKD1[70], PKD2[70] Fibrocystin[71] IFT88[72]
Rod-Cone dystrophy	RPGR[73]	RPGRIP1[74]		HRG4[75]
Senior-Løken syndrome	NPHP5[58]	NPHP4[76] NPHP1[77]	NPHP3[62] INVS[78]	
Sensenbrenner syndrome				WDR35[120] IFT122[121] IFT43[122]
Primary Ciliary Dyskinesia	OFD1[87,88] RPGR[89] CCNO[90]			DNAI1 [91],DNAH5[92] DNAI2[93] TXNDC3[94] DNAL1[95] CCDC114[96] ARMC4[97] CCDC151[98] CCDC103[99] KTU(DNAAF2)[100] LRRC50(DNAAF1) [101] DNAAF3[102] DYX1C1[103] HEATR2[104] LRRC6[105] ZMYND10[106] SPAG1[107] C21orf59[108] CCDC39[109] CCDC40[109] CCDC164[110] CCDC65[108] RSPH4A[111]

				RSPH9[111] PSPH1[112] HYDIN [113] DNAH11[114]

REFERENCES FOR CAUSATIVE GENES OF CILIOPATHIES

1. Alvarez-Satta, M., Castro-Sanchez, S., and D. Valverde. (2015). Alstrom syndrome: Current perspectives. *Appl clin Genet.* 8:171-179.

2. Kyttala, M., Tallila, J., et al. (2006). MKS1, encoding a component of the flagellar apparatus basal body proteome, is mutated in Meckel syndrome. *Nat Genet* 38, 155-157.

3. Mykytyn, K., Nishimura, D. Y., et al. (2002). Identification of the gene (BBS1) most commonly involved in Bardet-Biedl syndrome, a complex human obesity syndrome. *Nat Genet* 31, 435-438.

4. Nishimura, D. Y., Searby, C. C., et al. (2001). Positional cloning of a novel gene on chromosome 16q causing BardetBiedl syndrome (BBS2). *Hum Mol Genet* 10, 865-874.

5. Fan, Y., Esmail, M. A., et al. (2004). Mutations in a member of the Ras superfamily of small GTP-binding proteins causes Bardet-Biedl syndrome. *Nat Genet* 36, 989-993.

6. Chiang, A. P., Nishimura, D., et al. (2004). Comparative genomic Analysis identifies an ADP-ribosylation factor-like gene as the cause of Bardet-Biedl syndrome (BBS3). *Am J Hum Genet* 75, 475-484.

7. Mykytyn, K., Braun, T., et al. (2001). Identification of the gene that, when mutated, causes the human obesity syndrome BBS4. *Nat Genet* 28, 188-191.

8. Li, J. B., Gerdes, et al. (2004). Comparative genomics identifies a flagellar and basal body proteome that includes the BBS5 human disease gene. *Cell* 117, 541-552.

9. Katsanis, N., Beales, P. L., et al. (2000). Mutations in MKKS cause obesity, retinal dystrophy and renal malformations associated with Bardet-Biedl syndrome. *Nat Genet* 26, 67-70.

10. Badano, J. L., Ansley, S. J., et al. (2003). Identification of a novel Bardet -Biedl syndrome protein, BBS7, that shares structural features with BBS1 and BBS2. *Am J Hum Genet* 72, 650-658.

11. Ansley, S. J., Badano, J. L., et al. (2003). Basal body dysfunction is a likely cause of pleiotropic Bardet-Biedl syndrome. *Nature* 425, 628-633.

12. Nishimura, D. Y., Swiderski, R. E., et al. (2005). Comparative genomics and gene expression analysis identifies BBS9, a new Bardet-Biedl syndrome gene. *Am J Hum Genet* 77, 1021- 1033.

13. Stoetzel, C., Laurier, V., et al. (2006). BBS10 encodes a vertebrate -specific chaperonin-like protein and is a major BBS locus. *Nat Genet* 38, 521-524.

14. Chiang, A. P., et al. (2006). Homozygosity mapping with SNP Arrays identifies TRIM32, an E3 ubiquitin ligase, as a Bardet-Biedl syndrome gene (BBS11*). Proc Natl Acad Sci* U S A 103, 6287-6292.

15. Stoetzel, C., et al. (2007). Identification of a novel BBS gene (BBS12) highlights the major role of a vertebrate-specific branch of chaperonin-related proteins in Bardet-Biedl syndrome. *Am J Hum Genet* 80, 1-11.

16. Shaheen, R., Schmidts, M, et al. (2015). A founder CEP120 mutation in Jeune Asphyxiating thoracic dystrophy expands the role of centriolar proteins in skeletal ciliopathies. *Hum Mol Genetics.* 5:1410-9.

17. Shaheen R., Shamseldin H.E., et al. (2014). Mutations in *CSPP1*, encoding a core centrosomal protein, cause a range of ciliopathy phenotypes in humans. *Am. J. Hum. Genet*. 94:73-79.

18. Schmidts M., Vodopiutz J., et al. (2013). Mutations in the gene encoding IFT Dynein Complex Component WDR34 cause Jeune asphyxiating thoracic dystrophy. *Am.J. Hum. Genet*.93:932-944.

19. McInerney-Leo A.M., Schmidts M., et al. (2013) Short-rib polydactyly and Jeune syndromes are caused by mutations in *WDR60*. *Am. J. Hum. Genet*. 93:515-523.

20. Schmidts M., Hou Y., et al. (2015). TCTEX1D2 mutations underlie Jeune Asphyxiating Thoracic dystrophy with impaired retrograde intraflagellar transport. *Nat commun.* 6:7074.

21. Halbritter J., Bizet A.A., et al. (2013) Defects in the IFT-B component IFT172 cause Jeune and Mainzer-Saldino Syndromes in humans. *Am. J. Hum. Gene*t. 93:915-925.

22. Beales P.L., Bland E., et al. (2007) IFT80, which encodes a conserved intraflagellar transport protein, is mutated in Jeune asphyxiating thoracic dystrophy. *Nat. Genet*. 39:727-729.

23. Bredrup C., Saunier S., et al. (2011). Ciliopathies with skeletal anomalies and renal insufficiency due to mutations in the IFT-A gene *WDR19*. *Am. J. Hum.Genet.* 89:634-643.

24. Schmidts M., Frank V., et al. (2013). Combined NGS approaches identify mutations in the intraflagellar transport gene IFT140 in skeletal ciliopathies with early progressive kidney disease. *Hum. Mutat*. 34:714-724.

25. Davis E.E., Zhang Q., Liu Q., Diplas B.H., Davey L.M., Hartley J., Stoetzel C., Szymanska K., Ramaswami G., Logan C.V. TTC21B contributes both causal and modifying alleles across the ciliopathy spectrum. *Nat. Genet*. 2011;43:189-196.

26. Ferland, R. J., Eyaid, W., Collura, R. V., Tully, L. D., Hill, R. S., Al-Nouri, D., AlRumayyan, A., Topcu, M., Gascon, G., Bodell, A., et al. (2004). Abnormal cerebellar development and axonal decussation due to mutations in AHI1 in Joubert syndrome. *Nat Genet* 36, 1008-1013.

27. Dixon-Salazar, T., et al. (2004). Mutations in the AHI1 gene, encoding jouberin, cause Joubert syndrome with cortical polymicrogyria. *Am J Hum Genet* 75, 979-987.

28. Lee, J.E., Silhavy, J.L., Zaki, M.S., Schroth, J., Bielas, S.L., and et al. (2012). CEP41 is mutated in Joubert syndrome and is required for tubulin glutamylation at the cilium. *Nat Genet.* 44(2)193-9.

29. Arts, H. H., Doherty, D., et al. (2007). Mutations in the gene encoding the basal body protein RPGRIP1L, a nephrocystin-4 interactor, cause Joubert syndrome. *Nat Genet.* 39, 882-888.

30. Tuz K., Bachmann-Gagescu R., et al. (2014). Mutations in *CSPP1* cause primary cilia abnormalities and Joubert syndrome with or without Jeune asphyxiating thoracic dystrophy. *Am. J. Hum. Genet*. 94:62-72.

31. Adly N, Alhashem A, Ammari A, Alkuraya FS. 2014. Ciliary genes TBC1D32/C6orf170 and SCLT1 are mutated in patients with OFD type IX. *Hum Mutat.* 35:36-40.

32. Parisi, M. A., Bennett, C. L., et al. (2004). The NPHP1 gene deletion associated with juvenile nephronophthisis is present in a subset of individuals with Joubert syndrome. *Am J Hum Genet* 75, 82-91.

33. Valente, E.M., Silhavy, J.L., et al. (2006). Mutations in CEP290, which encodes a centrosomal protein, cause pleiotropic forms of Joubert syndrome. *Nat Genet.* 38(6):623-5.

34. Tallila, J., Jakkula, E., et al. (2008). Identification of CC2D2A as a Meckel syndrome gene adds an important piece to the ciliopathy puzzle. *Am J Hum Genet* 82, 1361-1367.

35. Cantagrel, V., et al. (2008). Mutations in the cilia gene ARL13B lead to the classical form of Joubert syndrome. *Am J Hum Genet* 83, 170-179.

36. Baala, L., Audollent, S., et al. (2007a). Pleiotropic effects of CEP290 (NPHP6) mutations extend to Meckel syndrome. *Am J Hum Genet* 81, 170-179.

37. Sohocki, M. M., et al. (2000). Mutations in a new photoreceptor-pineal gene on 17p cause Leber congenital amaurosis. *Nat Genet* 24, 79-83.

38. Freund, C. L., et al. (1998). De novo mutations in the CRX homeobox gene

associated with Leber congenital amaurosis. *Nat Genet* 18, 311-312.

39. Perrault, I., Rozet, J. M., et al. (1996). Retinal-specific guanylate cyclase gene mutations in Leber's congenital amaurosis. *Nat Genet* 14, 461-464.
40. den Hollander, A. I., et al. (2006). Mutations in the CEP290 (NPHP6) gene are a frequent cause of Leber congenital amaurosis. *Am J Hum Genet* 79, 556-561.
41. Lotery, A. J., Jacobson, S. G., et al. (2001). Mutations in the CRB1 gene cause Leber congenital amaurosis. *ArchOphthalmol* 119, 415-420.
42. den Hollander, A. I., et al. (2001). Leber congenital amaurosis and retinitis pigmentosa with Coats-like exudative vasculopathy are associated with mutations in the crumbs homologue 1 (CRB1) gene. *Am J Hum Genet* 69, 198-203.
43. Marlhens, F., Bareil, C., et al. (1997). Mutations in RPE65 cause Leber's congenital amaurosis. *Nat Genet* 17, 139-141.
44. den Hollander, A. I., Koenekoop, R. K., et al. (2007). Mutations in LCA5, encoding the ciliary protein lebercilin, cause Leber congenital amaurosis. *Nat Genet* 39, 889-895.
45. Smith, U.M., Consugar, M., et al. (2006). The transmembrane protein meckelin (MKS3) is mutated in Meckel-Gruber syndrome and the wpk rat. *Nat Genet.* 38(2)191-196.
46. Gorden, N. T., Arts, H. H., et al. (2008). CC2D2A is mutated in Joubert syndrome and interacts with the ciliopathy associated basal body protein CEP290. *Am J Hum Genet* 83, 559-571.

47. Bialas, N.J., et al. (2009). Functional interactions between the ciliopathy -associated Meckel syndrome 1 (MKS1) protein and two novel MKS1-related (MKSR) proteins. *J Cell Sci.* 122(5):611-24.

48. Smith, U. M., Consugar, M., et al. (2006). The transmembrane protein meckelin (MKS3) is mutated in Meckel-Gruber syndrome and the wpk rat. *Nat Genet* 38, 191-196.

50. Delous, M., Baala, L., et al. (2007). The ciliary gene RPGRIP1L is mutated in cerebello-oculo-renal syndrome (Joubert syndrome type B) and Meckel syndrome. *Nat Genet* 39, 875-881.

51. Bergmann, C., Fliegauf, M., et al. (2008). Loss of nephrocystin-3 function can cause embryonic lethality, Meckel-Gruber-like syndrome, situs inversus, and renal-hepatic-pancreatic dysplasia. *Am J Hum Genet* 82, 959-970.

52. Karmous-Benailly, H., Martinovic, J., et al. (2005). Antenatal presentation of Bardet-Biedl syndrome may mimic Meckel syndrome. *Am J Hum Genet* 76, 493-504.

53. Failler M, Gee HY, et al. (2014). Mutations of CEP83 Cause infantile nepronophthisis and intellectual disability. *Am J HumGenet.* 94(6): 905-14.

54. Chaki, M, Airik R, Ghosh AK, et al. 2012. Exome capture reveals ZNF423 and CEP164 mutations, linking renal ciliopathies to DNA damage response signaling. *Cell*. 150: 533-548.

55. Mollet, G., Salomon, R., et al. (2002). The gene mutated in juvenile nephronophthisis type 4 encodes a novel protein that interacts with nephrocystin. *Nat Genet* 32, 300-305.

56. Winklebauer, M.E., J.C. Schafer, C.J. Haycraft, P. Swoboda, B.K. Yoder. (2005) The *C.elegans* homologs of nephrocystin-1 and nephrocystin-4 are cilia transition zone proteins involved in chemosensory perception *J. Cell Sci*., 118; 5575–5587.

57. Hildebrandt, F., Otto, E., et al. (1997). A novel gene encoding an SH3 domain protein is mutated in nephronophthisis type 1. *Nat Genet* 17, 149-153.

58. Otto, E. A., et al. (2005). Nephrocystin-5, a ciliary IQ Domain Protein, is mutated in Senior-Loken syndrome and interacts with RPGR and calmodulin. *Nat Genet* 37, 282-288.

59. Attanasio, M., et al. (2007). Loss of GLIS2 causes nephronophthisis in humans and mice by increased apoptosis and fibrosis. *Nat Genet* 39, 1018-1024.

60. Wolf, M. T., et al. (2007). Mutational analysis of the RPGRIP1L gene in patients with Joubert syndrome and nephronophthisis. *Kidney Int* 72, 1520-1526.

61. Otto, E. A., Schermer, B., et al. (2003). Mutations in INVS encoding inversin cause nephronophthisis type 2, linking renal cystic disease to the function of primary cilia and left-right axis determination. *Nat Genet* 34, 413-420.

62. Olbrich, H., Fliegauf, M., et al. (2003). Mutations in a novel gene, NPHP3, cause Adolescent nephronophthisis, tapeto-retinal degeneration and hepatic fibrosis. *Nat Genet* 34, 455-459.

63. Otto, E. A., Trapp, M. L., Schultheiss, U. T., Helou, J., Quarmby, L. M., and Hildebrandt, F. (2008). NEK8 mutations affect ciliary and centrosomal localization and may cause nephronophthisis. *J Am Soc Nephrol* 19, 587-592.

64. Delous, M., Gaude, H.M., Saunier S. (2013). Genetic bases and pathogenic mechanisms of nephronophthisis. *Drug Discov. Today Dis. Mech.*

65. Ferrante, M.I., Z. Zullo, et al. (2006). Oral–facial–digital type I protein is required for primary cilia formation and left–right axis specification. *Nat. Genet*., 38: 112–117.

66. Romio, L., A.M. Fry, P.J. Winyard, S. Malcolm, A.S. Woolf, S.A. (2004) Feather OFD1 is a centrosomal/basal body protein expressed during mesenchymal–epithelial transition in human neurogenesis *J. Am. Soc. Nephrol*., 15;2566–2568.

67. Ooi, J., 2015. Mutations in C2CD3 cause oral-facial-digital syndrome through deregulation of centriole length. *Clin Genet.* 87(4)328-9.

68. Thauvin-Robinet, C., Lee JS, Lopez E, Herranz-Perez V et al. 2014. The oral-facial-digital syndrome gene C2CD3 encodes a positive regulator of centriole elongation. *Nat Genet.* 46(8)905-11.

69. Roberson E.C., Dowdle, W.E., Ozanturk, A., Garcia-Gonzalo, F.R., Li, C., Halbritter J., et al. (2015). TMEM231,mutated in orofaciodigital and Meckel syndromes, organizes the ciliary transition zone. *JCB.* 209 (1):129.43.

70. Boucher, C., and Sandford, R. (2004) Autosomal dominant polycystic kidney disease(ADPKD, MIM 173900, PKD1 and PKD2 genes, protein products known as polycystin-1 and polycystin-2). *Eur J Hum Genet.* 12 (5):347-54.

71. Ward, C.J., et al. (2002). The gene mutated in autosomal recessive polycystic kidney disease encodes a large, receptor-like protein. *Nat Genet*. 30(3):259-69.

72. Pazour GJ, et al. (2000). *Chlamydomonas* IFT88 and its mouse homologue, polycystic kidney disease gene Tg737, are required for assembly of cilia and flagella. *JCB.* 151(3):709-718.

73 Shu X., A.M. et al. (2005) Trojan RPGR OFR15 isoform co-localizes with RPGRIP1 at centrioles and basal bodies and interacts with nucleophosmin. *Hum. Mol. Genet*., 14;1193–1197.

74. Hameed, A., Abid, A., Aziz, A., Ismail, M., Mehdi, S.Q., and S. Khaliq. (2003) Evidence of RPGRIP1 gene mutations associated with recessive cone-rod dystrophy. *J Med Genet.* 40(8):616-619.

75. Kobayashi, A., et al. (2000) HRG (UNC119) mutation found in cone-rod dystrophy causes retinal degeneration in a transgenic model. *Invest. Ophthalmol. Vis. Sci.,* 41:3268–3277.

76. Otto, E., et al. (2002). A gene mutated in nephronophthisis and retinitis pigmentosa encodes a novel protein, nephroretinin, conserved in evolution. *Am J Hum Genet* 71, 1161-1167.

77. Hildebrandt, F., and Zhou, W. (2007). Nephronophthisis-associated ciliopathies. *JAmSoc Nephrol.* 18, 1855-1871.

78. O'Toole, J. F., Otto, E. A., Frishberg, Y., and Hildebrandt, F. (2006). Retinitis pigmentosa and Renal failure in a patient with mutations in INVS. *Nephrol Dial Transplant* 21, 1989-1991.

79. Valente, E. M., et al. (2006). Mutations in CEP290, which encodes a centrosomal protein, cause pleiotropic forms of Joubert syndrome. *Nat Genet* 38, 623-625.

80. Baala, L., Romano, S., Khaddour, R., Saunier, S., Smith, U. M., Audollent, S., Ozilou, C., Faivre, L., Laurent, N., Foliguet, B., et al. (2007b). The Meckel-Gruber syndrome gene, MKS3, is mutated in Joubert syndrome. *Am J Hum Genet* 80, 186-194.

81. S. J., Sullivan, L. S., et al. (2006). Spectrum and frequency of mutations in IMPDH1 associated with autosomal dominant retinitis pigmentosa and leber congenital amaurosis. *Invest Ophthalmol Vis Sci* 47, 34-42.

82. Perrault, I., et al. (2004). Retinal dehydrogenase 12 (RDH12) mutations in leber congenital amaurosis. *Am J Hum Genet* 75, 639-646.

83. Sayer, J. A., et al. (2006). The centrosomal protein nephrocystin-6 is mutated in Joubert syndrome and activates transcription factor ATF4. *Nat Genet* 38, 674-681.

84. Leitch, C. C., et al. (2008). Hypomorphic mutations in syndromic encephalocele genes are associated with Bardet- Biedl syndrome. *Nat Genet* 40, 443-448.

85. Badano, J. L., et al. (2006). Dissection of epistasis in oligogenic Bardet-Biedl syndrome. *Nature* 439, 326-330.

86. Dryja, T. P., et al. (2001). Null RPGRIP1 alleles in patients with Leber congenital amaurosis. *Am J Hum Genet* 68, 1295-1298.

87. Moore A, et al. (2006). RPGR is mutated in patients with a complex X linked phenotype combining primary ciliary dyskinesia and retinitis pigmentosa. *J Med Genet* 43:326–33.

88. Bukowy-Bieryłło Z, et al. (2013). RPGR mutations might cause reduced orientation of respiratory cilia. *Pediatr Pulmonol* 48:352–63.

89. Budny B, et al. (2006). A novel X-linked recessive mental retardation syndrome comprising macrocephaly and ciliary dysfunction is allelic to oral-facial-digital type I syndrome. *Hum Genet* 120:171–8.

90. Wallmeier J, et al. (2014). Mutations in CCNO result in congenital mucociliary clearance disorder with reduced generation of multiple motile cilia. *Nat Genet* 46:646–51.

91. Pennarun G, et al. (1999) Loss-of-function mutations in a human gene related to *Chlamydomonas reinhardtii* dynein IC78 result in primary ciliary dyskinesia. *Am J Hum Genet* 65:1508–19.

92. Olbrich H, et al. (2002). Mutations in DNAH5 cause primary ciliary dyskinesia and randomization of left-right asymmetry. *Nat Genet* 30:143–4.

93. Loges NT, et al. (2008) DNAI2 mutations cause primary ciliary dyskinesia with defects in the outer dynein arm. *Am J Hum Genet* 83:547–58.

94. Duriez B, et al. (2007). A common variant in combination with a nonsense mutation in a member of the thioredoxin family causes primary ciliary dyskinesia. *Proc Natl Acad Sci* USA 104:3336–41.

95. Mazor M, et al. (2011) Primary ciliary dyskinesia caused by homozygous mutation in DNAL1, encoding dynein light chain 1. *Am J Hum Genet* 88:599–607.

96. Onoufriadis A, et al. (2013) Splice-site mutations in the axonemal outer dynein arm docking complex gene CCDC114 cause primary ciliary dyskinesia. *Am J Hum Genet* 92:88–98.

97. Hjeij R, et al. (2013) ARMC4 mutations cause primary ciliary dyskinesia with randomization of left/right body asymmetry. *Am J Hum Genet* 93:357–67.

98. Alsaadi MM, et al. (2014) Nonsense mutation in coiled coil domain containing 151 gene (CCDC151) causes Primary ciliary dyskinesia. *Hum Mutat*. 35(12)1446-1448.

99. Panizzi J, et al. (2013) CCDC103 mutations cause primary ciliary dyskinesia by disrupting assembly of ciliary dynein arms. *Nat Genet* 44:714–19.

100. Omran H, et al. (2008) Ktu/PF13 is required for cytoplasmic pre-assembly of axonemal dyneins. *Nature* 456:611–16.

101. Loges NT, et al. (2009) Deletions and point mutations of LRRC50 cause primary ciliary dyskinesia due to dynein arm defects. *Am J Hum Genet* 85:883–9.

102. Mitchison HM, Schmidts M, Loges NT, Freshour J, Dritsoula A, Hirst RA, O'Callaghan C, Blau H, et al. (2012) Mutations in axonemal dynein assembly factor DNAAF3 cause primary ciliary dyskinesia. *Nat Genet* 44:381–9.

103. Tarkar A, Loges NT, Slagle CE, Francis R, Dougherty GW, Tamayo JV, Shook B, et al. (2013) DYX1C1 is required for axonemal dynein assembly and ciliary motility. *Nat Genet* 45:995–1003.

104. Horani A, Druley TE, Zariwala MA, Patel AC, Levinson BT, Van Arendonk LG, Thornton KC, et al. (2012) Whole-exome capture and sequencing identifies HEATR2 mutation as a cause of primary ciliary dyskinesia. *Am J Hum Genet* 91:685–93.

105. Kott E, Duquesnoy P, Copin B, Legendre M, Dastot-Le Moal F, et al (2012) Loss-of-function mutations in LRRC6, a gene essential for proper axonemal assembly of inner and outer dynein arms, cause primary ciliary dyskinesia. *Am J Hum Genet* 91:958–64.

106. Zariwala MA, et al. (2013) ZMYND10 is mutated in primary ciliary dyskinesia and interacts with LRRC6*. Am J Hum Genet* 93:336–45.

107. Knowles MR, Ostrowski LE, et al. (2013) Mutations in SPAG1 cause primary ciliary dyskinesia associated with defective outer and inner dynein arms. *Am J Hum Genet* 93:711–20.

108. Austin-Tse C, Halbritter J, Zariwala MA, Gilberti RM, Gee HY, Hellman N, et al (2013) Zebrafish ciliopathy screen plus human mutational analysis identifies C21orf59 and CCDC65 defects as causing primary ciliary dyskinesia. *Am J Hum Genet* 93:672–86.

109. Blanchon S, Legendre M, Copin B, Duquesnoy P, Montantin G, Kott E, Dastot F, et al (2011) Delineation of CCDC39/CCDC40 mutation spectrum and associated phenotypes in primary ciliary dyskinesia. *J Med Genet* 49:410–16.

110. Wirschell M, Olbrich H, Werner C, Tritschler D, Bower R, Sale WS, et al (2013) The nexin-dynein regulatory complex subunit DRC1 is essential for motile cilia function in algae and humans. *Nat Genet* 45:262–8.

111. Castleman VH, Romio L, Chodhari R, Hirst RA, de Castro SC, Parker KA, et al (2009) Mutations in radial spoke head protein genes RSPH9 and RSPH4A cause PCD with central-microtubular-pair abnormalities. *AJHG* 84:197–209.

112. Kott E, Legendre M, Copin B, Papon JF, Dastot-Le Moal F, Montantin G, et al. (2013) Loss-of-function mutations in RSPH1 cause primary ciliary dyskinesia with central-complex and radial-spoke defects. *Am J Hum Genet* 93:561–70.

113. Olbrich H, Schmidts M, et al. (2012) Recessive HYDIN mutations cause primary ciliary dyskinesia without randomization of left-right body asymmetry. *Am J Hum Genet* 91:672–84.

114. Pifferi M, Michelucci A, Conidi M, Cangiotti A, Simi P, Macchia P, Boner (2010) A New DNAH11 mutations in primary ciliary dyskinesia with normal axonemal ultrastructure. *Eur Respir J* 35:1413–16.

115. Travaglini L, Brancati F, Silhavy J, Iannicelli M, Nickerson E, et al. (2013). Phenotypic spectrum and prevalence of INPP5E mutations in Joubert syndrome and related disorders. *Eur J Hum Genet.* 21(10):1074-8.

116. Jacoby M, Cox JJ, Gayral S, Hampshire DJ, AyubM, et al. (2009) INPP5E mutations cause primary cilium signaling defects, ciliary instability and ciliopathies in human and mouse. *Nat Genet.* 41(9):1027-31.

117. Bachmann-Gahescu R, Phelps IG, Dempsey JC, Sharma VA, et al. (2015) KIAA0586 is mutated in Joubert syndrome. *Hum Mutat.* 36(9):831-5.

118. Perrault I, Halbritter J, Porath JD, Gerard X, Braun DA, et al (2015). IFT81, encoding an IFT-B core protein, as a very rare cause of a ciliopathy phenotype. *J Med Genet.* [epub ahead of print]

119. Perrault I, Saunier S, Hanein S, Filhol E, Bizet AA, et al. (2012) Mainzer -Saldino syndrome is a ciliopathy caused by IFT40 mutations. *Am J Hum Genet.* 90(5):864-70.

120. Hoffer JL, et al. (2013) Novel WDR35 mutations in patients with cranioectodermal dysplasia (Sensenbrebber syndrome). *Clin Genet.* 83(1)92-5.

121. Walczak-Sztulpa J, Eggenschwiler J, Osborn D, Brown DA, Emma F, et al. (2010) Cranioectodermal Dysplasia, Sensenbrenner syndrome, is a ciliopathy caused by mutations in the IFT122 gene. *Am J Hum Genet.* 86(6):949-56.

122. Arts HH, Bongers EM, Mans DA, van Beersum Se, e t al. (2011) C14ORF179 encoding IFT43 is mutated in Sensenbrenner syndrome. *J Med Genet.* 48(6)390-5.